Topological properties of superconducting nanostructures

Repin, E.

DOI
10.4233/uuid:b06f8d39-0c8b-405f-ad60-4df46f291ab8

Publication date
2021

Document Version
Final published version

Citation (APA)
Repin, E. (2021). *Topological properties of superconducting nanostructures*. [Dissertation (TU Delft), Delft University of Technology]. https://doi.org/10.4233/uuid:b06f8d39-0c8b-405f-ad60-4df46f291ab8

TOPOLOGICAL PROPERTIES OF SUPERCONDUCTING NANOSTRUCTURES

TOPOLOGICAL PROPERTIES OF SUPERCONDUCTING NANOSTRUCTURES

Proefschrift

ter verkrijging van de graad van doctor
aan de Technische Universiteit Delft,
op gezag van de Rector Magnificus Prof.dr.ir. T.H.J.J. van der Hagen
voorzitter van het College voor Promoties,
in het openbaar te verdedigen op dinsdag 6 april 2021 om 12:30 uur

door

Evgeny REPIN

Master in Applied Mathematics and Physics,
Moscow Institute of Physics and Technology, Russia,
born in Tambov, Russia.

Dit proefschrift is goedgekeurd door de

promotor: prof. dr. Y.V. Nazarov

Samenstelling promotiecommissie:

Rector Magnificus,	voorzitter
Prof. dr. Y.V. Nazarov,	Technische Universiteit Delft, promotor

Onafhankelijke leden:

Prof. dr. Y. Blanter	Technische Universiteit Delft
Prof. dr. W. Belzig	Universität Konstanz, Germany
Prof. dr. M.I. Katsnelson	Radboud Universiteit, Netherlands
Dr. M. Houzet	CEA Grenoble, France
Prof. dr. A.F. Otte	Technische Universiteit Delft
Prof. dr. R.A. Duine	TU Eindhoven, Utrecht University, Netherlands
Prof. dr. ir. H. van der Zant	Technische Universiteit Delft, reservelid

Printed by: GILDEPRINT

ISBN 978-90-8593-471-4

Casimir PhD-series number 2021-05

An electronic version of this dissertation is available at
http://repository.tudelft.nl/.

Zankoku na tenshi no te-ze

Plastic world has won, the brick turned out to be stronger
O-o-o... My defense...

«My defense» by Civil Protection

CONTENTS

Summary ix

Samenvatting xi

Preface xiii

1 Introduction 1
- 1.1 Preface . . . 2
- 1.2 Topology overview . . . 2
  - 1.2.1 Homotopy and cohomology groups . . . 3
  - 1.2.2 Fiber bundles . . . 6
  - 1.2.3 Characteristic classes . . . 9
  - 1.2.4 Classifying bundles and K-theory . . . 11
- 1.3 Topology in condensed matter . . . 15
  - 1.3.1 Weyl semimetal . . . 15
  - 1.3.2 Topological superconductor . . . 15
- 1.4 Superconducting nanostructures . . . 16
  - 1.4.1 Spacially inhomogeneous superconductivity . . . 16
  - 1.4.2 Scattering formalism . . . 18
  - 1.4.3 Action formalism . . . 19
- 1.5 Structure of the thesis . . . 20
  - 1.5.1 Chapter 2 . . . 20
  - 1.5.2 Chapter 3 . . . 20
  - 1.5.3 Chapter 4 . . . 21
  - 1.5.4 Chapter 5 . . . 21

References . . . 21

2 Topological properties of multiterminal superconducting nanostructures: Effect of a continuous spectrum 27
- 2.1 Introduction . . . 28
- 2.2 Multi-terminal superconducting nanostructure . . . 30
- 2.3 Action . . . 31
  - 2.3.1 Stationary phases . . . 33
- 2.4 Response function of the currents . . . 34
- 2.5 Weak energy dependence of the $S-$matrix . . . 38
  - 2.5.1 Energy-independent $S-$matrix: . . . 39
  - 2.5.2 Contribution from the large scales: . . . 41
- 2.6 The vicinity of a Weyl point . . . 43
  - 2.6.1 Vanishing spin-orbit coupling . . . 44
  - 2.6.2 Weak Spin-Orbit Coupling . . . 45

2.7 Energy-dependent $S-$matrix: . . . 48
2.8 Summary and Conclusions . . . 49
2.9 Appendix A: derivation of the action . . . 50
2.10 Appendix B: derivation of the response function . . . 55
2.11 Acknowledgements . . . 57
References . . . 58

3 Topological numbers of quantum superpositions of topologically non-trivial bands 61
3.1 Introduction . . . 62
3.2 Adiabatic evolution of the superposition . . . 64
3.3 Topological constraint on the mixing matrix element . . . 66
3.4 Topological transition and Berry curvature distribution . . . 67
3.5 Many bands: general properties of the phase diagrams . . . 72
3.6 Example: bilayer Haldane model . . . 73
3.7 Summary and Conclusions . . . 79
3.8 Appendix A: Extended singularities in the bilayer Haldane model . . . 80
3.9 Acknowledgements . . . 81
References . . . 81

4 Braiding and all quantum operations with Majorana modes in 1D 83
4.1 Braiding and all quantum operations with Majorana modes in 1D . . . 84
4.2 Supplemental Materials . . . 90
4.2.1 Wave functions and matrix elements of gate voltages . . . 90
4.2.2 Relation between pulse parameters and gate voltage amplitudes . . . 91
4.2.3 Pulse sequences required for braiding . . . 91
4.2.4 Developer and fixer for initialization and measurement . . . 94
4.2.5 Residulal overlap of Majorana modes . . . 94
4.3 Acknowledgements . . . 94
References . . . 96

5 Weyl points in the multi-terminal Hybrid Superconductor-Semiconductor Nanowire devices 97
5.1 Weyl points in the multi-terminal Hybrid Superconductor-... . . . 98
5.2 Supplementary material . . . 104
5.2.1 Finding the spectrum . . . 104
5.2.2 Search for Weyl points . . . 106
5.3 Acknowledgements . . . 106
References . . . 106

Acknowledgements 109

Curriculum Vitæ 111

List of Publications 113

SUMMARY

One of the pillars of the scientific method is the fact that... Oh wait, it's a different one. One of the pillars of the technological development is the fact that if the existing design does not achieve the goal or cannot be applied in new conditions, one could propose a totally different design that may achieve the goal. The only constraints in this way being the laws of physics. This is the main message of the lecture by Richard Feynman on tiny machines. The role of different designs can also be noted on a purely theoretical level. There, changing the well-known model can have far reaching consequences on its properties and possible applications.

One of the main goals in the focus of modern quantum technology is realization of a quantum computer. The appeal of this device is in the difference from the classical analogous computer, being reasonable proposals for error correction. Another aspect is that one may use topological quantum states that are robust by themselves against certain noises. There is a lot of effort in trying different approaches and designs to experimentally realize and detect these states. Two main approaches are to either realize topological compounds or combine topologically trivial compounds to effectively realize non-trivial topological properties. There have been advances in both topological and non-topological quantum computation. One of the most famous examples being the achieved quantum supremacy (or, after censorship, quantum advantage). Despite that, the technology is still far away from being used at home. Also, during the process of development of technology other things may come about on the way. Anyhow, regardless of the outcome, the way itself is always more important than the resulting point. In this thesis we discuss certain theoretical findings discovered on the way.

For example, in Chapter 2 we discuss in detail the topological properties of multi-terminal superconducting nanostructures. Initially they were proposed to realize non-trivial topology in higher dimensions with the help of topologically trivial materials. This idea belongs to the framework discussed above. We find that these nanostructures may indeed possess non-trivial topological properties but the observation may be complicated by the presence of the continuous spectrum above the superconducting gap. On the other hand, there is always a possibility thay any complication may be turned into advantage later.

Next, in Chapter 3 we address a general question about topological properties of many-band systems without anti-unitary symmetries. We investigate the generalities of topological phase diagrams and find that the generic features of those differ from the usual phase diagrams. Namely, the common critical points in topological phase diagrams are quadruple as opposed to the case of triple points in the usual phase diagrams. We exemplify the general considerations taking an example of bilayer Haldane model.

Then, in Chapter 4 we investigate the ways to operate on the Majorana states in a simple model. We propose a scheme that allows to braid Majorana states by application

of resonant voltage pulses and not using the geometry of the device. As discussed above, control and operation on topological states is crucial for possible applications.

Finally, in Chapter 5 we investigate a modification of the well-known superconductor-semiconductor nanowire design that was initially proposed to realize Majorana states with topologically trivial materials. Taking experimental advances as a motivation, we complicate the model by increasing the number of terminals that cover the nanowire and investigate different from Majorana topological properties, namely Weyl points. First, we find that it is possible to find Weyl points in the spectrum of the system. Second, we find that again the presence of the continuum does have the effect on the topological properties of the model.

SAMENVATTING

Eén van de bouwstenen van de wetenschappelijke methode is het feit dat... Oh wacht, het is een andere. Een van de pijlers van de technologische ontwikkeling is het feit dat als het bestaande ontwerp het doel niet bereikt of niet kan worden toegepast in nieuwe omstandigheden, men een totaal ander ontwerp kan voorstellen dat het doel kan bereiken. De enige beperkingen op deze manier zijn de wetten van de fysica. Dit is de belangrijkste boodschap van de lezing door Richard Feynman over kleine machines. De rol van verschillende ontwerpen kan ook op puur theoretisch niveau worden opgemerkt. Daar kan het veranderen van het bekende model verstrekkende gevolgen hebben voor de eigenschappen en mogelijke toepassingen.

Een van de belangrijkste doelen in de focus van moderne kwantumtechnologie is de realisatie van een kwantumcomputer. De aantrekkingskracht van dit apparaat zit hem in het verschil met de klassieke analoge computer, omdat het redelijke voorstellen voor foutcorrectie zijn. Een ander aspect is dat men topologische kwantumtoestanden kan gebruiken die op zichzelf robuust zijn tegen bepaalde geluiden. Er is veel moeite gedaan om verschillende benaderingen en ontwerpen uit te proberen om deze toestanden experimenteel te realiseren en te detecteren. Twee belangrijke benaderingen zijn om ofwel topologische verbindingen te realiseren of topologisch triviale verbindingen te combineren om effectief niet-triviale topologische eigenschappen te realiseren. Er zijn vorderingen gemaakt in zowel topologische als niet-topologische kwantumberekeningen. Een van de bekendste voorbeelden is de bereikte kwantumovermacht (of, na censuur, kwantumvoordeel). Desondanks is de technologie nog ver verwijderd van thuisgebruik. Ook kunnen er tijdens het proces van technologische ontwikkeling onderweg andere dingen gebeuren. Hoe dan ook, ongeacht de uitkomst, de weg zelf is altijd belangrijker dan het resulterende punt. In dit proefschrift bespreken we bepaalde theoretische bevindingen die onderweg zijn ontdekt.

In Hoofdstuk 2 bespreken we bijvoorbeeld in detail de topologische eigenschappen van multi-terminale supergeleidende nanostructuren. Aanvankelijk werd voorgesteld om niet-triviale topologie in hogere dimensies te realiseren met behulp van topologisch triviale materialen. Dit idee behoort tot het hierboven besproken raamwerk. We vinden dat deze nanostructuren inderdaad niet-triviale topologische eigenschappen bezitten, maar de waarneming kan gecompliceerd zijn door de aanwezigheid van het continue spectrum boven de supergeleidende spleet. Aan de andere kant is er altijd een mogelijkheid dat elke complicatie later in voordeel kan worden omgezet.

Vervolgens behandelen we in Hoofdstuk 3 een algemene vraag over topologische eigenschappen van veelbandsystemen zonder anti-unitaire symmetrieën. We onderzoeken de algemeenheden van topologische fasediagrammen en vinden dat de generieke kenmerken hiervan verschillen van de gebruikelijke fasediagrammen. De gemeenschappelijke kritische punten in topologische fasediagrammen zijn namelijk viervoudig in tegenstelling tot het geval van tripelpunten in de gebruikelijke fasediagrammen. We il-

lustreren de algemene overwegingen door een voorbeeld te nemen van een dubbellaag Haldane-model.

Vervolgens onderzoeken we in hoofdstuk 4 de manieren om in een eenvoudig model te opereren op de Majorana-staten. We stellen een schema voor waarmee Majorana-toestanden kunnen worden gevlochten door toepassing van resonante spanningspulsen en niet door de geometrie van het apparaat te gebruiken. Zoals hierboven besproken, is controle en werking op topologische toestanden cruciaal voor mogelijke toepassingen.

Ten slotte onderzoeken we in Hoofdstuk 5 een modificatie van het bekende supergeleider-halfgeleider nanodraadontwerp dat aanvankelijk werd voorgesteld om Majorana-toestanden te realiseren met topologisch triviale materialen. Door experimentele vooruitgang als motivatie te nemen, maken we het model gecompliceerder door het aantal terminals te vergroten dat de nanodraad bedekt en andere topologische eigenschappen dan Majorana te onderzoeken, namelijk Weyl-punten. Ten eerste vinden we dat het mogelijk is om Weyl-punten in het spectrum van het systeem te vinden. Ten tweede vinden we dat opnieuw de aanwezigheid van het continuüm effect heeft op de topologische eigenschappen van het model.

PREFACE

You **have** *to enjoy it!*

Quote without author № 3

The word "task" is not a synonym to "problem".

Quote without author № 15

The word "complicated" means it was complicated by someone.

Quote without author № 51

There are many ways of being stupid.

Quote without author № 100

This is why a pole at the end of the cut is impossible
folding a piece of paper into a cone and showing

Quote without author № 1

Pull the other leg!

Quote without author № 11

-We use different definitions here...
-Why don't you take mine?!

Quote without author № 12

Arguing with a manipulator is like shearing a pig:
lots of squeal and little gain.

Quote without author № 7

Jupyter notebooks will lead to the death of science.

Nostradamus

Without initiation rite or orthogonality catastrophe no adulthood or qualitatively new property is possible.

Quote without author № (-1)

Do this, do that
People who can't do anything are lame?
Excessive expectations invite failure
Feel free to gracefully avert your eyes
After all, this is basically
a tactical retreat!

«Declaration of complete resignation» by Nanawo Akari

Bob Wilson: "Any other expectations we might have are a matter of luck.
When we hire a professor, we're taking all the risks."
...and it released me from the feeling of guilt.
So I got this new attitude.
I'm going to play with physics, whenever I want to, without
worrying about any importance whatsoever.

from «Surely You're Joking, Mr. Feynman!»

The weak can overcome the strong;
The supple can overcome the stiff.
The truth often seems paradoxical.

Tao Te Ching - Lao Tzu - chapter 78

Quality of the time spent on projects
is much more important than the results.

Quote without author № 0

1

INTRODUCTION

...error correction is applied by repeating three steps:
1. Errors are accumulated over a short piece of the computation.

from PhD thesis by Tom O'Brien (2019)

1

1.1. PREFACE

The recent decades have seen the advent of topological concepts[1, 2] in condensed matter physics. This includes the theoretical developments[3, 4] including the description of topological properties[5, 6] or possible applications[7] of those as well as experimental results[8–12]. Generally, topological systems are interesting due to various unusual properties, among which there are anomalous response functions[13], edge states protected against localization[14], non-Abelian statistics of excitations[15]. The latter is a promising platform to realize topological quantum computation[7]. An alternative, but closely related, direction of research is non-topological quantum computations[16]. This involves making qubits without topological protection, for example superconducting qubits[17], qubits on quantum dots[18], etc. One of the most famous successful examples of non-topological quantum computation is the reported achieved quantum supremacy[19, 20].

Realization of topological structures and finding ways to use the topological properties is a problem of physics. One way is to search for or manufacture topological compounds experimentally[12, 21, 22]. In this way topological properties emerge due to a nontrivial bandstructure of the material itself. The other way is to investigate the topological properties of heterostructures[23, 24], where the topological properties may come about due to the interplay of different materials. In this Thesis we focus on this approach and investigate the topological properties of various heterostructures made of non-topological materials. In any case, the active use of topological concepts shows that the detailed knowledge of topology as a mathematical discipline is required if not vital. Due to this we make a brief review of topology in this Introduction.

A general problem providing additional motivation to this introduction is the problem of language, or rather interplay of different languages. The so-called continental philosophy[25, 26] had arrived at the conclusion of equivalence of different discourses. Discourse roughly means a descriptive system, e.g. a discourse of condensed matter physics, a discourse of biophysics, a discourse of high energy physics, etc. So, the statement about equivalence is relevant when different discourses address the same problem. The lack of understanding of this may bring significant problems to scientific research both on the level of personal interaction as well as on the level of interplay of different branches of science. The first part of the Introduction is an attempt to make a bridge between two discourses: the discourse of mathematics and the discourse of modern condensed matter physics.

So, in the first part of the Introduction we discuss the topological notions and concepts relevant for the present thesis. Then, in the second part we discuss models and approaches to description of condensed matter systems relevant for this Thesis in which topological concepts play a key role. The main purpose of the following Chapters is to discuss the novel topological properties of several heterostructures.

1.2. TOPOLOGY OVERVIEW

In this section we briefly review the relevant topological constructions and present a dictionary (see Table1.1) to make correspondence between mathematical notions with the usual thesaurus of condensed matter physics. In general, topology is the study of spaces

vector bundle	quantum system
section	wavefunction
base space	parameter space, Brillouin zone
fiber	Hilbert space
bundles isomorphism classes	topological phases
curvature 2-form for 1-dimensional complex bundle	Berry curvature

Table 1.1: Dictionary between mathematical notions and possible condensed matter analogues.

by means of formalization of how to describe properties that do not change upon continuous (or smooth) mappings/transformations. We do not mention several important branches of topology at all, like knot and links theory (for a review see, e.g.[27]). Those have already found important applications in high energy mathematical physics[28]. One can expect that those may also find useful applications in condensed matter when one would need to describe the topology of extended structures. First, we will review the general notions and constructions relevant for the thesis and then restrict to the specific case of smooth manifolds when the convenient differential geometry analysis may be applied. In the last part we discuss general classification approaches that can be applied to spaces without differential structure. Anywhere where there is an abstract topological notion appearing we will try to provide the natural analoges from condensed matter language. The exact conditions of applicability of statements are not always stated but can be easily found in the literature[29, 30]. A common requirement being the compactness of spaces under consideration, this would guarantee convergence of integrals over them. Some statements have a wider range of applicability, e.g. not compact but locally compact spaces like R^d. See Ref.[31] for more detail.

1.2.1. HOMOTOPY AND COHOMOLOGY GROUPS

In this subsection we review the basic notions and concepts used in the subsequent subsections. Topological spaces are the ones for which the notion of openness and thus continuousness of maps is defined.

We now discuss the notion of topological equivalence for different objects. First, topological equivalence of two maps can be formalized as a homotopy between maps. In a way it is as formalization for a path between maps. More precisely, two maps of spaces $f, g : X \to Y$ are homotopic $f \sim g$ if there exists a continuous map $F : [0;1] \times X \to Y$ such that $F(0) = f$ and $F(1) = g$ and $[0;1]$ is a unit interval with endpoints included. For spaces the definition of equivalence is not so simple since a path in the space of spaces is hardly well-defined (all spaces form a cathegory, not a set). There are two general formalizations of topological equivalence of spaces. First one is homeomorphism: there exists a continuous one-to-one map between spaces and inverse is also continuous. It does correspond to the intuitive picture of topological equivalence being a possibility to continuously deform one space into the other. The second one is homotopy equivalence of spaces: a pair of continuous maps f, g exist sich that $fg \sim id_X$ and $gf \sim id_Y$, where e.g. id_X is an identical map of X to itself. The homotopy equivalence is the one most widely used (theorems mostly state something about this particular equivalence relation) but it does not completely correspond to the intuitive picture of equivalent spaces. For example, a $d-$dimensional real space R^d or any other contractible (over itself) space that

consists of more than one point is homotopy equivalent to a point pt, but they are not homeomorphic.

Directly checking topological equivalence of spaces may be a formidable task. Therefore, one may think about what kind of topological invariants may help distinguish topological spaces. The first candidate is homotopy groups. For a given space X they are defined as homotopy classes of maps of spheres S^n into X called spheroids. Homotopy classes of spheroids are denoted as $[S^n, X]$. One also requires that there is one fixed pre-chosen point x_0 for all maps. Fixation of this basepoint allows one to introduce a group operation on these homotopy classes making it into a group denoted as $\pi_n(X, x_0)$. Rougly speaking, a product of spheroids of the same dimension is a composite spheroid made of two intial ones. The map for the product is as follows: one takes a sphere, its whole equator is mapped into x_0 and the upper and lower halves of the sphere become two spheroids that we want to multiply. For $n > 1$ the groups turn out to be commutative, for $n = 1$ not necessarily. The reason is actually the same as why fermions with repulsion are special in 1 dimension: one cannot push them through each other to exchange positions. For a path-connected X (there exists a path between any two points) the dependence on the basepoint is not essential (all groups corresponding to different basepoints are isomorphic), so one usually does not specify it. If X consists of identical components, like e.g. $O(n)$ being two copies of $SO(n)$, then $\pi_n(X)$ will be defined as a group computed for one component. For example, in accordance with the intuition for $n > 0$ $\pi_n(S^n) = Z$, this integer is called degree of mapping. Also $\pi_r(S^n) = 0$ for $r < n$. However, in the general case even the homotopy groups of spheres turn out to be very difficult to obtain. For example, an unexpected result is $\pi_3(S^2) = Z$ so homotopy groups are complicated invariants in general despite expectation. Also, by definition, a 0-dimensional sphere S^0 = point$\bigsqcup$point is a disjoint unit of two points, which is a boundary of a 1-dimensional disk B^1 - line segment with endpoints included. With this $\pi_0(X)$ is a number of connected components of X and $\pi_0(S^0) = Z_2$. In the subsequent section about K-theory 0-th homotopy groups give the simplest way to understand the groups arising in the well-known topological periodic table[32, 33]. Despite being a complicated invariant, homotopy groups generally do not completely specify the homotopy type of the space. But spaces with different groups are certainly not equivalent. Homotopy groups can be readily applied to classifications of stable defects[34], e.g. by considering classes of mappings of S^n to the space of order parameters. This sphere is then thought of as consisting of all points at infinity, i.e. "boundary" of the R^{n+1} parameter space of the system .

A somewhat simpler invariant (easier to compute and having properties corresponding to intuition) is homology and cohomology. Due to relative simplicity, these invariants are even weaker than homotopy but still allow to distinguish non-equivalent spaces. Also, widely used characteristic classes belong to cohomology groups. The basic idea of homology is also to consider mappings of spheres or other surfaces into X but present them as composed of elementary simplices. Then we will investigate if this surface will be a boundary of some region within X. If not - then the surface probes non-trivial topology. For the investigation of boundaries we will need orientation of each simplex: the order of its faces which are simplices of a dimension smaller by 1. So we will map $d-$dimensional simplices $\sigma^d \xrightarrow{f} X$ and introduce an operation of the sum of images of

those simplices as units of geometric objects $C_d = \Sigma_i n^i f(\sigma_i^d)$ where now all $n^i = 1$. Next, we consider arbitrary integer coefficients $n^i \in Z$, negative ones will make sense when we define the boundary of a simplex. Then this sum is called a $d-$dimensional chain. The boundary of the chain is a chain with dimensionality smaller by 1 $\partial C_d = \Sigma_i n^i f(\partial\sigma_i^d)$ consisting of linear combinations of boundaries of original simplices. The boundary of each simplex σ is a chain equal to the sum of all faces σ' of this simplex with alternating signs $\partial\sigma = \Sigma_j(-1)^j\sigma'_j$. Alternation of the signs in this definition is crucial. This operation is also called differential for the reasons discussed below. If the chain is itself a boundary of some other chain then we call it trivial. This suggests the notion of topological equivalence here called homology of chains: they are equivalent if they differ by a boundary. If the boundary of the chain is empty than we call it a cycle. Boundary of a boundary is empty: $\partial^2 = 0$, so we can factor d-dimensional cycles by d-dimensional boundaries, $d \geq 0$, the result being an abelian homology group $H_d(X)$. Roughly speaking, these groups probe the same topology as homotopy groups but these are different homotopy invariants.

Next, in the case when X is a smooth manifold (manifold means topological space every point of which has an open neighbourhood homeomorphic to R^d and smooth means that the notion of tangent vector and differentiation with respect to it $\partial/\partial x_m$ is also defined), one may consider integrals of real functions over these simplices which obviously result in numbers $C_d \to R^1$. Actually, the integration of functions is an operation not accurately defined (one has to keep track of the Jacobian), so instead one can introduce differential forms where the functions $\phi(x)$ will be coefficients in the basis of antisymmetric products of differentials of local coordinates $\omega = \phi(x)dx_1 \wedge dx_2 ... \wedge dx_k$. The product symbol defined on coordinate differentials $dx \wedge dy = -dy \wedge dx$ is just an antisymmetric product. Antisymmetric product will ensure the correct Jacobian upon coordinate transformation. The integral of a differential form over simplex is defined as the usual integral of the coefficient function $\phi(x)$ after one just sets the order of differentials in correspondence with the orientation of the simplex. The integral defined like this is invariant under coordinate transformations.

From the definition we see that differential forms are antisymmetric tensor fields defined on a manifold. For differential forms the usual differential operation $d(\phi(x)dx_1 \wedge ... \wedge dx_k) = \sum_m \frac{\partial\phi(x)}{\partial x_m} dx_m \wedge dx_1 \wedge ... \wedge dx_k$ has the property that is analogous to differentiation of simplices $d^2 = 0$. This is because the second derivative of smooth functions is symmetric w.r.t. the order of differentiation. Proceeding completely analogous to homology, let us define topological equivalence of differential forms: two forms are equivalent if they differ by a complete differential. Therefore, in complete analogy to homology one can introduce a factor group of forms that have trivial differential $d\omega = 0$ over forms that are themselves differentials of some other form $\omega = d\eta$. These classes of $d-$dimensional differential forms are called elements of de Rham cohomology groups with real coefficients $H^d(X, R^1)$. In the case of a general space when the notion of differentiation is not defined one can also define cohomology as a space of linear functions over homology. This is analogous to the duality of vectors and covectors in standard linear algebra. Thus, the linear space of differential forms can be seen as a dual space of linear functionals to homology. Finally, there is a deep relation between geometric differentiation of simplices ∂ and usual differentiation operation d. Stokes theorem is an

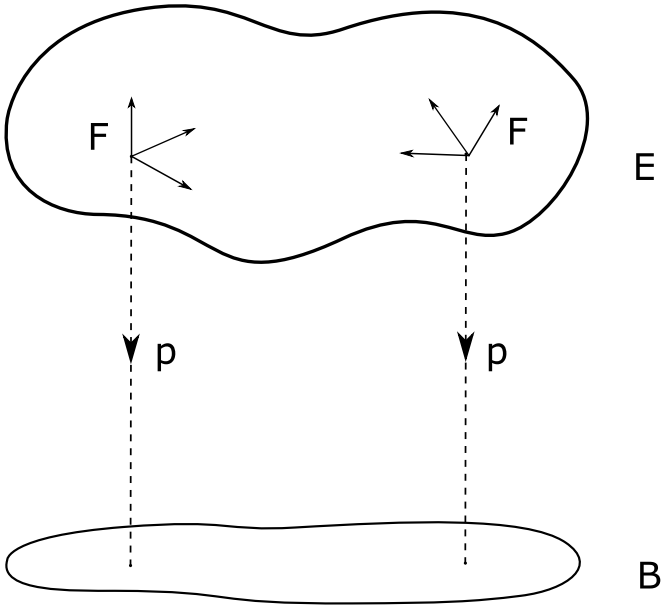

Figure 1.1: An illustration for vector bundle definition over space B: total space E is mapped to B by a bundle projection p, the fiber, a linear space in this case, denoted as F, is mapped to each point in B. Fibers living in E can be glued non-trivially making a non-trivial bundle. Trivial bundle corresponds to just a product of spaces $E = F \times B$, so fibers in E are glued in a trivial way.

exact statement about how they are related.

1.2.2. FIBER BUNDLES

The natural way to think about most of the topological properties discussed in condensed matter so far is in terms of the topology of locally trivial vector fiber bundles. A locally trivial fiber bundle by definition is a structure involving 3 topological spaces: E, B, and F and a surjective continuous map $p : E \to B$ such that each point $x \in B$ has an open neighborhood U such that $p^{-1}(U)$ is homeomorphic to $U \times F$. The way to understand this abstract definition is to note that over each point in B there is a fiber space that lives in E and is projected into the point upon bundle projection p (see Fig.1.1). In order to avoid exotic examples we also require that the homeomorphism $\overline{p}$: $U \times F \to p^{-1}(U)$ is compatible with p, i.e., $pr_1(U \times F) = p(\overline{p}(U \times F))$; here pr_1 is a projection onto the first factor. The map p is called the bundle projection, B is the base of the bundle, F is the fiber, and E is the total space of the bundle.

Next, one may consider a base space as a space made of a set of overlapping open patches $\{U\}$ (so-called open covering) over each of which the bundle is just a direct product, i.e. trivial. The main issue is where any two patches overlap one has to match or glue the fibers defined over separate overlapping patches and this can be done in a topologically non-trivial way thus producing a *globally* non-trivial bundle. Topological properties of the base itself play a huge role, for example any bundle over R^d is trivial. Another useful notion is the section of the bundle: a continuous map s from base space B to total

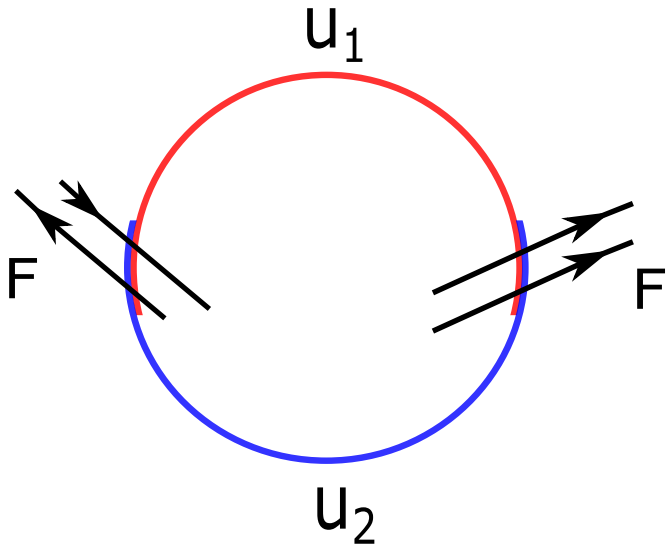

Figure 1.2: An illustration for a simplest non-trivial real vector bundle, fiber being R^1. Total space is the Mobius band. Base space is a circumference S^1. As discussed in the text, the base space is covered by two open patches: red U_1, blue U_2. In the region where regions overlap we need to glue 1-dimensional fibers R^1. There are two options, as shown in the figure, orientation preserving or changing. A non-trivial bundle corresponds to choosing orientation preserving on one overlap and orientation flipping on the other overlap, as shown. Then, it can be viewed as fibers living in E being glued non-trivially making a Mobius band (without a boundary).

space E such that $ps = id_B$. This map defines an element in fiber space dependent on B.

A linear bundle is a bundle where fibers F are linear spaces of fixed dimension. It can be vector or tensor space. In this case the gluing between fibers over overlapping patches is just a linear map. In the case of vector bundles sections are vector fields over a base. The simplest example of a non-trivial real vector bundle is provided by the Mobius band: the Mobius band itself is a total space E, the base is a circumference $B = S^1$ and the fiber is 1-dimensional real space R^1. The bundle projection p can be seen as projection of the Mobius band onto the circumference embedded in the middle of the band. The base S^1 can be separated into two overlapping open intervals, over each one the bundle is trivial. Gluing of fibers over two regions of overlap is done by a linear map $R^1 \to R^1$. This map can be orientation preserving or not. If on one overlap region the orientation is preserved and on the other not, we get a Mobius bundle (see Fig.1.2). A 2-dimensional cylinder without boundary is a trivial 1-dimensional bundle because it is globally a Cartesian product $S^1 \times R^1$. These two examples are the only possibilities of a 1-dimensional real bundle over S^1 as can be proven by an application of Stiefel-Whitney classes discussed below.

A usual condensed matter analogue of a base space is a Brillouin zone or a parameter space. A fiber space is Hilbert space (complete linear metric space, i.e. there are no "holes" in it: any sequence of vectors convergent by the metric does converge to a vector from the same space) of states. A wavefunction is then a section of the bundle, i.e. a map from Brillouin zone to the fibers consistent with the global bundle structure. Total space

and bundle projection are needed to complete the structure of the bundle. A specific vector bundle corresponds to a description of all states a physical system and topological classes of bundles correspond to topological phases. Equivalence of linear bundles over the same base B is a homeomorphism of total spaces $E_1 \to E_2$ such that its restriction to any fiber is an isomorphism of linear spaces.

A theorem says that if there is a globally defined basis of sections (wavefunctions) then the bundle is trivial. Let us consider the textbook example of the complex bundle over S^2 with an obstruction to defining the globally well-defined section. We parametrize the sphere by two angles $\theta \in [0;\pi]$ and $\phi \in [0,2\pi]$. Let us also introduce two topologically trivial patches as discussed above. Denote U_1 is $\theta \in [0;\pi/2+\epsilon]$ and $\phi \in [0,2\pi]$; U_2 is $\theta \in [\pi/2-\epsilon;\pi]$ and $\phi \in [0,2\pi]$. Then consider the wavefunction

$$\psi_2 = \begin{pmatrix} \sin\frac{\theta}{2} \\ \cos\frac{\theta}{2} e^{i\phi} \end{pmatrix} \tag{1.1}$$

is not well defined at $\theta = 0$ but is well-defined on U_2 We can move the singularity to $\theta = \pi$ by applying a gauge transformation to obtain $\psi_1 = e^{-i\phi}\psi_2$ but cannot get rid of it, the argument for it is provided by characteristic classes discussed below. And ψ_1 is a section well-defined on U_1. As discussed above, we glue the 1-dimensional fibers along the overlap of patches - vicinity of $\theta = \pi/2$. It will be done precisely with the gauge transformation $e^{i\phi} \in U(1)$. This realizes a nontrivial map from the equator homotopy equivalent to S^1 to the group of admissible linear transformations. We see now how 1-dimensional complex bundles with no additional symmetries over S^2 are classified by $\pi_1(U(1)) = Z$. Analogous statement applies in higher dimensions.

Finally, we mention that in the case of smooth manifolds a tangent bundle can be defined. The name is self-explanatory: the fibers can be associated with tangent spaces at each point of the manifold. For example, a tangent bundle to S^2 is non-trivial despite having no non-trivial characteristic classes discussed below. Tangent vectors play a special role since they are useful for treating differentiation.

How does the Hamiltonian fit into this picture? Let us consider a Hamiltonian defined on a compact space of parameters (or a Brillouin zone). Diagonalizing a Hamiltonian provides an alternative way to define a bundle. If there are no degeneracies then the distinct eigenbasis wavefunctions can be chosen up to a global phase. Different values of energies are the reason not to make superpositions of wavefunctions, namely to consider wavefunctions separately as sections of 1-dimensional bundles over parameter space. Let us consider another case, an isolated degeneracy point of two energy levels in 3-dimensional parameter space being present. We will call it a Weyl point. Different energies wavefunctions are well-defined on a small sphere surrounding this point so, once again, they can be seen as sections of 1-dimensional bundles over this sphere. Each bundle can have any integer first Chern number n (the sum of all of them will vanish due to completeness of the basis), the definitions and way to compute Chern numbers are discussed below. In the case of two wavefunctions the absolute value of this arbitrary integer is usually called a topological charge. The nonzero value of the topological charge imples the topological protection of the level crossing: it is directly related to non-triviality of the corresponding 1-dimensional bundle and its topological non-equivalence to the trivial bundle with $n = 0$. If the spectrum is such that degener-

acy happens along an extended subspace of parameter space, then the superpositions of wavefunctions with coinciding energies are natural and these wavefunctions can form a many-dimensional basis of sections. In this many-dimensional bundle case the topological classification is different from the previous 1-dimensional case. A well-known example is Yang monopole[5, 35] with two pairs of degenerate wavefunctions defined on a sphere S^4.

Now we need to consider different symmetry classes of systems, i.e. what the additions of usual anti-unitary symmetries change in this picture. These symmetries impose restrictions on bundles and may change the topological properties. More precisely, symmetries change the way the fibers can be glued over overlapping patches. Also, in the many-level case when K-theory discussed below can be applied, the indices of K-groups that are classifying the topological phases change upon addition of symmetries.

1.2.3. CHARACTERISTIC CLASSES

The next thing to consider is how to establish topological equivalence or difference of bundles thus classifying topological phases over a given parameter space. The strategy is same as for spaces: introduce possible invariants that do not change upon topologically equivalent mappings and assume different values for different bundles. A convenient candidate for bundles is characteristic classes: certain elements of the cohomology group of the base associated with the bundle.

Since all the spaces in physics are assumed to be smooth (at least if there is no special reason for exception), we will focus on the case of smooth manifolds and differential-geometric approach in the rest of this subsection. Then the notion of a tangent vector, differentiation with respect to it and integration is defined. Then the elements of cohomology groups are classes of differential forms. The characteristic class becomes a certain differential form, an integral of this differential form over a compact space is an integer invariant, e.g. a Chern number for complex bundles. In order to obtain the explicit expressions for characteristic classes we need to review some standard notions of differential geometry.

Let us recall the differential operator acting on a tensor that results in a tensor is a covariant derivative. In the language of linear vector or tensor bundles it is called a connection: a map from sections to sections. We introduce a local basis of sections $\{e_\alpha\}$. Using this basis we write the derivative of a section vector field $\psi = \psi^\alpha e_\alpha$ with respect to a tangent vector X^i as

$$\nabla_X \psi = X^i \left(\frac{\partial \psi^\beta}{\partial x^i} dx^\beta + \omega^\beta_{i,\alpha} \psi^\alpha \right) e_\beta \tag{1.2}$$

The coefficients ω are given by the derivatives of the basis vectors $\{e_\gamma\}$ of the sections $\nabla e_\alpha = \omega^\beta_\alpha e_\beta$, so $\omega^\beta_\alpha = \omega^\beta_{i,\alpha} dx^i$ is a differential 1-form, it is called connection form. Everywhere summation over repeated indices is implied. In general the object $\omega^\beta_{i,\alpha}$ has 2 types of indices: Greek ones take values in the dimension of the fibers and the Latin one takes values in the dimensionality of the base, i.e. dimensionality of tangent vectors space. For example, if the bundle is 1-dimensional, then the Greek indices are trivial and we just end up with a usual connection (pseudo)vector A_i. It shows that in general gauge fields can be seen as connections in corresponding bundles. Another example is pro-

vided by general relativity where one considers a tangent bundle or tensor products of tangent bundles. Therefore, in that case all the indices take values in the dimensionality of the base and the connection is called Christoffel symbols Γ^k_{ij}. In this case connection coefficients play the role of gravity field strength. The next thing to notice is that ω is not a globally well-defined tensor since upon the change of the basis $e \to eT$

$$\omega \to T^{-1}\omega T + T^{-1}dT \tag{1.3}$$

which physically means the gauge dependence of gauge potentials A_i or possibility to change or even eliminate gravity Γ^k_{ij} in the infinitesimal volume by choosing a corresponding frame. An operator

$$F = \nabla^2 = d\omega + \omega \wedge \omega \tag{1.4}$$

is however a well-defined globally differential 2-form $F \to T^{-1}FT$. It corresponds to physical gauge independence of fields or coordinate frame covariance of components of the curvature tensor in the examples. In general, $F = F^{\beta}_{ij,\alpha}$ has 2 indices in the fibers and 2 indices in the tangent vectors. It is proven in the literature that both ω and F are either antisymmetric or antihermitian (with respect to indices in fibers) for real and complex bundles correspondingly. For example, in the case of 1-dimensional bundle it implies that the connection A_i is purely imaginary. Using this it can be proven that F is a closed 2-form $dF = F \wedge \omega - \omega \wedge F = 0$, so it well defines de Rham cohomology classes. So, introduction of curvature form allows us to finally obtain characteristic classes in a standard way. Namely, for a complex bundle we consider the expansion in powers of the matrix elements of F of the following determinant

$$\det(1 + \frac{iF}{2\pi}) = 1 + c_1(F) + ... + c_n(F) = 1 + \mathrm{tr}\frac{iF}{2\pi} + ... + \det\frac{iF}{2\pi} \tag{1.5}$$

where n is dimensionality of the fibers. It is called total Chern class and the motivation here is to consider a determinant invariant under basis transformations in fibers that will yield a polynomial in F. The expansion coefficients $c_i(F)$ are precisely the Chern classes. Another theorem states that that these classes actually belong to cohomology group with integer coefficients instead of real numbers $c_i(F) \in H^{2i}(B, Z)$. It comes from the specifics of the topology of Grassmann manifolds (we will not go into details here). It is a main result of this construction: we have obtained cohomology classes that will take only integer values, Chern numbers. The way to obtain Chern numbers is to consider products of Chern classes (as differential forms) that the resulting rank will match the dimensionality of the base and than integrate over a base. Therefore, a complex vector bundle over an m-dimensional base space can have at most $k =$ (number of partitions of m) independent Chern numbers. If we restrict to compact bases then the convergence of integrals will be guaranteed.

For real bundles we consider the expansion of a slightly different determinant

$$\det(1 + \frac{F}{2\pi}) = 1 + p_1(F) + ... + p_n(F) = 1 + \mathrm{tr}(\frac{F}{2\pi})^2 + ... + \det(\frac{F}{2\pi})^2 \tag{1.6}$$

which is called total Pontryagin class. The expansion coefficients $p_i(F) \in H^{4i}(B, Z)$ are called the Pontryagin classes. These are 4-forms $p_i(F) \in H^{4i}(B, Z)$ in integer coefficient

cohomology. Pontryagin numbers can be obtained in the same way as Chern numers by integrating the products of Pontryagin classes.

The last invariant that can be obtained with F in real case is Euler class

$$e(F) = \mathrm{Pf}\frac{F}{2\pi} \tag{1.7}$$

which is a n-form $e(F) \in H^n(B, Z)$. It is well defined when its sign cannot be changed by orthogonal transformations, that is in even dimensionality of the fibers $n = 2k$. For a tangent bundle integral of it over the whole base space yields Euler characteristic $\chi(B)$.

As a result, we obtain a set of topological invariants - characteristic classes of cohomology associated with a bundle. These invariants are in fact not complete: if the classes of the bundle are not all zero, then the bundle is non-trivial, but conversely non-trivial bundles with all zero classes do exist. The important practical conclusion here is that since the resulting coefficients of the cohomology groups are integer, any integral over a compact base (or compact subspace for a restriction of the bundle) will yield an integer.

The last standard type of characteristic classes are Stiefel-Whitney classes defined for real bundles $w_i \in H^i(B, Z_2)$. They are axiomatically defined by a set of axioms that are real analogues of those for Chern classes but one cannot obtain explicit differential geometric expressions for Stiefel-Whitney classes. One of the axioms for all characteristic classes is that they are stable, i.e. do not change upon taking a direct sum with a trivial bundle (except Euler class that explicitly depends on fiber dimensionality n). This property closely relates characteristic classes with K-theory discussed below.

As for anti-unitary symmetries, they may surely affect characteristic classes, for example by changing the space to which F will belong. An example discussed in literature[36] concerns the bundle initially without symmetries over 2-dimensional base after imposition of an additional time-reversal symmetry. This is then a model for a time reversal-invariant topological insulator. As a result, it changes the invariant from the integer Chern number to the Chern number defined modulo 2. In general, there are relations between different types of characteristic classes when they are mapped onto each other upon complexification of the bundle or conversely forgetting the complex structure, or cohomology coefficients mapping[30]. For example, forgetting the complex structure of the bundle $\xi_C \to \xi$ gives

$$(-1)^i c_{2i}(\xi_C) = p_i(\xi) \tag{1.8}$$

we will not discuss those theorems in detail here.

1.2.4. CLASSIFYING BUNDLES AND K-THEORY

Now we discuss some approaches that were developed to classify bundles, i.e. topological phases, completely, which is in general a formidable task. Characteristic classes are useful for this purpose in lowest dimensions: for a good base space the complex bundles are precisely classified by the first Chern class and real bundles are classified by a first Stiefel-Whitney class

$$\mathrm{Vect}^1_C(B) \overset{c_1}{\simeq} H^2(B, Z), \quad \mathrm{Vect}^1_R(B) \overset{w_1}{\simeq} H^1(B, Z_2) \tag{1.9}$$

For example, there are Z 1-dimensional complex bundles over S^2 and over torus T^2; and Z_2 real 1-dimensional bundles over S^1 discussed above. In general, the way to clas-

1

r \n	1	2	3	4	5	6
1	Z	Z	Z	Z	Z	Z
2	0	0	0	0	0	0
3	0	Z	Z	Z	Z	Z
4	0	Z_2	0	0	0	0
5	0	Z_2	Z	Z	Z	Z
6	0	Z_{12}	Z_6	0	0	0
7	0	Z_2	0	Z	Z	Z
8	0	Z_2	Z_{12}	Z_{24}	0	0
9	0	Z_3	Z_3	Z_2	Z	Z
10	0	Z_{15}	Z_{30}	$Z_{120} \bigoplus Z_2$	Z_{120}	0

Table 1.2: Table of the first homotopy groups $\pi_r(U(n))$, taken from Ref.[37]

sify bundles is to consider how the fibers are glued along all the overlaps of patches, which in principle can be achieved by considering the corresponding homotopy classes of mappings of the subspaces along which the gluing takes place into the gluing group allowed by the symmetry that glues fibers. For example, the $n-$dimensional complex bundles without additional restricting symmetries over a sphere S^{r+1} will be classified by $\pi_r(U(n))$ as discussed above. Some results are presented in Table1.2. In this Table we see a regular pattern above the diagonal $r = 2n$. This regular pattern corresponds to the usual topological periodic table[33] in the complex case. This is a domain of applicability of K-theory that assigns a set of abelian groups $K^q(B)$ to a space B that have this regular pattern. Below this diagonal the classification is complicated which indicates interesting topological properties.

An alternative equivalent approach is based on a theorem that states that the real or complex bundles without additional symmetries can be classified by the homotopy classes of maps of the base space into a certain classifying space called real or complex Grassmannian $\text{Vect}^n(B) = [B, G_n^\infty]$. A complex Grassmannian $G_n^\infty(C)$ is a space of all $n-$dimensional linear subspaces in infinite-dimensional complex space C^∞. This definition somehow clarifies the statement of the theorem: the image of any point in B is a linear subspace associated with fiber space and infinite dimensionality allows to orient these subspaces totally freely for gluing.

In general, computation and analysis of these homotopy classes is very complex. It turns out that if we do not restrict the dimensionality of the fibers then the computation is much simpler. It corresponds to the many-band case (compared to the dimensionality of the base e.g. see the condition $r > 2n$ in Table1.2, exact conditions are discussed below). It results in the usual topological periodic table classification[33]. This is the subject of the topological K-theory[32]. We note that the same classification was developed with the analysis of the topology of the Q-field of the non-linear sigma model for disor-

dered systems[33]. Releasing the fiber dimensionality we define a zeroth reduced complex K-group $\tilde{K}^0(B) = [B, G_\infty^\infty(C)]$. In the real case one has to take a real Grassmannian and the corresponding groups are denoted as $\widetilde{KO}^0(B)$. These are groups of classes of vector bundles with a group operation being a direct sum. Dimensionality unrestricted classes are defined by the following equivalence relation: two bundles are called stably equivalent $\xi \sim \eta$ iff the augmentation of one $\xi \bigoplus 0^m$ is isomorphic in a standard way to the augmentation of the other $\eta \bigoplus 0^n$, where $0^m, 0^n$ are trivial $m-$ and $n-$dimensional bundles, possibly $m \neq n$. For example, if $B = S^2$ the 1-dimensional stably equivalent classes of real bundles over a circumference S^1 are classified by $\widetilde{KO}^0(S^1) = Z_2$ and these elements are the Mobius bundle and a trivial bundle discussed above.

Another useful notion[30] is unreduced K-group. It deals with a different equivalence relation of bundles: in the stable equivalence described above we now require $m = n$, this is called stable isomorphism. The resulting classes with an operation of direct sum form a semigroup: inverse elements are not defined. In order to make it into a group one formally introduces virtual bundles as classes of formal differences $[\xi - \eta] \sim [a - b]$ iff $\xi \bigoplus b \bigoplus 0^m$ is isomorphic to $a \bigoplus \eta \bigoplus 0^m$ for some m. The resulting group does not literally consist of classes of bundles but still can be used in classification. Example: for a base space being one point a bundle is just a projection of a vector space into a point. In the stably equivalent case $\tilde{K}^0(\text{pt}) = 0$ because augmentation of any dimensional linear space leads to equivalent element of the group. In the case of virtual stably isomorphic classes $K^0(\text{pt}) = Z$ because two elements are equivalent only if they are augmented by the same dimensional vector space, and the elements $k \in Z$ are precisely the dimensionalities of the virtual bundles, that can be negative. For compact B the unreduced complex zeroth K-groups are also given by the homotopy classes but the classifying space is different $K^0(B) = [B, Z \times G_\infty^\infty(C)]$ and analogous for real case. There is a general relation $K^0(B) = [B, Z] \bigoplus \tilde{K}^0(B)$ and same relation holds for real case.

Then the case when additional anti-unitary symmetries are present one can use K-groups with a general index q. For a compact B one can define $K^{p-q}(B) = [B, Grad_C^{p-q}]$ and $KO^{p-q}(B) = [B, Grad_R^{p-q}]$ where $Grad_{R,C}^{p-q}$ are classifying spaces[38] strongly related to Clifford algebras, which in turn are strongly related to anti-unitary symmetries in condensed matter. More precisely, index $p - q$ is directly related to the number and type of symmetries[32]. Classification of Hamiltonians up to augmentation by an arbitrary number of trivial bands was reduced by Kitaev to the problem of computation of unreduced K-groups (it was shown that spaces of Hamiltonians are homotopy equivalent to classifying spaces). For example, in consistency with definitions above $Grad_C^0 = G_\infty^\infty(C) \times Z$, $Grad_R^0 = G_\infty^\infty(C) \times Z$ and $Grad_R^{-4} = G_\infty^\infty(\text{H}) \times Z$, H being quaternion algebra. Considering a base space being just a point, we can easily obtain $K^0(\text{pt}) = K^{-4}(\text{pt}) = Z$ as just numbers of connected components of corresponding classifying spaces. Same in the complex case $K^0(\text{pt}) = Z$. These are precisely the Z entries in the topological periodic table. Two other nontrivial entries in the table are provided by the real case classifying spaces $Grad_R^{-1} = \lim_{s\to+\infty} O(s)$ and $Grad_R^{-2} = \lim_{s\to+\infty} O(2s)/U(s)$. Since these spaces consist of two connected components, $[\text{pt}, Grad_R^{-2}] = \pi_0(O(2s)/U(s))|_{s\to+\infty} = Z_2 = \pi_0(O(2s))|_{s\to+\infty} = [\text{pt}, Grad_R^{-1}]$ these yield Z_2 entries in the periodic table. The other classifying spaces only have one connected component, so they yield trivial entries in the periodic table.

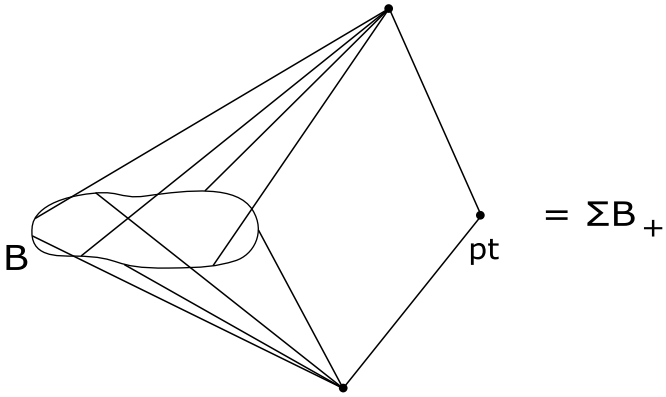

Figure 1.3: An illustration for a suspension construction over a space B_+. Starting with space B one has to make a disjoint unit with a point $B_+ = B \sqcup \text{pt}$. Then one constructs two cones over B_+. Formally one has to take a product with a closed interval $B_+ \times [0;1]$ and factor the spaces at the ends of the interval 0 and 1 into points.

On the other hand, the classification of stably equivalent bundles is given by the reduced K-groups $\tilde{K}^0$, $\widetilde{KO}^0$. In the case of arbitrary negative index $q < 0$ they can be defined topologically as $\tilde{K}^{-q}(B) = \tilde{K}(\Sigma^q B)$ and similarly for real case, where Σ is an operation of suspension resulting in a new topological space. Suspension is defined as construction of two cones over a space, see Fig.1.3. For example, $\Sigma S^n = S^{n+1}$.

The main result of K-theory is Bott periodicity: all the classifying spaces and all the resulting groups are periodic in index with period 8 and 2 in real and complex cases. This also allows to extend the definitions of K-groups above to arbitrary integer q. We note that this periodicity can in a certain sense be understood as geometric periodicity in dimensionality of the base (see definition of K-groups with suspension construction discussed above). For spheres exactly the same sequence of groups as in the periodic table is obtained since $K^{-q}(\text{pt}) = \tilde{K}^{-q}(\text{pt}_+) = \tilde{K}(\Sigma^q S^0) = \tilde{K}(S^q)$. For example, in the complex case the application of Bott periodicity yields $\tilde{K}(S^n) = 0$ for odd n, and $\tilde{K}(S^n) = Z$ for even n. For an arbitrary base B the relation between the two K-theoretic groups is not so transparent: $K^{-n}(B) = \tilde{K}(\Sigma^n B_+)$, where $B_+ = B \sqcup \text{pt}$ a disjoint union of B and a point.

So as we see, with the K-theoretic approach one classifies bundles only up to augmentation by an arbitrary number of trivial bands. This means that formally this classification applies to many-band case only ($2n > r - 1$ for complex case and $n > r$ for real case where r is the dimensionality of the base space), whereas the toy models like Kitaev model discussed below illustrating topological properties are usually low-dimensional. For real case the Z invariants present in the periodic table can be captured by Pontryagin classes, but Z_2 invariants are generally not captured by Stiefel-Whitney classes except lowest dimensions[30] despite naive expectation.

We stress that even in the dimensionality unrestricted case for arbitrary base B there can be different K-groups and therefore different classification than in the periodic table (an example being weak topological insulator[39] in the case of a torus[32] $B = T^3$). Another way outside of topological periodic table is to restrict the fiber dimensionality.

1.3. TOPOLOGY IN CONDENSED MATTER

In this section we discuss some condensed matter models in which the topological concepts discussed above play a key role.

1.3.1. WEYL SEMIMETAL

Weyl semimetals were introduced in a seminal paper[40]. Weyl semimetal is a system defined by special properties of the spectrum[41]. Namely, it is a system where topologically protected point-like band crossings are present in the $3d$ momenta space. Such systems have been reported to be realized in several compounds[42] e.g. in tantalum arsenide (TaAs)[43]. We do not consider so-called Type-II semimetals[44] with nodal lines in the spectrum. Knot theory not outlined in the introduction can be useful to describe their topological properties[6].

A generic crossing of two bands (if an effective Hamiltonian linear in deviations from the crossig point contains 3 independent parameters) will have the wavefunctions of these bands defined on the small sphere S^2 surrounding the crossing corresponding to the topological charge $q = \pm 1$ discussed above (as first Chern numbers of these two 1-dimensional complex bundles), higher singularities $|q| > 1$ are also possible. One may also consider arbitrary $2d$ smooth and periodic subspace of the $3d$ Brillouin zone outside of band crossings and restrict the gapped spectrum to this $2d$ subspace. Thus, one will obtain locally well-defined wavefunctions that, as sections of 1-dimensional bundles over this $2d$ subspace, may have nontrivial Chern numbers. Therefore, one will obtain a 2-dimensional Chern insulator[45]. Some details of the topology of $2d$ Chern insulators in the many-band case are discussed in Chapter 3.

1.3.2. TOPOLOGICAL SUPERCONDUCTOR

We consider symmetry class D in dimensionality $d = 1$ from the periodic table. The Hamiltonian has particle-hole symmetry but no time-reversal and therefore no chiral. Particle-hole symmetry affects topology as discussed above and so it is classified by Z_2 invariant. In accordance with the general statement above we claim that despite being stable this invariant cannot be captured by characteristic classes. A simple 2×2 model that has the same topological classification and the same symmetry is Kitaev model[46]. Let us consider spacially homogeneous case with periodic boundary conditions first. Then the Hamiltonian in $q-$space reads

$$H = (-2t \cos q - \mu)\tau_z + 2\Delta \sin q \tau_y \tag{1.10}$$

where the quasimomentum $q \in [-\pi, \pi]$, τ matrices act in Nambu space, superconducting gap Δ is chosen real, μ is a chemical potential and t being the nearest sites real hopping amplitude. The aforementioned Z_2 invariant distinguishing between two classes of bundles is the sign of the product of pfaffians

$$P = \mathrm{sgn}\mathrm{Pf}(iH_A(q=0))\mathrm{Pf}(iH_A(q=\pi)) \tag{1.11}$$

where H_A is an antisymmetrised form of the Hamiltonian. Using Eq.1.10, we obtain that one of the pfaffians changes sign at $\mu = 2|t|$ and the other one at $\mu = -2|t|$, these are the conditions for the topological phase transitions. The same conditions yield the gap

closing either at $q = 0$ or $q = \pi$. Diagonalization of Eq.1.10 results in two bands defined on a S^1 $q-$space. Let us fix $t > 0$. Then for $\mu \gg |t|$ the positive energy wavefunction $\psi_+ \simeq \begin{pmatrix} 0 \\ 1 \end{pmatrix}$, and exactly equal for $q = 0$ and $q = \pi$. It is topologically equivalent to a trivial constant wavefunction. In the topological regime it cannot be tuned to a trivial wavefunction since at $q = \pi$ it is pinned as $\psi_+ \propto \begin{pmatrix} 1 \\ 0 \end{pmatrix}$ and for $q = 0$ the asymptotic does not change. This change happens after closing the gap at $q = \pi$ upon decreasing $\mu < 2t$ but keeping $\mu > -2t$. In general, there are no nontrivial complex bundles over S^1 because $H^2(S^1, Z) = 0$ but class D with additional symmetry is described by real K-theory. If we associate the wavefunction $\begin{pmatrix} 0 \\ 1 \end{pmatrix}$ with a positive Jacobian in the Mobius bundle described above and the wavefunction $\begin{pmatrix} 1 \\ 0 \end{pmatrix}$ with a negative one, all possible choices of these wavefunctions at $q = 0$ and $q = \pi$ result in the same classification options as the real bundles over S^1: Mobius and trivial cylinder.

1.4. SUPERCONDUCTING NANOSTRUCTURES

In this section we consider topology of other model examples, namely heterostructures. The initial idea of this approach is to realize topological materials without actually fabricating them. One of the first proposals was to realize a 2-dimensional topological superconductor placing films of the trivial superconductors on top of the topological insulator[47]. Other proposals focus on realizing Kitaev model[46] or a topologically equivalent model being an example of 1-dimensional $p-$wave pairing superconductor. The reason being boundary Majorana modes, potentially useful for topological quantum computation[48, 49] due to topological protection[7, 50], forming at the ends of the wire in the topological regime. Majorana bound states form one fermionic state that can be either filled or empty leading to degenerate ground state - another peculiarity of the model. In the finite system in the topological regime Majoranas are not exactly at zero energy but the splitting $\sim e^{-L/\xi}$ is exponentially small in the system size L, where ξ is Majorana localization length. Realization of Weyl fermion physics with multi-terminal superconducting nanostructures is also thinkable (see recent proposal[23]). In the latter proposal the dimensionality of parameter space (superconducting phases) is not restricted by $d \leq 3$, so one could expect to have topological properties related to higher dimensionalities.

1.4.1. SPACIALLY INHOMOGENEOUS SUPERCONDUCTIVITY

Since we discuss heterotructures in this section, we need to address the spacially inhomogeneous systems in general and spacially inhomogeneous superconductivity in particular. The standard way to describe an inhomogeneous system with superconducting regions is to solve the eigen-basis problem for the BdG Hamiltonian. Let us sketch the standard derivation. We start with a BCS[51] Hamiltonian in the spacially dependent

case. For example, for point-like interaction corresponding to $s-$pairing[52]

$$H = \int d^3r \left(\sum_\sigma \psi_\sigma^\dagger H_0 \psi_\sigma + V_0 \psi_\uparrow^\dagger \psi_\downarrow^\dagger \psi_\downarrow \psi_\uparrow \right) \tag{1.12}$$

where the first term being being a normal state Hamiltonian

$$H_0 = \epsilon(-i\hbar\nabla - e\mathbf{A}) + U(\mathbf{r}) - \mathbf{E_F} + \mathbf{g}\mu_\mathbf{B}(\sigma, \mathbf{h}) + \mathbf{i}\mathbf{V}_{\mathrm{SO}}(\mathbf{r})\sigma \times \nabla \tag{1.13}$$

where $\epsilon(\mathbf{p})$ is electrons dispersion relation, $\mathbf{A}$ being external vector-potential, e is electron charge, $U(\mathbf{r})$ is external potential that may contain disorder, E_F is Fermi energy, $g\mu_B(\sigma, \mathbf{h})$ is Zeeman splitting due to external magnetic field, $V_{\mathrm{SO}}(\mathbf{r})$ is spin-orbit coupling. And the second term in Eq.1.12 being an attractive $s-$pairing electron interaction with $V_0 < 0$ interaction strength. In the weak interaction limit the 4-fermion interaction can be decoupled by the introduction of superconducting order parameter $\Delta(r)\psi_\uparrow^\dagger \psi_\downarrow^\dagger + h.c.$

$$\Delta(r) = V_0 \langle \psi_\uparrow(r) \psi_\downarrow(r) \rangle \tag{1.14}$$

In the normal regions we set $V_0 = 0$, so $\Delta(r) = 0$. Introducing an additional structure - Nambu space one can conveniently reformulate the problem to solving the eigenbasis problem for a spacially dependent BdG Hamiltonian[53]

$$H_{\mathrm{BdG}} = \begin{pmatrix} H_0 & \Delta(r) \\ \Delta^\star(r) & -H_0^T \end{pmatrix} \tag{1.15}$$

This approach allows one to describe a large variety of physical systems: nanostructures, nanowires, heterostructures with topological materials etc.

One can consider a general case[52] of position-dependent electron interaction in Eq.1.12. Then one can also obtain different types of pairing corresponding to scattering with higher orbital numbers $l > 0$. As an example of $p-$pairing corresponding to $l = 1$ one can consider a spacially inhomogeneous Kitaev chain[46]

$$H = -\sum_n \mu_n c_n^\dagger c_n - \sum_n (t_n c_{n+1}^\dagger c_n + h.c.) + \sum_n (\Delta_n c_{n+1}^\dagger c_n^\dagger + h.c.) \tag{1.16}$$

where c_n is a usual fermion annihilation operator on the $n-$th site and the parameters are the same as in Eq.1.10 but can be non-constant from site to site, e.g. $\mu = \mu_n$. Taking spacially-dependent parameters one may realize several regions of topological or non-topological regimes within the wire and, therefore, more Majorana bound states.

Another example[54] is the model that was proposed as a way to realize the topological superconductor in class D with topologically trivial materials. It consist of a semiconductor nanowire with strong spin-orbit coupling in proximity to ordinary s-wave superconductor and external magnetic field. The continuous limit BdG Hamiltonian reads

$$H_{\mathrm{BdG}} = \left(\frac{p^2}{2m} - \alpha\sigma_z p - \mu \right) \tau_z + B\sigma_x + \mathrm{Re}\Delta\tau_x - \mathrm{Im}\Delta\tau_y \tag{1.17}$$

where σ matrices act in spin space, τ matrices act in particle-hole space, p is electron momentum in a wire, m is effective mass, α is spin-orbit strength, B is external magnetic

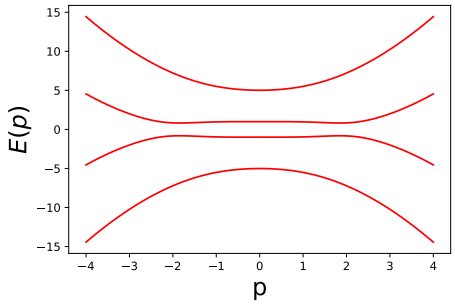

Figure 1.4: An example of the spectrum of the model Eq.1.17 in the topological regime. The parameters are $m = \alpha = 1$, $B = 3$, $\Delta = 1.5$, $\mu = -1.34$.

field and Δ is induced superconducting order parameter in the wire due to proximity effect. This model is nontrivial topologically at $|B| > \sqrt{|\Delta|^2 + \mu^2}$ and $\alpha \neq 0$.

In Chapters 3 and 4 we consider modifications of this model introducing position dependent parameters, e.g. $\mu(x)$. In order to investigate the topological properties of the model we proceed in two different ways in Chapters 3 and 4. In Chapter 4 we analyze the spectrum by explicit direct diagonalization of the discretized version of the model. In Chapter 3 we use the trick to reformulate the problem of finding the band crossings of the Hamiltonian into minimization of a certain determinant alongside with its derivative - see Chapter 4 for details.

1.4.2. SCATTERING FORMALISM

As a yet another example a suggestion was proposed[23] to realize topological materials with multi-terminal superconducting nanostructures. In the case of nanostructures the general problem Eq.1.15 can be simplified to the scattering problem. In this case the model of the nanostructure consists of a short structure off which the electrons scatter. This scatterer is connected to several (superconducting) terminals (see Figure and more details on multi-terminal nanostructures in Chapter 2). For the applicability of the scattering approach one needs a sufficiently short nanostructure and negligible inelastic processes. Within the scattering formalism[55] the scatterer is described by a single (probably energy-dependent) scattering S-matrix denoted as S. In the case of superconducting structure, the phases of superconducting terminals form a many-dimensional parameter space in which one can study topological properties of the states of the system. Therefore, one is not restricted by small dimensionality $d \leq 3$ of parameter (base) space as in the case of topological compounds.

Superconducting nanostructures may host Andreev bound states that exist due to Andreev scattering processes[56, 57] at the energies smaller than the superconducting gap in the terminals. Successive Andreev scatterings of a quasiparticle living inside of the nanostructure with the energy lower than the gap lead to a finite motion and, therefore, discrete energy levels. The condution of matching the wavefunction[55] of the quasiparticle returning to its original state after the process of two Andreev reflections off the

boundaries of the scatterer yields a condition[58]

$$\det(1 - e^{-2i\chi(E)} S e^{i\hat{\phi}} S^* e^{-i\hat{\phi}}) = 0 \tag{1.18}$$

where $\chi(E) = \arccos(E/|\Delta|)$ and $\hat{\phi}$ is a vector composed of all phases of superconducting terminals. Eq.1.18 allows to find the energies of the bound states. One can investigate the topology of the band structure of Andreev bound states in the parameter space of superconducting phases of the terminals.

We rederive Eq.1.18 in Chapter 1 within action formalism. It was shown previously that indeed one can find nontrivial topological configurations in this system[23], however the presence of the continuous spectrum above the superconducting gap in the terminals may complicate the observation, which is the main subject of Chapter 2.

1.4.3. ACTION FORMALISM

Another simplification to the general problem of Eq.1.12 can be done provided that certain subset of the degrees of freedom of the system can be averaged out. Within this approach one describes the system with an effective action[59] S_{eff} instead of a full Hamiltonian 1.15. The effective action is a functional of physically relevant degrees of freedom (e.g. superconducting phases) describing their effective dynamics, it is obtained upon integrating out the irrelevant degrees of freedom (e.g. electron dynamics in reservoirs). The response functions of the system and quantum correlators of the relevant degrees of freedom can be derived from this action. The equation for minimization of the action is usually a semiclassical equation of motion for a Green's function. For example, a saddle point equation for a sigma-model action in replica formalism[60]

$$S_{\text{eff}}[Q] = \frac{\pi\nu}{8} \int d\mathbf{r} \text{Tr}[D(\nabla Q)^2 - 4\hat{G}Q] \tag{1.19}$$

where ν is electron density of states, D is diffusion coefficient and $\hat{G} = \begin{pmatrix} \epsilon_n & \Delta \\ \Delta^* & -\epsilon_n \end{pmatrix}_N$ is a matrix in Nambu space and Matsubara frequency ϵ_n space. This action defines a nonlinear field theory for a matrix field $Q^2 = 1$ describing diffusive superconductors. On the saddle point level the matrix Q is a semiclassical Green's function and minimization of the action yields Usadel equation[61]

$$D\nabla(Q\nabla Q) + [\hat{G}, Q] = 0 \tag{1.20}$$

In this example what is integrated out are ballistic scales much larger than inverse mean free time $\epsilon \gtrsim \tau^{-1}$ leaving effective diffusive degrees of freedom.

Another example is an action for a Josephson contact, in this case the effective degrees of freedom is a terminals superconducting phase difference ϕ and the fast electrons degrees of freedom responsible for dissipation are integrated out[62, 63]. In imaginary time $\tau \in [0, \beta]$

$$S_{\text{eff}}[\phi] = \int_0^\beta d\tau \frac{C}{2} \left(\frac{1}{2e}\frac{\partial\phi}{\partial\tau}\right)^2 - \int_0^\beta d\tau \int_0^\beta d\tau' (\alpha(\tau - \tau') \cos\frac{\phi(\tau) - \phi(\tau')}{2} -$$
$$- \beta(\tau - \tau') \cos\frac{\phi(\tau) + \phi(\tau')}{2}) \tag{1.21}$$

where C is geometric capacitance and kernels $\alpha(\tau)$, $\beta(\tau)$ are obtained with electrons Green's functions in the leads and junction tunneling amplitude.

This consideration was generalized to the action for a multi-terminal contact in real-time Keldysh formalism[64]:

$$S_{\text{eff}}[\phi] = \text{Tr}\log\left(\frac{1-\hat{g}}{2} + \frac{1+\hat{g}}{2} S \frac{1+\hat{g}}{2}\right) \tag{1.22}$$

where phases $\hat{\phi}$ can be ascribed to the normalized analytic continuation of $\hat{G}$ Green's functions of the terminals $\hat{g}^2 = 1$ or to the S-matrix describing the scatterer. We rederive the action 1.22 in imaginary time formalism in Chapter 1.

1.5. STRUCTURE OF THE THESIS

1.5.1. CHAPTER 2

In this Chapter, we investigate how the continuous spectrum that is intrinsically present in all physical systems, affects topological properties. For this we consider a model of the nanostructure within scattering formalism. We derive the imaginary time action and the current response function. This allow to introduce a re-definition of Berry curvature for a system with a continuous spectrum present.

As a result, we have found that the re-defined Berry curvature for a nanostructure may have a non-topological phase-independent contribution that may add a non-quantized part to the transconductances. This additional contribution vanishes in the case of a time-reversible scattering matrix. Also, we have found convenient expressions for the re-defined Berry curvature in the cases of weak energy dependence of the scattering matrix. In the cases of spin-orbit coupling absent and present, we have investigated the vicinity of Weyl singularities in the spectrum.

1.5.2. CHAPTER 3

In this Chapter, we address the general definition and values of topological numbers of superpositions of the topologically distinct bands. This problem is simple in essence, but one can formulate it as a paradox: quantum superposition naively implies non-integer Chern numbers which should be prohibited by general topology.

First, we investigate superpositions created dynamically and ones created by a stationary mixing. We find that the results are different in these two cases. In the case of dynamical superpositions, we have found that there is an observable that does not exhibit topological properties in general but is topological for eigenstates of the Hamiltonian. In the case of static superpositions, as expected from the general topology, the resulting bands retain integer Chern numbers. We illustrate the restoration of the quantization of Chern number upon avoided crossing of topologically different bands. The unavoided band crossings may result in the exchange of Chern numbers between the bands upon changing the parameters of the Hamiltonian. This is a topological phase transition. We investigate complicated phase diagrams arising in this context. We show that the triple critical points are generally absent and that quadruple critical points are common features. This distinguishes the topological phase diagrams from the common

phase diagrams. We investigate an example of a bilayer Haldane model to illustrate these features.

1.5.3. CHAPTER 4

In this Chapter we propose a novel scheme to perform all unitary operations on Majorana modes in 1D. The scheme is based on using the geometry of the device, but rather a resonant manipulation involving the first excited state at the superconducting gap that overlaps well with all the localized states. The detection of the filling of the excited state also allows to achieve initialization and read-out. We illustrate the scheme in detail with a concrete device.

1.5.4. CHAPTER 5

In this Chapter we investigate topological properties of multi-terminal superconductor-semiconductor wires. We focus on the possibility to realize an additional to Majorana fermions topological feature, namely Weyl singularities in the spectrum. As a result, we find an abundance of Weyl points for devices with intermediate size of the electrodes (size being comparable with a typical Andreev bound states localization length). We investigate the properties of these and the ways the Weyl points emerge and disappear upon change of the parameters of the model.

REFERENCES

[1] M. Z. Hasan and C. L. Kane, *Colloquium: Topological insulators,* Rev. Mod. Phys. **82**, 3045 (2010).

[2] X.-L. Qi and S.-C. Zhang, *Topological insulators and superconductors,* Rev. Mod. Phys. **83**, 1057 (2011).

[3] M. S. Foster, H.-Y. Xie, and Y.-Z. Chou, *Topological protection, disorder, and interactions: Survival at the surface of three-dimensional topological superconductors,* Phys. Rev. B **89**, 155140 (2014).

[4] F. Schindler, A. M. Cook, M. G. Vergniory, and et. al, *Higher-order topological insulators,* Science Advances **4**, eaat0346 (2018).

[5] E. Demler and S.-C. Zhang, *Non-abelian holonomy of bcs and sdw quasiparticles,* Annals of Physics **271**, 83 (1999).

[6] B. Lian and S.-C. Zhang, *Weyl semimetal and topological phase transition in five dimensions,* Phys. Rev. B **95**, 235106 (2017).

[7] A. Y. Kitaev, *Fault-tolerant quantum computation by anyons,* Annals of Physics **303** (2002), 10.1016/S0003-4916(02)00018-0.

[8] S. M. Albrecht, A. P. Higginbotham, and et.al., *Exponential protection of zero modes in majorana islands,* Nature **531**, 206 (2016).

[9] M. T. Deng, S. Vaitiekenas, and et.al., *Majorana bound state in a coupled quantum-dot hybrid-nanowire system,* Science **354**, 1557 (2016).

[10] M. T. Deng, C. L. Yu, and et.al., *Anomalous zero-bias conductance peak in a nb–insb nanowire–nb hybrid device,* Nano Lett. **12**, 6414 (2012).

[11] J. Chen, P. Yu, and et.al., *Experimental phase diagram of zero-bias conductance peaks in superconductor/semiconductor nanowire devices,* Sci. Adv. **3**, e1701476 (2017).

[12] S.-Y. Xu, N. Alidoust, and et.al., *Discovery of lorentz-violating type ii weyl fermions in laalge,* Sci. Adv. **3**, e1603266 (2017).

[13] A. A. Zyuzin and A. A. Burkov, *Topological response in weyl semimetals and the chiral anomaly,* Phys. Rev. B **86**, 115133 (2012).

[14] C. L. Kane and E. J. Mele, *Z_2 topological order and the quantum spin hall effect,* Phys. Rev. Lett. **95**, 146802 (2005).

[15] G. Moore and N. Read, *Nonabelions in the fractional quantum hall effect,* Nuc. Phys. B **360**, 362 (1991).

[16] M. A. Nielsen and I. L. Chuang, *Quantum Computation and Quantum Information* (Cambridge University Press, 2000).

[17] J. Koch, T. M. Yu, J. Gambetta, A. A. Houck, D. I. Schuster, J. Majer, A. Blais, M. H. Devoret, S. M. Girvin, and R. J. Schoelkopf, *Charge-insensitive qubit design derived from the cooper pair box,* Phys. Rev. A **76**, 042319 (2007).

[18] D. Loss and D. P. DiVincenzo, *Quantum computation with quantum dots,* Phys. Rev. A **57**, 120 (1998).

[19] F. Arute, K. Arya, R. Babbush, and et. al., *Quantum supremacy using a programmable superconducting processor,* Nature **574** (2019), https://doi.org/10.1038/s41586-019-1666-5.

[20] C. Palacios-Berraquero, M. Houzet, L. Mueck, and D. M. Persaud, *Instead of 'supremacy' use 'quantum advantage',* Nature **576**, 213 (2019).

[21] Y.-L. Chen, J. G. Analytis, J.-H. Chu, and et. al, *Experimental realization of a three-dimensional topological insulator, bi_2te_3,* Science **325** (2009), 10.1126/science.1173034.

[22] K. Kuroda, M. Arita, K. Miyamoto, M. Ye, J. Jiang, A. Kimura, E. E. Krasovskii, E. V. Chulkov, H. Iwasawa, T. Okuda, K. Shimada, Y. Ueda, H. Namatame, and M. Taniguchi, *Hexagonally deformed fermi surface of the 3d topological insulator* bi_2se_3, Phys. Rev. Lett. **105**, 076802 (2010).

[23] R.-P. Riwar, M. Houzet, J. S. Meyer, and Y. V. Nazarov, *Multi-terminal josephson junctions as topological matter,* Nature Communications **7**, 11167 EP (2016).

[24] M. König, S. Wiedmann, C. Brüne, and et. al, *Quantum spin hall insulator state in hgte quantum wells,* Science **318**, 766 (2007).

[25] G. Deleuze and F. Guattari, *A Thousand Plateaus: Capitalism and Schizophrenia* (University of Minnesota Press, 1980).

[26] J. Baudrillard, *Simulacra and Simulations: I. The Precession of Simulacra* (1981).

[27] V. V. Prasolov and A. B. Sossinsky, *Knots, Links, Braids and 3-Manifolds: An Introduction to the New Invariants in Low-dimensional Topology* (American Mathematical Soc., 1997).

[28] E. Witten, *Global aspects of current algebra,* Nuclear Physics B **223**, 422 (1983).

[29] A. Fomenko and D. Fuchs, *A course in homotopy topology* (Moscow, Nauka, 1989).

[30] A. Hatcher, *Vector Bundles and K-Theory* (2003).

[31] M. Nakahara, *Geometry, topology and physics* (Institute of Physics Publishing, Bristol and Philadelphia, 2003).

[32] A. Kitaev, *Periodic table for topological insulators and superconductors,* Advances in Theoretical Physics: Landau Memorial Conference. AIP Conference Proceedings **1134**, 22 (2009).

[33] S. Ryu, A. P. Schnyder, A. Furusaki, and A. W. W. Ludwig, *Topological insulators and superconductors: tenfold way and dimensional hierarchy,* New Journal of Physics **12** (2010).

[34] V. P. Mineev, *Topologically Stable Defects and Solitons in Ordered Media* (CRC Press, 1998).

[35] C. N. Yang, *Generalization of dirac's monopole to su2 gauge fields,* Journal of Mathematical Physics **19**, 320 (1978).

[36] B. A. Bernevig and T. L. Hughes, *Topological Insulators and Topological Superconductors* (Princeton University Press, 2013).

[37] T. Püttmann and A. Rigas, *Presentations of the first homotopy groups of the unitary groups,* Comment. Math. Helv. **78**, 648 (2003).

[38] M. Karoubi, *K-Theory* (Springer-Verlag Berlin Heidelberg, 1978).

[39] L. Fu, C. L. Kane, and E. J. Mele, *Topological insulators in three dimensions,* Phys. Rev. Lett. **98**, 106803 (2007).

[40] X. Wan, A. M. Turner, A. Vishwanath, and S. Y. Savrasov, *Topological semimetal and fermi-arc surface states in the electronic structure of pyrochlore iridates,* Phys. Rev. B **83**, 205101 (2011).

[41] S. Jia, S. Xu, and M. Hasan, *Weyl semimetals, fermi arcs and chiral anomalies,* Nature Materials **15**, 1140–114 (2016).

[42] L. Lu, Z. Wang, D. Ye, L. Ran, L. Fu, J. D. Joannopoulos, and M. Soljačić, *Experimental observation of weyl points,* Science **349**, 622 (2015).

[43] S.-Y. Xu, I. Belopolski, N. Alidoust, and et. al, *Discovery of a weyl fermion semimetal and topological fermi arcs,* Science **349**, 613 (2015).

[44] A. Soluyanov, D. Gresch, Z. Wang, and et. al., *Type-ii weyl semimetals,* Nature **527**, 495–498 (2015).

[45] F. D. M. Haldane, *Model for a quantum hall effect without landau levels: Condensed-matter realization of the "parity anomaly",* Phys. Rev. Lett. **61**, 2015 (1988).

[46] A. Y. Kitaev, *Unpaired majorana fermions in quantum wires,* Physics-Uspekhi **44** (2001), 10.1070/1063-7869/44/10S/S29.

[47] L. Fu and C. L. Kane, *Superconducting proximity effect and majorana fermions at the surface of a topological insulator,* Phys. Rev. Lett. **100**, 096407 (2008).

[48] D. P. DiVincenzo and P. W. Shor, *Fault-tolerant error correction with efficient quantum codes,* Phys. Rev. Lett. **77**, 3260 (2996).

[49] P. W. Shor, *Algorithms for quantum computation: Discrete logarithms and factoring,* Symposium on Foundations of Computer Science (1994).

[50] C. Nayak, S. H. Simon, A. Stern, M. Freedman, and S. Das Sarma, *Non-abelian anyons and topological quantum computation,* Rev. Mod. Phys. **80**, 1083 (2008).

[51] J. Bardeen, L. N. Cooper, and J. R. Schrieffer, *Microscopic theory of superconductivity,* Phys. Rev. **106**, 162 (1957).

[52] V. P. Mineev and K. V. Samokhin, *Introduction to unconventional superconductivity* (Gordon and Breach Science Publishers, 1999).

[53] P. G. D. Gennes, *Superconductivity ofMetals and Alloys* (CRC Press, 2018).

[54] R. M. Lutchyn, J. D. Sau, and S. Das Sarma, *Majorana fermions and a topological phase transition in semiconductor-superconductor heterostructures,* Phys. Rev. Lett. **105**, 077001 (2010).

[55] Y. Nazarov and Y. Blanter, *Quantum Transport* (Cambridge University Press, 2009).

[56] A. A. F., *The thermal conductivity of the intermediate state in superconductors,* Sov. Phys. JETP **19**, 1228 (1964).

[57] G. E. Blonder, M. Tinkham, and T. M. Klapwijk, *Transition from metallic to tunneling regimes in superconducting microconstrictions: Excess current, charge imbalance, and supercurrent conversion,* Phys. Rev. B **25**, 4515 (1982).

[58] C. W. J. Beenakker, *Universal limit of critical-current fluctuations in mesoscopic josephson junctions,* Phys. Rev. Lett. **67** (1991), 10.1103/PhysRevLett.67.3836.

[59] P. M. E. and D. V. Schroeder, *An Introduction To Quantum Field Theory* (Avalon Publishing, 1995).

[60] D. Belitz and T. R. Kirkpatrick, *The anderson-mott transition,* Rev. Mod. Phys. **66**, 261 (1994).

[61] K. D. Usadel, *Generalized diffusion equation for superconducting alloys,* Phys. Rev. Lett. **25**, 507 (1970).

[62] V. Ambegaokar, U. Eckern, and G. Schön, *Quantum dynamics of tunneling between superconductors,* Phys. Rev. Lett. **48**, 1745 (1982).

[63] G. Schön and A. Zaikin, *Quantum coherent effects, phase transitions, and the dissipative dynamics of ultra small tunnel junctions,* Physics Reports **198**, 237 (1990).

[64] Y. V. Nazarov, *Block-determinant formalism for an action of a multi-terminal scatterer,* Physica E: Low-dimensional Systems and Nanostructures **74**, 561 (2015).

2

TOPOLOGICAL PROPERTIES OF MULTITERMINAL SUPERCONDUCTING NANOSTRUCTURES: EFFECT OF A CONTINUOUS SPECTRUM

Recently, it has been shown that multi-terminal superconducting nanostructures may possess topological properties that involve Berry curvatures in the parametric space of the superconducting phases of the terminals, and associated Chern numbers that are manifested in quantized transconductances of the nanostructure. In this Article, we investigate how the continuous spectrum that is intrinsically present in superconductors, affects these properties. We model the nanostructure within scattering formalism deriving the action and the response function that permits a re-definition of Berry curvature for continuous spectrum.

We have found that the re-defined Berry curvature may have a non-topological phase-independent contribution that adds a non-quantized part to the transconductances. This contribution vanishes for a time-reversible scattering matrix. We have found compact expressions for the redefined Berry curvature for the cases of weak energy dependence of the scattering matrix and investigated the vicinity of Weyl singularities in the spectrum.

Phys. Rev. B **99**, 165414 (2019), this publication was done jointly with Y.Chen, it is also to be used in his thesis; http://doi.org/10.5281/zenodo.4376665

2.1. INTRODUCTION

The study of topological materials has been on the front edge of the modern research in condensed matter physics for the past decade [1–5]. These materials are appealing from fundamental point of view and for possible applications (TI-based Photodetector[6, 7], spintronics[8], field-effect transistor[9], catalyst[10] and quantum computing[11, 12]). The basis for applications is the topological protection of quantum states, which makes the states robust against small perturbations and leads to many unusual phenomena, e.g. topologically protected edge states[13–15]. The topological superconductors[16–19] and Chern insulators[20–23] are the classes of topological materials that are relevant for the present Chapter. In the case of the Chern insulator the topological characteristic is an integer Chern number[24, 25] computed with the Green's function of electrons occupying the bands in a Brillouin zone of a material - WZW form[26–29]. The first Chern number reduces to the sum of first Chern numbers of the filled bands. For each band, the first Chern number is defined as an integral of the Berry curvature over the Brillouin zone[30, 31]. The Berry curvature is commonly defined[32] as $B_{\alpha\beta} = 2\mathrm{Im}\langle\partial_\alpha k|\partial_\beta k\rangle$ with $|k\rangle$ being the wavefunction in this band and α, β being the parameters: in this case two components of a wavevector. If the Chern number of a crystal is not zero, the edge states necessarily appear at the interface between the crystal and the vacuum (since the Chern number of the vacuum is zero). The dimensionality of topological materials in real space is restricted by three from above, which significantly limits possible topological phases.

However, there is a way to circumvent this fundamental limitation. Recently, the multi-terminal superconducting nanostructures with conventional superconductors were proposed to realize the topological solids in higher dimensions[33]. Such nanostructures host discrete spectrum of so called Andreev bound states[34–36]. The energies and wavefunctions of these states depend periodically on the phases of superconducting terminals. This sets an analogy with a bandstructure that depends periodically on the wavevectors. The dimensionality of this bandstructure is the number of terminals minus one. Also, as it was noted[33], the multi-terminal superconducting nanostructures cannot be classified as the high-dimensional topological superconductors from the standard periodic table of topological phases[37]. The authors of [33] have considered in detail 4-terminal superconducting nanostructures and proved the existence of Weyl singularities[38, 39] in the spectrum. The Weyl singularity is manifested as level crossing of Andreev bound states at a certain point in 3-dimensional phase space. Each Weyl singularity can be regarded as a point-like source of Berry curvature. Owing to this, a nonzero two-dimensional Chern number can be realized and is manifested as a quantized transconductance of the nanostructure. This transconductance is the response of the current in one of the terminals on the voltage applied to the other terminal in the limit of small voltage, this signifies an adiabatic regime.

The peculiarity of the system under consideration is the presence of a continuous spectrum next to the discrete one. These states are the extended states in the terminals with energies above the superconducting gap. Were a spectrum discrete, the adiabaticity condition would imply the level spacing being much larger than the driving frequency. The level-spacing is zero for a continuous spectrum, so this complicates the adiabaticity conditions. This has been pointed out already in Ref.[33] but was not investigated in detail. We note the generality of the situation: a generic gapped system might have

a continuous spectrum above the certain threshold, and the adiabaticity condition required for the manifestations of topology needs to be revisited in this situation.

The aim of the present article is to investigate this question in detail for a generic model of a superconducting nanostructure. We have studied the linear response of currents on the changes of superconducting phases in the terminals. We model a multi-terminal superconducting nanostructure within the scattering approach[40]. In this approach the terminals of the nanostructure are described with semiclassical Green's functions and the scatterer coupled to the terminals is described by a unitary (in real time) S-matrix. Although it is not crucial, we made use of Matsubara formalism which conveniently allows us to concentrate on the ground state of the system and the limit of zero temperature is formally achieved by considering continuous Matsubara frequencies. So we do the calculations in imaginary time formalism[41]. At the first step, we obtain the general effective action describing the nanostructure in terms of the S-matrix and time-dependent semiclassical Green's functions of the terminals. At the second step, we expand the action to the second power in time-dependent phases of the terminals. At the third step, we concentrate on the limit of small voltage and driving frequency, to obtain the response function relevant for topological properties.

We can use the properly anti-symmetrized response function as a generalized definition of the Berry curvature that is suitable for the systems with and without a continuous spectrum. The main result of the present Chapter is that so-defined Berry curvature is contributed to by a continuous spectrum as well as discrete one even in the case of energy-independent S-matrix. We derive an explicit formula for it. This solves the paradox mentioned in [33]: the Berry curvature associated with discrete Andreev bands is discontinuous when the highest Andreev bound state merges with the continuum, which indicates that the integral of the Berry curvature defined only for discrete spectrum will not reduce to an integer. The redefined Berry curvature that we find is continuous. It gives rise to integer Chern numbers if the S-matrix is time-reversible. If it does not we reveal a specific additional non-topological contribution that does not depend on the superconducting phases. We note the the importance of the energy scales much larger than superconducting gap $|\Delta|$ in this context. This is why we also discuss in detail the case of an energy-dependent S-matrix the energy scale of variation of which may be in any relation with superconducting gap. We find that the non-topological contribution depends on the regularization of the S-matirx at large energies. In particular, it vanishes if the S-matrix is regularized as $S_{\pm\infty} = 1$, this corresponds to no conduction between the terminals.

The Chapter is organized as follows. In Sec. 2.2 we introduce the details of a model of a multi-terminal superconducting nanostructure and review the main aspects of a scattering matrix approach formalism in this case. The derivation and discussion of the response function are given in Sec. 2.4. In Sec. 2.6 we discuss the specific behaviour near the Weyl singularities, in the absence and presence of a weak spin-orbit coupling. In Sec. 2.5 we apply the general formulae to the case of a scattering matrix that varies only slightly on the scale of the superconducting gap $|\Delta|$. In Sec. 2.7 we address the energy-dependent S-matrices at arbitrary energy scale for a specific model of an energy dependence. We conclude the Chapter with the discussion of our results (Sec. 2.8). The technical details of the derivations are presented in Appendices.

2.2. MULTI-TERMINAL SUPERCONDUCTING NANOSTRUCTURE

Generally a multi-terminal superconducting nanostructure (Fig. 2.1) is a small conducting structure that connects n superconducting leads. The leads are macroscopic and are characterized by the phases of the superconducting order parameter. Each lead labeled by $\alpha \in \{0, 1, \cdots, n-1\}$ has its own superconducting phase ϕ_α and one of the leads' phase can be set to zero value $\phi_0 = 0$, according to the overall gauge invariance. The nanostructure design and these phases determine the superconducting currents I_α in each lead, that are the most relevant quantities to observe experimentally.

We aim to describe a general situation without specifying the nanostructure design. To this end, we opt to describe the system within the scattering approach pioneered by Beenakker [42]. The superconducting leads are treated as terminals: they are regarded as reservoirs which contain macroscopic amount of electrons and are in thermal equilibrium. A common assumption that we also make in this Chapter is that all terminals are made from the same material and thus have the same modulus of the superconducting order parameter $|\Delta|$. At sufficiently low temperatures and applied voltages one can disregard possible inelastic processes in the nanostructure and concentrate on elastic scattering only. Following the basics of the scattering approach[40], we assume N_α spin-degenerate transport channels in terminal α. The conducting structure connecting the terminals is a scattering region and is completely characterized by a scattering matrix S which generally depends on energy ε and is a unitary matrix at any ε. In Matsubara formalism we use imaginary energy ϵ and the matrix S satisfies the condition $S_\epsilon S^\dagger_{-\epsilon} = 1$. All the details of the nanostructure design are incorporated into the scattering matrix.

The electrons and holes in the superconducting transport channels involved in the scattering process may be described as plane waves that scatter in the region of the nanostructure and then return to the corresponding terminals. Amplitudes of incoming and outgoing waves are linearly related by the S-matrix. The numbers of transport channels in the terminal α denoted as N_α determines the dimension of the scattering matrix: $\dim S = M \times M$, where $M = 2_S \sum_\alpha N_\alpha$ and 2_s counts for the spin. The electrons and holes experience Andreev reflection in the superconducting terminals: the electrons are converted into holes and turn back, the same happens to holes. The Andreev reflection is complete at the energies smaller than the superconducting gap Δ. Therefore, electron-hole waves may be confined in the nanostructure giving rise to discrete energy levels called Andreev bound states (ABS). The amplitudes and phases of these confined states are determined by the scattering matrix and Andreev reflection phases that involve the superconducting phases of the corresponding terminals. One can find the energies of the ABS ε through Beenakker's determinant equation[36]:

$$\det(e^{2i\chi} - S_\varepsilon e^{i\phi}\sigma_y (S^T_{-\varepsilon})^{-1}\sigma_y e^{-i\phi}) = 0, \quad \chi = \arccos(\frac{\varepsilon}{\Delta}) \tag{2.1}$$

where S_ε is the S-matrix at the real energy ε, $\sigma_y = \begin{pmatrix} 0 & -i \\ i & 0 \end{pmatrix}$ is a Pauli matrix acting in the spin space and $e^{i\phi}$ is the diagonal matrix in channel space ascribing the stationary superconducting phases of the terminals to the corresponding channels, $e^{i\phi} \to \delta_{ab} e^{i\phi_\alpha}$ where a, b label the channels and α is the terminal corresponding to the channel a. The

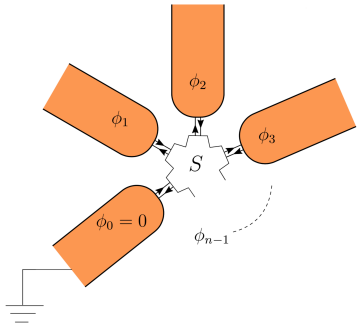

Figure 2.1: A multi-terminal superconducting nanostructure. Superconducting terminals are characterized by the corresponding superconducting phases. Electrons and holes coming from a terminal are scattered at the scattering region and can go to any other terminals. At least 4 terminals with 3 independent phases are required for a nanostructure to simulate a 3-dimensional bandstructure with topological properties.

ABS energies and the corresponding eigenvectors in the space of the channels depend parametrically on $n-1$ independent phases $\phi_\alpha \in [0, 2\pi]$ and thus can be viewed as a bandstructure defined in a "Brilluoin zone" of phases. It was noted[33] that (without spin-orbit interaction) three independent parameters are needed to tune the $n-1$ dimensional band structure of energy levels of ABS to reach the Weyl singularity at zero energy. It was also noted[33] that only one parameter is required to satisfy the condition for the highest ABS to touch the continuum above the gap ($\varepsilon = |\Delta|$). The ABS merges the continuum in this case and this implies that one cannot change this level adiabatically even for arbitrarily slow change of the parameters. When the incommensurate small voltages are applied to two terminals to sweep the phases[33], the system passes the points where the highest level merges with the continuum. This makes it questionable to apply the adiabaticity reasoning in this case. This makes it necessary to consider the contribution of the continuous spectrum to the response function of the currents in the limit of slow change of the parameters.

2.3. ACTION

The most general way to describe the nanostructure under consideration is to use an action method. This method has been pioneered in the context of a simple Josephson junction in [41]. In this method one deals with an action of the nanostructure that depends on the time-dependent superconducting phases $\phi_\alpha(\tau)$. The transport properties of the nanostructure as well as quantum fluctuations of the phases in case the nanostructure is embedded in the external circuit [41], can be derived from this action.

One of the advances of this Chapter is the derivation of such action for multi-terminal nanostructure and arbitrary S-matrix in Matsubara formalism. The details of the derivation are given in 2.9. Here we give the answer:

$$2L = -\mathrm{Tr}\log[\Pi_+ + \Pi_- \hat{S}_\epsilon], \quad \Pi_\pm = \frac{1 \pm g}{2} \tag{2.2}$$

here $\Pi_\pm$ and $\hat{S}_\epsilon$ are matrices in a space that is a direct product of the space of channels,

the imaginary-time space, spin and Nambu space. The matrix $\hat{S}_\epsilon$ is diagonal in the corresponding energy representation, therefore it depends on the difference of the imaginary time indices only. Its Nambu structure is given by

$$\hat{S}_\epsilon = \begin{pmatrix} S_\epsilon & 0 \\ 0 & S^T_{-\epsilon} \end{pmatrix} \tag{2.3}$$

where S_ϵ is the electron energy-dependent S-matrix (see App. 2.9). The matrix g is composed of the matrices diagonal in energy and diagonal in time in the following way:

$$g = U^\dagger \tau_z U, \quad U^\dagger = \begin{pmatrix} e^{\frac{i\phi(\tau)}{2}} & 0 \\ 0 & e^{\frac{-i\phi(\tau)}{2}} \end{pmatrix} \begin{pmatrix} A_{-\epsilon} & A_\epsilon \\ A_\epsilon & A_{-\epsilon} \end{pmatrix} \tag{2.4}$$

where

$$A_\epsilon = \sqrt{\frac{E+\epsilon}{2E}}, \quad E = \sqrt{\epsilon^2 + |\Delta|^2}, \tag{2.5}$$

where τ_z is the 3rd Pauli matrix acting in Nambu space and the Nambu structure has been made explicit in $U^\dagger$. This form assumes that $|\Delta|$ is the same in all the terminals. If it is not so, the matrix A_ϵ also acquires the dependence on the channel index. It is worth noting that $g^2 = 1$ so that $\Pi_\pm$ are projectors. The matrix g can be associated with the semiclassical Green's function in a terminal[40, 43]: $e^{i\phi(\tau)}$ is the diagonal matrix in channel space ascribing the time-dependent superconducting phases of the terminals to the corresponding channels, $e^{i\phi(\tau)} \to \delta_{ab} e^{i\phi_a(\tau)}$ where a, b label the channels and α is the terminal corresponding to the channel a. We note the gauge invariance of the action: due to the invariance of the trace under unitary transformations, the superconducting phases can be ascribed to the terminal Green's functions g as well as to the scattering matrix. Let us assume that the matrix S_ϵ does not depend on spin. Then the trace over spin is trivial. It is convenient to apply the unitary transformation $U^\dagger$ as in (2.4) to all the matrices in (2.2). This transforms the matrix g to τ_z. Then the projectors take a simple form $\Pi_\pm \to \frac{1\pm\sigma_z}{2}$ and the matrix in (2.2) reduces to the lower block-triangular form in Nambu space. The determinant is then equal to the determinant of the lower right block of the transformed matrix $\tilde{S}_\epsilon$. Then the action takes the form

$$-2L = 2_S \mathrm{Tr} \log[A_\epsilon e^{\frac{-i\phi(\tau)}{2}} S_\epsilon e^{\frac{i\phi(\tau)}{2}} A_\epsilon +$$

$$+ A_{-\epsilon} e^{\frac{i\phi(\tau)}{2}} S^T_{-\epsilon} e^{\frac{-i\phi(\tau)}{2}} A_{-\epsilon}] \tag{2.6}$$

the S-matrix in Matsubara formalism is subject to the unitarity constraint,

(2.7)

In what follows we concentrate on the zero-temperature limit $k_B T \ll |\Delta|$, so the summations over discrete frequencies are replaced with integrations $\int \frac{d\epsilon}{2\pi}$.

2.3.1. STATIONARY PHASES

In the stationary case $\phi(\tau) = \phi + \delta\phi(\tau)$ with constant ϕ and $\delta\phi(\tau) \equiv 0$ the value of the action gives the stationary phase-dependent ground state energy of the nanostructure $E_g = \lim_{k_B T \to 0} TL_0$.

$$E_g = -\frac{2_S}{2}\int \frac{d\epsilon}{2\pi}\mathrm{Tr}\log Q_\epsilon \tag{2.8}$$

$$Q_\epsilon = A_\epsilon^2 S_\epsilon + A_{-\epsilon}^2 S_{-\epsilon}^T \tag{2.9}$$

where Trace is now over the channel space and the Trace over spin space is taken explicitly as a factor of 2_S unless specifically addressed. The operator Q_ϵ introduced here has the properties of the inverse of the Green's function although it is not related to an operator average: its determinant as function of complex ϵ vanishes, $\det Q_\epsilon = 0$, at imaginary values $\epsilon = \pm i\varepsilon_k$ corresponding to the ABS energies (compare with (2.1)). In addition to these singularities the operator Q_ϵ has two cuts in the plane of complex ϵ corresponding to the presence of a continuous spectrum in the terminals above the gap $|\Delta|$. We choose the cuts as shown in Fig. 2.2. The expression (2.8) can be simplified in the case when the S-matrix does not depend on energy

$$E_g = -\tfrac{2_S}{2}\int \tfrac{d\epsilon}{2\pi}\mathrm{Tr}\log\left(\tfrac{E+\epsilon}{2E} + \tfrac{E-\epsilon}{2E}SS^*\right) + \tag{2.10}$$

$$+\tfrac{2_S}{2}\int \tfrac{d\epsilon}{2\pi}\log\det(S^T) \tag{2.11}$$

the second (divergent) contribution here does not depend on the superconducting phases so we omit it. To compute the integral it is convenient to choose the basis in which the unitary matrix $\Lambda = SS^*$ is diagonal. This is a unitary matrix, so the eigenvalues are unimodular complex numbers. The phases of the eigenvalues are related to the energies of ABS: $\Lambda_k = e^{2i\chi_k}$, $\chi_k = \arccos[\epsilon_k/|\Delta|]$, $\chi \in [-\pi/2;\pi/2]$. The eigenvalue $\Lambda_k = 1$ is doubly degenerate and corresponds to the values $\epsilon_k = \pm|\Delta|$. The eigenvalues come in complex conjugated pairs $\Lambda_k^* = \Lambda_{-k}$, where $(-k)$ corresponds to the Nambu-counterpart of the $k-$th eigenvector. So only the eigenvalues $\mathrm{Im}\Lambda_k > 0$ correspond to the quasiparticle states with positive energies. We will label them with positive indices k. In what follows we define a "bar" operation that links these pairs $|\bar{k}\rangle = S|k^\star\rangle = |-k\rangle$ where $|k\rangle$ is some eigenvector of Λ. We note, however, that this operation is not a convolution, since $|\bar{\bar{k}}\rangle = \Lambda_k|k\rangle$.

In this basis we can rewrite the integral as

$$E_g = -\frac{2_S}{2}\sum_{k>0}\int \frac{d\epsilon}{2\pi}\log[\frac{(E+\epsilon)^2 + (E-\epsilon)^2 + 2\cos 2\chi_k}{4(\epsilon^2+|\Delta|^2)}] \tag{2.12}$$

Evaluation of the integral brings to the known result

$$E_g = -\frac{2_S}{2}\sum_{\epsilon_k>0}\epsilon_k \tag{2.13}$$

where ϵ_k are the stationary phase-dependent ABS energies, as discussed above. The derivative of the ground state energy with respect to a stationary phase in terminal α gives the stationary current in the corresponding terminal,

$$I_\alpha = 2e\frac{\partial E_g}{\partial \phi_\alpha^{(0)}}. \tag{2.14}$$

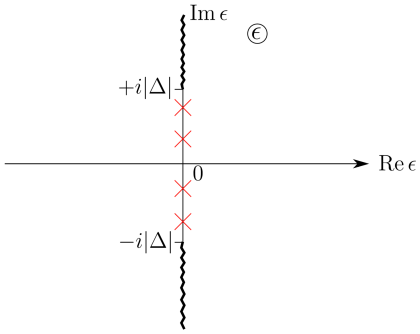

Figure 2.2: Singularities of the matrix Q_ϵ in the complex plane of energy ϵ. The symmetric cuts $[\pm i|\Delta|, \pm\infty]$ manifest the states of continuous spectrum. The isolated zeroes of the determinant of the matrix are situated at the imaginary axis within the interval $[-i|\Delta|, +i|\Delta|]$ (red crosses in the Figure). Their positions correspond to the ABS energies.

We expect this relation to hold in the adiabatic limit. In the following Section, we will access the time-dependent currents concentrating on the next order correction in the limit of small frequencies.

2.4. RESPONSE FUNCTION OF THE CURRENTS

To compute the response function of the currents we assume small nonstationary phase addition to the stationary phases ϕ, $\phi(\tau) = \phi + \delta\phi(\tau)$, $\delta\phi(\tau) \ll 2\pi$ and expand the action to the second order in $\delta\phi(\tau)$ (first order vanishes automatically since $\delta\phi(\tau)$ is nonstationary $\int_0^\beta d\tau\delta\phi(\tau) = 0$). We give the details in Append. 2.10. The total contribution to the action reads

$$\delta L = \sum_{\alpha,\beta} \int \frac{d\omega}{2\pi} \frac{\delta\phi_\omega^\alpha \delta\phi_{-\omega}^\beta}{2} R_\omega^{\alpha\beta}, \tag{2.15}$$

$\delta\phi_\omega$ being the Fourier transform of $\delta\phi(\tau)$. The frequency-dependent response function of the current $R_\omega^{\alpha\beta}$ is given by

$$
\begin{aligned}
&R_\omega^{\alpha\beta} = \\
&-2_S \int \frac{d\epsilon}{2\pi} \mathrm{Tr}\Big\{ Q_\epsilon^{-1} A_\epsilon^2 [\frac{I_\alpha}{2}(S_{\epsilon-\omega} - S_\epsilon)\frac{I_\beta}{2} + \\
&+ \frac{I_\beta}{2}(S_{\epsilon+\omega} - S_\epsilon)\frac{I_\alpha}{2}] + \qquad (2.16)\\
&+ \frac{1}{2} Q_\epsilon^{-1} \frac{\partial^2 Q_\epsilon}{\partial\alpha\partial\beta} - \qquad (2.17)\\
&- \frac{1}{2} Q_{\epsilon+\omega}^{-1} (A_{-(\epsilon+\omega)} (\frac{iI_\alpha}{2} S_{-\epsilon}^T - S_{-(\epsilon+\omega)}^T \frac{iI_\alpha}{2}) A_{-\epsilon} - \\
&- A_{\epsilon+\omega} (\frac{iI_\alpha}{2} S_\epsilon - S_{\epsilon+\omega} \frac{iI_\alpha}{2}) A_\omega) \times \\
&\times Q_\epsilon^{-1} (A_{-\epsilon} (\frac{iI_\beta}{2} S_{-(\epsilon+\omega)}^T - S_{-\epsilon}^T \frac{iI_\beta}{2}) A_{-(\epsilon+\omega)} - \\
&- A_\epsilon (\frac{iI_\beta}{2} S_{\epsilon+\omega} - S_\epsilon \frac{iI_\beta}{2}) A_{\epsilon+\omega}) \Big\} \qquad (2.18)
\end{aligned}
$$

here the stationary phases are ascribed to the S-matrix. We use a shorthand notation $\partial/\partial_\alpha = \partial/\partial_{\phi_\alpha}$ and define a set of matrices that project channel space onto the space of the channels in the terminal α, $(I^\alpha)^{ab} = \delta^{ab}$ if a is a channel in terminal α and $(I^\alpha)^{ab} = 0$ otherwise. The first term in (2.18) vanishes at zero frequency and in the case of the energy-independent S-matrix. The second term does not depend on frequency ω. In the limit of zero frequency the second and the third terms reproduce the stationary response function of the currents

$$\lim_{\omega\to 0} R_\omega^{\alpha\beta} = -\frac{2_S}{2} \frac{\partial^2}{\partial\alpha\partial\beta} \int \frac{d\epsilon}{2\pi} \mathrm{Tr} \log Q_\epsilon = \frac{\partial^2 E_g}{\partial\alpha\partial\beta} \qquad (2.19)$$

Let us consider the limit of small $\omega \ll |\Delta|$ and concentrate on the first order correction to the adiabatic limit

$$R_\omega^{\alpha\beta} = \frac{\partial^2 E_g}{\partial\alpha\partial\beta} + \omega B_{\alpha\beta} + O(\omega^2) \qquad (2.20)$$

We note that the response function is analytic in the vicinity of $\omega = 0$. This is guaranteed by the gap in the density of states, which is given by the energy of the lowest ABS. Away from the zero-energy Weyl singularity it can be estimated as $|\Delta|/N$ with N being the total number of ABS in the nanostructure. The vicinity of a Weyl singularity has to be treated more carefully as we discuss in Sec. 2.6. Let us note that for any system with a discrete spectrum the quantity $B_{\alpha\beta}$ can be related to the *Berry curvature*[30–32]. For any state in the discrete spectrum the Berry curvature corresponding to this state is given by $B_{\alpha\beta}^{(i)} = 2\mathrm{Im}\langle\partial_\alpha i|\partial_\beta i\rangle$ with i labeling discrete states and $|i\rangle$ being the wavefunction of the corresponding state. In our case we are interested in the total Berry curvature of the superconducting ground state defined as $B_{\alpha\beta} = -\frac{1}{2}\sum_i B_{\alpha\beta}^{(i)}$ where i labels the (spin-degenerate) wavefunctions of the BdG equation with positive eigenvalues[33]. However,

the adiabaticity condition which justifies the expansion in (2.20) for the case of discrete spectrum requires the frequency to be much smaller than the smallest energy spacing between the levels.

In our system, the continuous spectrum above the superconducting gap is present. In principle, any continuous spectrum can be approximated with a discrete spectrum with a vanishing level spacing $\overline{\delta} \to 0$. By doing this we can utilize the previous expression for the response function $B_{\alpha\beta}$ since it is valid for the discrete spectrum. However, the adiabaticity condition which is necessary for this expression to be valid would reduce to $\omega \ll \overline{\delta} \to 0$. This condition contains an artificially introduced $\overline{\delta}$ and is by construction very restrictive in ω. On the other hand, the expansion in Eq. (2.20) is valid under a physically meaningful and less restrictive condition $\omega \ll |\Delta|/N$. Taken all that into account, we conclude that the response function $B_{\alpha\beta}$ defined in Eq (2.20) does not have to reduce to the expression for a total Berry curvature of a superconducting ground state of a system discussed above. The topological properties of this quantity also have to be investigated separately.

One may conjecture that the resulting response function in Eq. (2.20) reduces to the sum of the Berry curvatures of the discrete ABS spectrum, so that it is not contributed to by the continuous spectrum. This conjecture relies on the analogy between the expressions for the total Berry curvature and the superconducting ground state energy. In the case when the S-matrix is energy-independent, only the discrete states contribute to the ground state energy. Thus motivated, in the following we investigate the response function $B_{\alpha\beta}$ defined by means of Eq (2.20) in detail. We find that there is a contribution from the continuous spectrum to this quantity as well as from the discrete one. We also find that in general the integral of $B_{\alpha\beta}$ over the phases ϕ_α, ϕ_β that would normally define an integer Chern number, is not integer. Therefore, $B_{\alpha\beta}$ contains a non-topological contribution. This non-topological part is contributed by the continuous as well as the discrete part of the spectrum.

The tensor $B_{\alpha\beta}$ defined in Eq. (2.20) is antisymmetric (since $R_{\omega}^{\alpha\beta} = R_{-\omega}^{\beta\alpha}$). The concrete expression for $B_{\alpha\beta}$ reads:

$$B_{\alpha\beta} = -\frac{2_S}{2}\int \frac{\mathrm{d}\epsilon}{2\pi}\left(\frac{1}{2}\mathrm{Tr}\left[Q_\epsilon^{-1}\frac{\partial Q_\epsilon}{\partial\epsilon}Q_\epsilon^{-1}\frac{\partial Q_\epsilon}{\partial\alpha}Q_\epsilon^{-1}\frac{\partial Q_\epsilon}{\partial\beta}\right] + \right.$$
$$\left. + \frac{\partial}{\partial\beta}\mathrm{Tr}\left[Q_\epsilon^{-1}A^2(\epsilon)\{\frac{\partial S_\epsilon}{\partial\epsilon}, \frac{iI_\alpha}{2}\}\right]\right) - (\alpha \leftrightarrow \beta) \tag{2.21}$$

The first term here resembles the usual WZW form[29] for a Chern number. Usually, the form contains the matrix Green's functions[29], in our case the form utilizes the matrix Q_ϵ defined by Eq. (2.9). We note however that in distinction from common applications of WZW forms here one cannot regard Q_ϵ as a smooth function of parameters $\phi_\alpha, \phi_\beta, \epsilon$ defined on a compact manifold without a boundary. This is because in general this matrix has different limits at positive and negative infinite energies $S_{-\infty}$ for $\epsilon \to -\infty$ and $S_{-\infty}^T$ for $\epsilon \to +\infty$ that also depend on the phases. Due to this reason the integral of the first term over a compact surface without a boundary in a space of phases does not have to reduce to an integer $\cdot(2\pi)^{-1}$. The second term in Eq. (2.21) has a form of a total derivative with respect to a phase of a periodic and smooth function, so the integral of this one over a compact surface will give zero.

In order to obtain the value of this integral let us consider first the variation of this value upon the small smooth variation of the matrix $Q_\epsilon \to Q_\epsilon + \delta Q_\epsilon$ that comes from the small variation of the S-matrix δS_ϵ, so $\delta Q_\epsilon = A_\epsilon^2 \delta S_\epsilon + A_{-\epsilon}^2 \delta S_{-\epsilon}^T$. The value of the integral of the second contribution in Eq. (2.21) does not contribute to the integral over a compact submanifold in phase space, so we needn't consider its variation. It is known [44] that the variation of the first contribution to $B_{\alpha\beta}$ reduces to the total derivatives

$$\delta\{\int \frac{d\epsilon}{2\pi} \mathrm{Tr}\left[Q_\epsilon^{-1}\frac{\partial Q_\epsilon}{\partial\epsilon}Q_\epsilon^{-1}\frac{\partial Q_\epsilon}{\partial\alpha}Q_\epsilon^{-1}\frac{\partial Q_\epsilon}{\partial\beta}e^{\alpha\beta}\right]\} =$$

$$= \int \frac{d\epsilon}{2\pi}\partial_\epsilon \mathrm{Tr}\left[Q_\epsilon^{-1}\delta Q_\epsilon Q_\epsilon^{-1}\frac{\partial Q_\epsilon}{\partial\alpha}Q_\epsilon^{-1}\frac{\partial Q_\epsilon}{\partial\beta}\right]e^{\alpha\beta} + \tag{2.22}$$

$$+ \int \frac{d\epsilon}{2\pi}\partial_\alpha \mathrm{Tr}\left[Q_\epsilon^{-1}\delta Q_\epsilon Q_\epsilon^{-1}(\frac{\partial Q_\epsilon}{\partial\beta}Q_\epsilon^{-1}\frac{\partial Q_\epsilon}{\partial\epsilon} - \right.$$

$$\left.\frac{\partial Q_\epsilon}{\partial\epsilon}Q_\epsilon^{-1}\frac{\partial Q_\epsilon}{\partial\beta})\right]e^{\alpha\beta} \tag{2.23}$$

The value of the integral of second term in (2.23) over a compact submanifold in phase space vanishes if the submanifold does not pass Weyl singularities corresponding to $\det Q_\epsilon^{-1} \to \infty$, because it has a form of a total derivative of a smooth function. Evaluation of the integral in (2.22) yields the following contribution to the variation of $B_{\alpha\beta}$

$$\frac{1}{2\pi}\delta\{\mathrm{Tr}[S_{-\infty}\frac{I_\alpha}{2}S_{+\infty}^\dagger\frac{I_\beta}{2}]\}e^{\alpha\beta} \tag{2.24}$$

We note that this contribution is generally nonzero and does not depend on phases.

Let us turn to the evaluation of the topological charge that is proven to be very useful in the field [28]. The value of the topological charge is defined in a usual way with the divergence of the topological field $\vec{E}$

$$2\pi q = \mathrm{div}\vec{E}, \quad E^\gamma \equiv \frac{1}{2}e^{\gamma\alpha\beta}B_{\alpha\beta} \tag{2.25}$$

To compute the topological charge we need to consider a special variation of the S-matrix that just corresponds to the stationary phase derivative $\delta S_\epsilon = [S_\epsilon, \frac{iI_\gamma}{2}]\delta\phi_\gamma$. Since the expression under the trace in (2.24) does not depend on phases, the topological charge vanishes at any point where the field $\vec{E}$ is well-defined, or alternatively $\det Q_\epsilon^{-1}$ is finite. The Weyl singularities give rise to the point-like integer charges being the sources of the field $\vec{E}$. We consider this in detail in Sec. 2.6. This situation is in complete analogy with that of the standard Berry curvature of a discrete spectrum where Weyl singularities correspond to band crossings. However, we have computed the topological charge for the particular phase-dependence of the S-matrix on phases $(e^{-\frac{i\phi}{2}}Se^{-\frac{i\phi}{2}})$. We have not considered the topological charge in the space of 2 phases ϕ_α, ϕ_β and some other parameter characterizing the scattering matrix, this charge could be nonzero and have a continuous distribution. The investigation of the general parametric dependence of the S-matrix is beyond the scope of the present Chapter.

We separate the field $\vec{E}$ into three parts: a part produced by the point-like charges, divergenceless field that is zero in average, and a constant part $\vec{\bar{E}}$. The value of the integral

$$2\pi C^{12} = \int_0^{2\pi}\int_0^{2\pi} d\phi_1 d\phi_2 \frac{B_{\alpha\beta}e^{\alpha\beta}}{2} = \int (d\vec{s},\vec{E}) \tag{2.26}$$

is given by the flux of the topological field through the corresponding surface. This flux reduces to the integer for the first contribution to $\vec{E}$, vanishes for the second divergenceless contribution and may result in some value for the constant part of the field. We stress that the last contribution being present is the main distinction from the common case. The value of this constant field is then given by the integration of the variation (2.24):

$$\bar{E}^{\gamma} = \frac{1}{2\pi}\{\mathrm{Tr}[S_{-\infty}\frac{I_\alpha}{2}S^{\dagger}_{+\infty}\frac{I_\beta}{2}]\}e^{\gamma\alpha\beta} \tag{2.27}$$

This constant field can contribute to the flux through any plane in the phase space.

$$C = n + 2\pi(\vec{\bar{E}},\vec{n}) \tag{2.28}$$

where $\vec{n}$ is the normal vector to this plane. As it has been shown in Ref. [33] the value of C^{12} is directly related to the observable transconductance between the leads α and β. Therefore, in contrast to the conclusions of Ref. [33] the value of transconductance does not always quantize although the change of transconductance with a phase can be quantized.

So, in principle a nonzero non-topological contribution to (2.28) can be present. This contribution is nonzero if the S-matrix is not regularized at infinite energy such that $[S_{-\infty}, I_\alpha] = 0$. If the S-matrix is regularized in this way, then the Q_ϵ matrix is defined on a compact space of parameters (ϵ,α,β), so the first contribution to Eq. (2.21) would reduce to an integer n (with proper normalization). If it is not regularized this way, then this boundary term leads to the presence of a non-topological contribution to the response function, that comes due to the presence of a continuous spectrum and, formally, from the fact that the matrix Q_ϵ is not defined on a compact space, as discussed above. In the limit of energy-independent S-matrix, this contribution reduces to the antisymmetric part of the Landauer conductance[40, 45]. In this case, if the bare S-matrix (without the stationary phases of terminals ascribed) is non-symmetric (which means the breaking the time-reversibility condition) we obtain a nonzero value of (2.27). If the S-matrix is time-reversible, the non-topological contribution is zero and the integer quantization of transconductance is restored.

2.5. WEAK ENERGY DEPENDENCE OF THE $S-$MATRIX

In the description of the realistic nanostructure a reasonable approximation is to consider the S-matrix to be constant on the scale of $|\Delta|$. It corresponds to the case of a short nanostructure (smaller than the superconducting coherence length). So a logical approximation would be to describe the nanostructure with a constant S-matrix at all energies. The response function $B_{\alpha\beta}$ is given by an integral over energy in Eq. (2.21). Would this integral accumulate in the region $\epsilon \sim |\Delta|$, then the approximation of a constant S-matrix at all energies would be accurate. However, there can be a significant

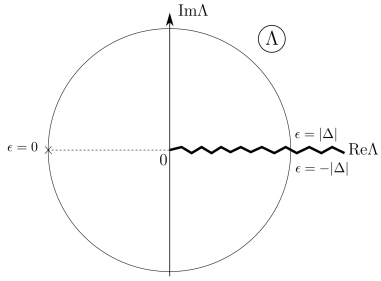

Figure 2.3: The choice of the branch cut of the logarithm in Eq. (2.29) in the plane of complex Λ.

contribution from the energy scales $\epsilon \gg |\Delta|$ to the integral yielding $B_{\alpha\beta}$. In this case the energy dependence of the S-matrix at the large energies becomes important. To investigate this we consider the contributions from the small scales $\epsilon \gtrsim |\Delta|$ and from the large scales $\epsilon \gg |\Delta|$ in the Subsections 2.5.1 and 2.5.2 respectively.

2.5.1. ENERGY-INDEPENDENT $S-$MATRIX:

In this Subsection we analyze the small-scale ($\epsilon \sim |\Delta|$) contribution to (2.21). For this we approximate the S-matrix to be constant at all energies and extend the integration limits to infinity. The second term in (2.21) vanishes since $\frac{\partial S_\epsilon}{\partial \epsilon} = 0$. The integral in the first term in (2.21) converges on the scale $\epsilon \gtrsim |\Delta|$. This statement only necessarily holds if the S-matrix is energy-independent. Otherwise, the contribution from the larger scales can be present and we investigate it in 2.5.2. Similarly to (2.12), the result of integration under consideration can be expressed in terms of the eigenvalues and eigenvectors of the unitary matrix $\Lambda = SS^*$. We use the same notations $|k\rangle$ and $|\bar{k}\rangle$ for the eigenvectors related to the complex conjugated eigenvalues pair Λ_k and Λ_k^* correspondingly as described after Eq.(2.11). We remind that the phase of the eigenvalue $\Lambda_k = e^{2i\chi_k}$ with $k > 0$ is related to the energy of ABS as $\chi_k = \arccos[\epsilon_k/|\Delta|]$. We also remind that $\Lambda_k = 1$ is degenerate and corresponds to the energy of one of the ABS $\epsilon_k = |\Delta|$. Upon crossing this point in phase space, this ABS state exchanges the wave function with its Nambu counterpart with the eigenvalue $\epsilon_{k'} = -|\Delta|$. Due to this we call such points gap touching singularities.

Evaluating the integral yields

$$4\pi B_{\alpha\beta} = -2\sum_k \big(\log\Lambda_k - \log(1 + i0sgn(k))\big)\langle\partial_\alpha k|\partial_\beta k\rangle - \\ -\sum_{k,j}(1 - \frac{\Lambda_k}{\Lambda_j})\langle\bar{j}|\partial_\alpha\bar{k}\rangle\langle j|\partial_\beta k\rangle - (\alpha \leftrightarrow \beta) \tag{2.29}$$

where k, j label the eigenvalues of Λ, and the summation goes over indices with both signs. If the number of channels is odd, there is an eigenvector of Λ corresponding precisely to the eigenvalue $\Lambda_k = 1$. Then the index $k = 0$ corresponds to this state. If the number of channels is even, the indices in Eq.(2.29) do not take the zero value. In the following we consider the number of channels to be even. The logarithm here has a branch cut along the real axis as $[0, +\infty]$ (see Fig. 2.3) to avoid the gap touching singularity ambiguity $\Lambda_k = 1$. Let us consider the behaviour of $B_{\alpha\beta}$ in the vicinity of the gap touching

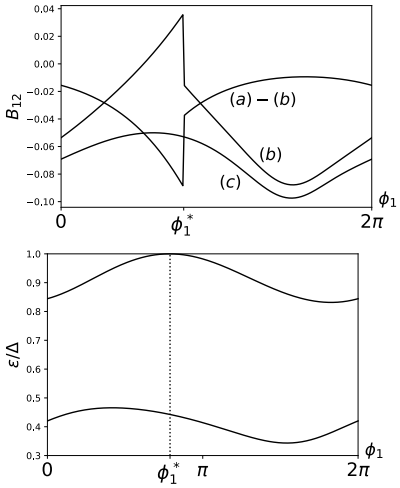

Figure 2.4: Example plots of B_{12}. To produce the plots, we chose one channel per terminal and took a random non-symmetric 4×4 scattering matrix describing the structure. We fix $\phi_2 = 1.20\pi, \phi_3 = 0.48\pi$ and change ϕ_1. (Upper panel) (a) the value of B_{12} as given (2.29). It is clearly a continuous function of ϕ_1. (b) The contribution of the discrete ABS to B_{12}. The contribution experiences a jump at a point where the highest ABS merges with the continuum. (a)-(b) is thus the contribution from the continuous spectrum (Lower panel) The ABS energies versus ϕ_1. The point where the highest level touches the gap egde by coincides with the point of discontinuity of the discrete spectrum contribution

singularity. Since the wave function corresponding to $\Lambda_k \to 1+i0$ is discontinuous upon crossing this singularity, it is not obvious that $B_{\alpha\beta}$ is continuous. However, one can observe that the first term is a sum of Berry curvatures of individual levels multiplied by the eigenvalue-dependent prefactors $\log\Lambda_k$. This prefactors vanish for the discontinuous wavefunctions at the gap touching degeneracy and guarantee the continuity of the first term. Also, one can show that the second term in Eq.(2.29) is continuous. Consequently, $B_{\alpha\beta}$ is continuous at this point (see Fig. 2.4). The only possibility for $B_{\alpha\beta}$ to be ill-defined at some points in phase space is the zero-energy Weyl singularity where $\det Q_\epsilon^{-1}$ diverges (see Sec.2.6).

The response function $B_{\alpha\beta}$ is expressed in terms of eigenvalues and eigenvectors of the matrix Λ. So is the ABS contribution to the ground state Berry curvature, which was conjectured as a result for $B_{\alpha\beta}$ (see Sec. 2.4). It was shown[33] that this ABS contribution is given by $B^{\mathrm{ABS}}_{\alpha\beta} = -\frac{2_S}{2}\sum_{k>0} B^{(k)}_{\alpha\beta}$, $B^{(k)}_{\alpha\beta} = 2\mathrm{Im}\langle\partial_\alpha k|\partial_\beta k\rangle$. Since one of the wavefunctions contributing to this sum is discontinuous at the gap touching singularity, we conclude that $B^{\mathrm{ABS}}_{\alpha\beta}$ is discontinuous contrary to $B_{\alpha\beta}$. One can understand the difference between $B_{\alpha\beta}$ and $B^{\mathrm{ABS}}_{\alpha\beta}$ by considering the computation of the integral in the first term in Eq. (2.21) by means of complex analysis (in the plane of complex ϵ). By shifting the integration contour to the upper half-plane, one can see that the integral is contributed to by the poles, corresponding to ABS and the cut above the gap (see Fig. 2.2). The contribution from the poles results in B_{ABS}, but the contribution from the cut, $B^{\mathrm{cut}}_{\alpha\beta} = B_{\alpha\beta} - B^{\mathrm{ABS}}_{\alpha\beta} \neq 0$, is equally important (see Fig. 2.4).

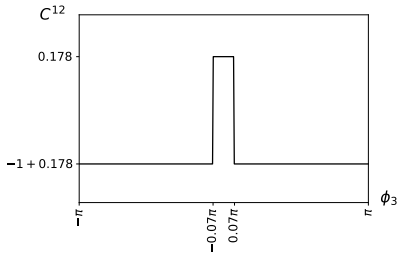

Figure 2.5: An example plot of the "Chern number" C_{12} defined as the integral of B_{12} over $\phi_{1,2}$ (see (2.28)). To produce the plot, we have chosen a randon 4×4 scattering matrix that is not invariant with respect to time reversal. We have found two Weyl singularities of opposite charge at $\phi_3 = \pm 0.07\pi$. We plot C_{12} versus ϕ_3 to demonstrate the integer jumps at the positions of Weyl singularities along with a non-integer, non-universal offset.

For the integrated $B_{\alpha\beta}$ we obtain in accordance with Eq. (2.28)

$$\int_0^{2\pi}\int_0^{2\pi} d\phi_1 d\phi_2 \frac{e^{\alpha\beta}B_{\alpha\beta}}{2} = 2\pi(n+\frac{1}{4}\mathrm{Tr}(S^\dagger I_\beta S I_\alpha)e^{\alpha\beta}) \tag{2.30}$$

so the value of transconductance is not necessarily quantized in the approximation of the energy-independent S-matrix.

2.5.2. CONTRIBUTION FROM THE LARGE SCALES:

In the previous Section we have shown that the non-topological contribution to the transconductance comes from the boundary terms at $\epsilon = \pm\infty$ (see Eq.(2.22)). This means that, contrary to intuition, there is an essential contribution to $B_{\alpha\beta}$ coming from the energy scales much larger than the energy gap. In order to investigate the large energy contribution we assume the regularization of the S-matrix at large energies. So, in this Subsection we consider $B_{\alpha\beta}$ for a particular energy-dependence of the S-matrix. It is chosen such that the S-matrix is regularized at infinity such that it varies slowly on the scale of a superconducting gap $|\Delta|$ and $S_{\pm\infty} = 1$. This S-matrix corresponds to a complete isolation of the terminals at the largest energies. With this regularization, the matrix Q_ϵ is defined on a compact parameter space (α,β,ϵ) and the first contribution in (2.21) must reduce to an integer. Due to the scale separation, there are two contributions to $B_{\alpha\beta}$. One comes from the scales $\epsilon \sim |\Delta|$ and is given by the same result (2.29). Another one comes from the scales $\epsilon \gg |\Delta|$.

For negative energies, the large scale contribution with asymptotic accuracy equals

$$\begin{aligned}
&-\frac{1}{2}e^{\alpha\beta}\int_{-\infty}^{0}\frac{d\epsilon}{2\pi}\mathrm{Tr}[\frac{\partial S^\dagger_{-\epsilon}}{\partial\epsilon}S_\epsilon\frac{\partial S^\dagger_{-\epsilon}}{\partial\alpha}\frac{\partial S_\epsilon}{\partial\beta}] = \\
&=-\frac{1}{2}e^{\alpha\beta}\int_{-\infty}^{0}\frac{d\epsilon}{2\pi}\partial_\epsilon\mathrm{Tr}[S^\dagger_{-\epsilon}\frac{iI_\alpha}{2}S_\epsilon\frac{iI_\beta}{2}] = \\
&=-\frac{1}{4\pi}e^{\alpha\beta}\mathrm{Tr}[S^\dagger\frac{iI_\alpha}{2}S\frac{iI_\beta}{2}]+\frac{1}{4\pi}e^{\alpha\beta}\mathrm{Tr}[S^\dagger_{+\infty}\frac{iI_\alpha}{2}S_{-\infty}\frac{iI_\beta}{2}]
\end{aligned} \tag{2.31}$$

with the notation $S = S_{\epsilon=0}$.

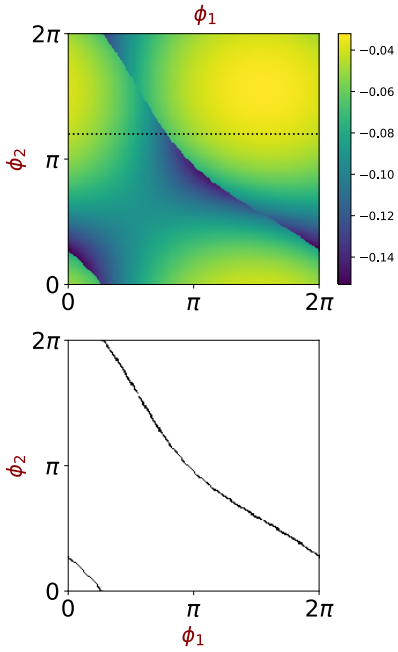

Figure 2.6: Example plots versus ϕ_1, ϕ_2. A random non-symmetric scattering matrix has been chosen to produce the plots, that varies slowly at the scale of $|\Delta|$, while $S_\infty = 1$. Upper panel: A density plot of the continuous spectrum contribution to B_{12} ((2.21))versus ϕ_1, ϕ_2 at $\phi_3 = 0.48\pi$. There is a discontinuity at the lines of the gap edge touching. Lower panel: the lines of the gap touching.

For positive ones:

$$-\frac{1}{2}e^{\alpha\beta}\int_0^{+\infty}\frac{d\epsilon}{2\pi}\mathrm{Tr}[\frac{\partial S_\epsilon^\star}{\partial\epsilon}S_{-\epsilon}^T\frac{\partial S_\epsilon^\star}{\partial\alpha}\frac{\partial S_{-\epsilon}^T}{\partial\beta}]=$$
$$=-\frac{1}{2}e^{\alpha\beta}\int_0^{+\infty}\frac{d\epsilon}{2\pi}\partial_\epsilon\mathrm{Tr}[S_\epsilon^\star\frac{iI_\alpha}{2}S_{-\epsilon}^T\frac{iI_\beta}{2}]=$$
$$=-\frac{1}{4\pi}e^{\alpha\beta}\mathrm{Tr}[S^\dagger\frac{iI_\alpha}{2}S\frac{iI_\beta}{2}]+\frac{1}{4\pi}e^{\alpha\beta}\mathrm{Tr}[S_{+\infty}^\dagger\frac{iI_\alpha}{2}S_{-\infty}\frac{iI_\beta}{2}]. \tag{2.32}$$

So, the both contributions give the following addition to the response function

$$\frac{1}{2\pi}e^{\alpha\beta}\mathrm{Tr}[S^\dagger\frac{I_\alpha}{2}S\frac{I_\beta}{2}]-\frac{1}{2\pi}e^{\alpha\beta}\mathrm{Tr}[S_{+\infty}^\dagger\frac{I_\alpha}{2}S_{-\infty}\frac{I_\beta}{2}] \tag{2.33}$$

Both terms here do not depend on phases. The first one is exactly equal to the constant part of the topological field defined previously with an opposite sign (computed for an energy-independent S-matrix case). So after integration over two phases, it cancels the non-topological contribution from small scales in (2.30). Since we assume a regularization $S_{\pm\infty}=1$, the second term is zero ($\mathrm{Tr}[S_{+\infty}^\dagger\frac{I_\alpha}{2}S_{-\infty}\frac{I_\beta}{2}]=0$), so the total mean value of the transconductance is quantized in correspondence with the theory of characteristic classes.

The second contribution to $B_{\alpha\beta}$ in Eq. (2.21) contains the energy-derivative of the S-matrix under the integral. Due to this the energy scale of its dependence drops out from the integral. So, one may expect that it contributes to the large scale contribution to $B_{\alpha\beta}$. However, with asymptotic accuracy it vanishes in the limit when the S-matrix varies slowly on the scale $|\Delta|$. Indeed, in the limit $|\epsilon|\gg|\Delta|$

$$Q_\epsilon^{-1}\simeq S_\epsilon^\star,\quad A_\epsilon^2\simeq 0,\quad \epsilon>0 \tag{2.34}$$
$$Q_\epsilon^{-1}\simeq S_{-\epsilon}^\dagger,\quad A_\epsilon^2\simeq 1,\quad \epsilon<0 \tag{2.35}$$

In this limit for $\epsilon<0$, the integrand equals

$$\frac{\partial}{\partial\beta}\mathrm{Tr}[Q_\epsilon^{-1}A^2(\epsilon)\{\frac{\partial S_\epsilon}{\partial\epsilon},\frac{iI_\alpha}{2}\}]\simeq$$
$$\simeq\partial_\beta\mathrm{Tr}[\frac{iI_\alpha}{2}(\frac{\partial S_\epsilon}{\partial\epsilon}S_{-\epsilon}^\dagger-\frac{\partial S_{-\epsilon}^\dagger}{\partial\epsilon}S_\epsilon)]=0 \tag{2.36}$$

with asymptotic accuracy, since the expression under the trace does not depend on phases. For $\epsilon>0$ the integrand vanishes since $A_\epsilon^2\to 0$ for $\epsilon\gg|\Delta|$.

2.6. THE VICINITY OF A WEYL POINT

In this Section, we investigate the Berry curvature in the vicinity of a Weyl singularity, that occurs at some point $\vec{\phi}_0$ in the 3-dimensional phase space. Such Weyl points have been analyzed in [33] assuming spin symmetry, in [46] the analysis has been extended to cover weak spin-orbit interaction. Without spin-orbit coupling, the Weyl points are situated at zero energy and $\det Q_{\epsilon=0}^{-1}$ diverges near the point. A conical spectrum of ABS is found in the vicinity of the point [33]. A weak spin-orbit coupling splits the energy cones in spin and shifts the Weyl point to a finite energy [46]. Further, we discuss separately the cases of vanishing and weak spin-orbit coupling.

2.6.1. VANISHING SPIN-ORBIT COUPLING

When the spin-orbit (SO) coupling is absent, the Weyl singularities are located at some points in the phase space $\vec{\phi}_0$ and occur at zero energy $\epsilon_\pm = 0$. To consider the vicinity of the singularity, we assume a small phase deviation $\delta\hat{\phi} = \hat{\phi} - \hat{\phi}_0 \ll 1$ from the singularity point and assign it to each channel via the diagonal matrix $e^{\delta\hat{\phi}}$. In the vicinity, $B_{\alpha\beta}$ defined by Eq. (2.21) only has non-zero contributions from the first term of quasi-WZW term. The second term vanishes asymptotically when the energy approaches zero, as shown in Eq. 2.34. Conform to these approximations, we extend the domain of the integration over the phases to infinity since $B^{\alpha\beta}$ is concentrated near the singularity point.

To compute $B^{\alpha\beta}$, we approximate the Q matrix near the Weyl point with the expression that keeps the first orders in ϵ and of the variation: $Q = (\epsilon + \frac{1}{2}\delta\Lambda)S^T = MS^T$, S being the scattering matrix in the singularity point at $\epsilon = 0$. Conveniently, we can replace Q with M in Eq.(2.21). We find the variation $\delta\Lambda$ by expanding the S-matrix in $\delta\vec{\phi}$:

$$S \to S + \delta_\phi S = e^{-i\delta\hat{\phi}/2} S e^{i\delta\hat{\phi}/2} = S - [\frac{i\delta\hat{\phi}}{2}, S] \tag{2.37}$$

$$\Lambda = SS^* \to \Lambda + \delta_\phi\Lambda = \Lambda + iS\delta\hat{\phi}S^\dagger\Lambda - i\delta\hat{\phi}\Lambda \tag{2.38}$$

We can contract the dimension of M projecting it to two eigenvectors of Λ that achieve singular values at the Weyl point. Following [33], we separate the singular part of M and write in the basis of ABS eigenvectors $|+\rangle$ and $|-\rangle$ satisfying $S|\pm\rangle = \pm|\mp\rangle^*$, $\Lambda|\pm\rangle = -|\pm\rangle$:

$$M = \epsilon + \frac{1}{2}\delta\Lambda \equiv \epsilon + \frac{i}{2}\vec{h}\cdot\vec{\tau} \tag{2.39}$$

where $\vec{\tau}$ are the Pauli matrices in the space of these two eigenvectors, and the components of $\vec{h}$ are proportional to the components of $\vec{\phi}$: $h_x + ih_y = 2\langle -|\delta\hat{\phi}|+\rangle$, $h_z = \langle +|\delta\hat{\phi}|+\rangle - \langle -|\delta\hat{\phi}|-\rangle$.

The form of M is similar to the generic form of Green's function of a two-level system. We expect that the two poles of M^{-1} should be positioned symmetrically on the imaginary axis ϵ due to BdG particle-hole symmetry. Indeed, we find these poles at $\epsilon_\pm = \pm i\frac{|\vec{h}|}{2}$. Using the trace relations of Pauli matrices, we reduce in the leading order $B_{\alpha\beta}$ to the Berry curvature of the corresponding levels :

$$\begin{aligned} B^{\alpha\beta} &= -\frac{1}{4}\int \frac{d\epsilon}{2\pi}\mathrm{Tr}\left(M_\epsilon^{-1}\frac{\partial M_\epsilon}{\partial\epsilon}M_\epsilon^{-1}\frac{\partial M_\epsilon}{\partial\alpha}M_\epsilon^{-1}\frac{\partial M_\epsilon}{\partial\beta}\right) \\ &= \frac{1}{8}\int\frac{d\epsilon}{2\pi}\sum_{\substack{a,b,c\\=x,y,z}}\frac{1}{(\det M)^2}\Big(h_a\partial_\alpha h_b\partial_\beta h_c\epsilon_{abc} - \\ &- (\alpha\leftrightarrow\beta)\Big) = \frac{\vec{h}}{4|\vec{h}|^3}\cdot\partial_\alpha\vec{h}\times\partial_\beta\vec{h} - (\alpha\leftrightarrow\beta) \end{aligned} \tag{2.40}$$

We note that in this section all the matrices have the spin index. For an N dimensional space of superconducting phases, the singularities are concentrated in the $N-3$ dimensions and the relevant space is reduced to a 3-dimensional subspace $\{\delta\phi_1, \delta\phi_2, \delta\phi_3\}$. For certainty, we set the indices $\alpha, \beta = 1, 2$, and consider the curvature defined in the $\phi_1 - \phi_2$ plane at a fixed phase ϕ_3.

The ϕ_3 dependence of the integral of the curvature with respect to superconducting phases ϕ_1, ϕ_2 witnesses the change of first Chern number C^{12} when the integration plane passes the singularity point. Since we only concentrate on the vicinity of the Weyl singularity, the integral under the approximations made can only indicate the change of the Chern number, rather than its total value that can be determined by integration over the regions far from the singularity point. To compute the integrated $B_{\alpha\beta}$, we notice from Eq.(2.39) that the energy spectrum is linear in $\delta\phi$, and introduce a linear relation $h_i = \sum_\alpha \delta\phi_\alpha T_{\alpha i}$ with $T_{\alpha i} = \partial_\alpha h_i$ being a real invertible matrix. The integrated B_{12} is then obtained as:

$$C^{12} = \frac{1}{2\pi}\int B_{12}\mathrm{d}\phi_1\mathrm{d}\phi_2 = \frac{1}{2}\mathrm{sgn}(\delta\phi_3 \det T) \tag{2.41}$$

$\mathrm{sgn}(\delta\phi_3)$ determining the orientation of the $\delta\phi_3$ deviation.

This implies that whenever the integration plane passes the Weyl point, the first Chern number is changed by $\Delta C^{12} = \frac{1}{2}\mathrm{sgn}(\delta\phi_3 \det T) - \frac{1}{2}\mathrm{sgn}(-\delta\phi_3 \det T) = \pm 1$. This manifest the the integer values of the topological charge. The integrated $B_{\alpha\beta}$ in Eq.(2.41) specifies the flux of the Berry field penetrating the plane which is either above or below the singularity point. This flux, owing to symmetry, is a half of the total flux, this explains the half-integer values. Therefore, the main contribution to Eq.(2.29) in the vicinity the Weyl point is given by the Berry curvatures of the two levels that are close to zero energy, and can be presented as

$$2\pi B_{\alpha\beta} = 2\pi i[\langle\partial_\alpha +|\ \partial_\beta +\rangle - \langle\partial_\alpha -|\ \partial_\beta -\rangle] \tag{2.42}$$

2.6.2. WEAK SPIN-ORBIT COUPLING

Let us turn on a weak spin-orbit interaction and take it into account perturbatively giving a small spin-dependent change to the scattering matrix that preserves its unitarity, as is done in [46]. The first order variation thus reads

$$\begin{aligned} S \to & e^{-i\delta\phi/2} S e^{i\vec{\sigma}\cdot\vec{K}} e^{i\delta\phi/2} \\ = & S + \delta_\phi S + iS(\vec{\sigma}\cdot\vec{K}) \end{aligned} \tag{2.43}$$

$$\begin{aligned} \Lambda = & S\sigma_y S^*\sigma_y \to \Lambda + \delta_\phi\Lambda + \delta_K\Lambda \\ = & \Lambda + \delta_\phi\Lambda + iS(\vec{\sigma}\cdot\vec{K})S^\dagger\Lambda + i\Lambda(\vec{\sigma}\cdot\vec{K}^*) \end{aligned} \tag{2.44}$$

where the last equality sign implies the commutation relation $\sigma_y\sigma_i^*\sigma_y = -\sigma_i$. Here, $\vec{\sigma}$ are the Pauli matrices in spin space and $\vec{K}$ being the corresponding Hermitian matrix in the channel space characterizing the spin-orbit effects. Owing to the time reversibility, $\vec{K}(\vec{\phi}) = -\vec{K}(-\vec{\phi})$, yet in the vicinity of the singularity we may disregard its dependence on superconducting phases.

As in the previous Subsection, we project the matrix Q onto singular subspace that has now dimension of 4 to account for spin, and replace it with the matrix M. Writing the latter in the basis of eigenvectors $|\pm\rangle|\uparrow(\downarrow)\rangle$:

$$M = \epsilon + \frac{1}{2}\delta\Lambda = \epsilon + \frac{i}{2}(\vec{h}\cdot\vec{\tau} - \vec{\sigma}\cdot\vec{K}') \tag{2.45}$$

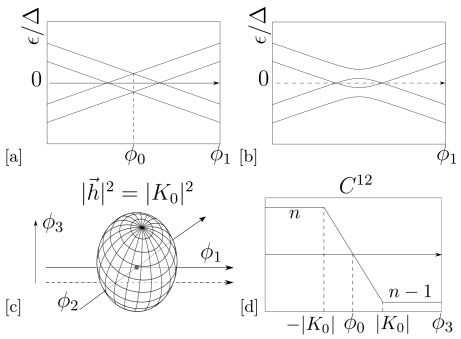

Figure 2.7: Spin-orbit splitting of Weyl singularity [a]: ABS energies versus ϕ_1 through the singularity for a choice $\phi_{2,3}$ corresponding to the singularity. The cone shifted upward(downward) specifies spin up (down). [b]: ABS energy with the same $\phi_{2,3}$ along the line ϕ_1 that misses the singularity. [c]: The ABS cross zero energy at the surface of the ellipsoid depicted. The ellipsoid encloses the singularity (central point). The ground state within the ellipsoid is of odd parity and the Berry curvature is zero. The central dot is the the Weyl singularity ϕ_0 enclosed in the ellipsoid. The ABS energies in [a,b] are plotted along the solid [a] and dashed [b]lines in the Figure. [d]: The "Chern number"C_{12} versus ϕ_3. The topological quantization is absent owing to the discontinuity of the ground state at the surface of the ellipsoid.

$\vec{K}' = \langle +|\vec{K}^*|+\rangle + \langle -|\vec{K}^*|-\rangle$. We can conveniently choose the spin quantization axis in the direction of $\vec{K}'$ replacing the operator $\vec{\sigma}\cdot\vec{K}'$ with its eigenvalues $\pm|K_0| = \pm\sqrt{|\vec{\sigma}\cdot\vec{K}'|}$ for spin up and down, respectively.

The spin-orbit coupling lifts the spin degeneracy of the ABS in the vicinity of a Weyl point. The poles at imaginary energies become $\epsilon_\uparrow = i(\pm\frac{|\vec{h}|}{2} + \frac{|K_0|}{2})$ for spin up and $\epsilon_\downarrow = i(\pm\frac{|\vec{h}|}{2} - \frac{|K_0|}{2})$ for spin down. Contrary to the spin-degenerate case, the singularities at $|\vec{h}| = 0$ are no longer at zero energy. Instead, they are shifted to $\pm i|K_0|$, see Fig. 2.7. The conical singularity of the spectrum remains and the topology is still protected, as we will explain below in detail.

The ABS energies cross zero energy when

$$|K_0| = |\vec{h}| = \sqrt{\sum \delta\phi_\alpha X_{\alpha\beta}\delta\phi_\beta} \tag{2.46}$$

is satisfied. (Here, we introduce a positively defined matrix $X_{\alpha\beta} = \sum_i T_{\alpha i}T_{i\beta}$. Eq.(2.46) defines an ellipsoidal surface in the 3D superconducting phase space that encloses the singularity at $\hat{\phi}_0$ where $|\vec{h}| = 0$. Outside the ellipsoid, two positive imaginary poles at $\epsilon_{+\uparrow(\downarrow)} = \frac{i}{2}(|\vec{h}| \pm |K_0|)$ hold a half of the residue of the spin degenerate pole ϵ_+ each. Two negative imaginary poles $\epsilon_{-\uparrow(\downarrow)}$ at $\epsilon_{-\uparrow(\downarrow)} = \frac{i}{2}(-|\vec{h}| \pm |K_0|)$ have the opposite residues. Inside the ellipsoid, poles of $\epsilon_{+\uparrow}$ and $\epsilon_{-\downarrow}$ exchange their values as well as wave functions, thus canceling the contributions from the other two poles. Thus, $B_{\alpha\beta}$ is zero inside the ellipsoid and is the same as in the spin-degenerate case outside the ellipsoid,

$$B^{\alpha\beta} = \begin{cases} \frac{\vec{h}}{4|\vec{h}|^3}\cdot\partial_\alpha\vec{h}\times\partial_\beta\vec{h} - [\alpha\leftrightarrow\beta], & |K_0| < |\vec{h}| \\ 0, & |K_0| > |\vec{h}| \end{cases} \tag{2.47}$$

The result of integration of B^{12} over two superconducting phases ϕ_1,ϕ_2 at a fixed $\delta\phi_3$ thus reads

$$C^{12} = \frac{1}{2\pi}\int \mathrm{d}\phi_1 \mathrm{d}\phi_2 B^{12}\theta(|\vec{h}| \geq |K_0|^2) \tag{2.48}$$

One can understand this result geometrically by presenting Eq. (2.48) as an integral over the corresponding plane in $\vec{h}$ space,

$$\begin{aligned} C^{12} &= \frac{1}{2\pi}\int_{|\vec{h}^2|>|K_0|^2} \Big(\frac{\vec{h}}{2|\vec{h}|^3}\cdot \hat{n}^h_{12}\Big)\mathrm{d}^2 h_{12} \\ &= \frac{\mathrm{sgn}(\delta\phi_3 \det T)}{4\pi}\int_{|\vec{h}^2|>|K_0|^2} \frac{\mathrm{d}^2 h_{12}}{h^2} \\ &= \frac{\mathrm{sgn}(\delta\phi_3 \det T)}{2}\frac{\Omega_{12}}{2\pi} \end{aligned} \tag{2.49}$$

where $\hat{n}^h_{12}$ is the vector normal of the corresponding plane and Ω_{12} is eventually the solid angle at which a part of the $\phi_1-\phi_2$ plane outside the ellipsoid is seen from the Weyl singularity (see Fig.2.7). Generally, this angle is expressed through elliptic integrals.

The integral can be simplified if we choose the coordinate system in 3D space of the phases in such a way that $T_{13} = T_{31} = T_{23} = T_{32} = 0$. With this, the integral can be evaluated as

$$\begin{aligned} C^{12} &= \frac{\mathrm{sgn}(\det T)\delta\phi_3}{2}\int_1^\infty \frac{(|K_0|^2 - T_{33}^2\delta\phi_3^2) r\,\mathrm{d}r}{[(|K_0|^2 - T_{33}^2\delta\phi_3^2)r^2 + T_{33}\delta\phi_3^2]^{\frac{3}{2}}} \\ &= \frac{1}{2}\mathrm{sgn}(\det T)\frac{\delta\phi_3}{|K_0|} \end{aligned} \tag{2.50}$$

We see that in the vicinity of a Weyl point the C^{12} is not a topologically protected quantity confined to the integer values: rather, it changes linearly in an interval of $\delta\phi_3$ defined by the strength of the spin-orbit coupling (Fig. 2.7)

To explain this, and eventually restore the topological protection of C_{12}, let us consider many-body states in the vicinity of the Weyl point. Their energies are given by the eigenvalues of the many-body Hamiltonian H_{MB}

$$H_{\mathrm{MB}} = E_\uparrow(\hat{n}_\uparrow - \frac{1}{2}) + E_\downarrow(\hat{n}_\downarrow - \frac{1}{2}) \tag{2.51}$$

where $E_{\uparrow(\downarrow)} = |\vec{h}| \pm |K_0|$ are the energies of quasiparticle excitations with spin up(down), $\hat{n}_{\uparrow(\downarrow)}$ are the number operators of the quasiparticles with the corresponding spin. The energy spectrum E_{MB} for each of the four possible states is given in Fig. 2.8. As we see from the Figure, the ground state of the superconducting nanostructure corresponds to $n_\uparrow = n_\downarrow = 0$ at $|\vec{h}| > |K_0|$ and to $n_\downarrow = 1, n_\uparrow = 0$ within the ellipsoid $|\vec{h}| < |K_0|$. These states differ in fermion parity, that is the conserving quantity for the superconducting Hamiltonian. This is why the parity transition that takes place at $|\vec{h}| = |K_0|$ is accompanied by the discontinuity of the wave functions, which violates the topological quantization of C^{12}. It is evident from Fig. 2.8 that the states of the odd fermion parity do not depend on phases in the vicinity of the Weyl point therefore corresponding to zero B^{12}.

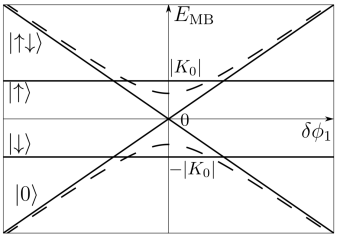

Figure 2.8: Many-body energy spectrum E_{MB} given by (2.51) corresponding to FIG. 2.7. The ground singlet state, single quasiparticle states of different spin and the excited singlet are labeled as $|0\rangle$, $|\downarrow(\uparrow)\rangle$ and $|\uparrow\downarrow\rangle$, respectively. The solid (dashed) lines correspond to the ABS plots FIG. 2.7 a (FIG. 2.7b). As the phase is varied, the ground state parity transition between $|0\rangle$ state and $|\downarrow\rangle$ state takes place at the point defined by (2.46).

The topological protection is restored if one considers the ground state at fixed parity. Then for the even ground state C^{12} is the same as for the spin-degenerate case and experiences an integer jump when the integration plane passes the singularity point. No change of topological charge occurs for the odd ground state and it remains topologically trivial.

2.7. ENERGY-DEPENDENT $S-$MATRIX:

In this Section we consider the effect of the energy dependence of the S-matrix on B_{12} given by (2.21) for arbitrary relation between the energy scales of the scattering matrix and the gap $|\Delta|$.

We make use of the following model scattering matrix:

$$S_\epsilon = \frac{i\epsilon - \mu - \mathscr{E}(\hat{H} + i\hat{\Gamma}/2)}{i\epsilon - \mu - \mathscr{E}(\hat{H} - i\hat{\Gamma}/2)}, \quad [\hat{H}, \hat{\Gamma}] = 0 \tag{2.52}$$

where $\hat{\Gamma}, \hat{H}$ are Hermitian dimensionless matrices with eigenvalues of the order of one. This expression can be regarded as a rather general polar decomposition of an energy-dependend scattering matrix. Since the matrices $\hat{\Gamma}, \hat{H}$ can be diagonalized simultaneously, the expession has poles at the complex energies $E = \mu + \mathscr{E}(H_n - i\Gamma_n/2)$ defined by the corresponding eigenvalues. The poles can be seen as the scattering resonances. The eigenvalues H_n set the energies of those resonances and the corresponding eigenvalues Γ_n give the inverse lifetimes of these resonances, Γ_n must be positive to assure the correct causal properties of the scatterimg. Real energy scale $\mathscr{E}$ then sets the typical spread of the poles in energy around their average position μ. We note that $S_\epsilon \to 1$ as $\epsilon \to \infty$, so the conditions of regularization described in a previous Section are fulfilled and the integral of B_{12} over a compact subspace in phase space that does not cross the Weyl singularities, reduces to an integer. We remind that the limit $S_\epsilon \to 1$ corresponds to isolated terminals. In distinction from the weak energy dependence case, the ABS energies defined by Eq. (2.1) can not be readily obtained and the resulting spectrum may

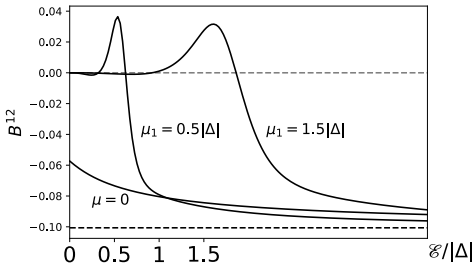

Figure 2.9: An example plot of B_{12} (Eq. 2.21 for a randomly chosen energy-dependent S versus the energy scale $\mathscr{E}$ for several choices of the energy scale μ at $\phi_1 = 0.22\pi, \phi_2 = -0.67\pi, \phi_3 = -\pi$. The dashed line gives the limiting value of B_{12} at $\mathscr{E} \gg |\Delta|$ where the energy dependence of the scattering matrix is weak.

be complicated with more ABS per transport channel. It is no more plausible to separate the contributions to $B_{\alpha\beta}$ coming from discrete and continuous spectrum. This, however, does not change the qualitative features of these contributions discussed above.

Let us consider and illustrate the dependence of B_{12} on these two energy scales. We choose random matrices $\hat{H}$, $\hat{\Gamma}$ that satisfy the conditions stated, and compute B_{12} from Eq. 2.21 at rather arbitrary settings of 3 phases. The integration over the imaginary energy in Eq. 2.21 permits the evaluation with no regard for the details of a complicated ABS spectrum. We plot the result versus the energy scale $\mathscr{E}$ at several settings of μ. (Fig. 2.9)

Let us consider $\mu \neq 0$ first. In this case, at $\mathscr{E} \to 0$ the transmission between the terminals is limited to a small circle of the radius $\simeq \mathscr{E}$ near μ. This suppresses the Andreev scattering that requires good transmission at opposite energies, and all quantities that depend on the phase differences including $B_{\alpha\beta}$. In Fig. 2.9, this is manifested as almost zero B_{12} at $\mathscr{E} < \mu$. The further increase of $\mathscr{E}$ restores the Andreev scattering bringing B_{12} to its typical values of $\sim (2\pi)^{-2}$. We note a non-monotonous dependence on $\mathscr{E}$ and explain it by the fact that different poles of the scattering matrix contribute to B_{12} with typically different signs, and the magnitude of the contribution depends on the position of the pole with respect to the energy scale $\simeq \Delta$. At $\mathscr{E} \gg \Delta$ the energy dependence of the scattering matrix is weak at $\epsilon \simeq \Delta$ and B_{12} saturates at a value that does not depend on μ and is given by Eqs. (2.29) and (2.33) (dashed line in the Figure 2.9).

The case of $\mu = 0$ is special at small $\mathscr{E}$ since the concentration of transmission in a small circle of energies does not suppress the Andreev scattering. The ABS in this case are concentrated in this small energy circle (see [47]) and depend on all phases. This is why B_{12} does not drop to 0 but rather approaches a finite limit at $\mathscr{E} \to 0$. At $\mathscr{E} \gg \Delta$ B_{12} still saturates at the value corresponding to the weak energy dependence case.

2.8. SUMMARY AND CONCLUSIONS

In this Chapter, we address the topological properties of multi-terminal superconducting nanostructures. This involves Berry curvatures in the parametric space of the superconducting phases of the terminals and associated Chern numbers that manifest themselves in quantized transconductances [33].

The specifics of the superconducting nanostuctures is the presence of continuous spectrum along with the discrete one. The Berry curvature is readily defined for a discrete spectrum. Its generalization for a (partly) continuous spectrum is not straightforward, and is a problem of general interest. It has not been solved in Ref. [33].

We perform the calculation in imaginary time, and model the nanostructure with an energy-dependend scattering matrix. We have derived a general action of superconducting nanostructure with time-dependent phases, this is a separate advance. We expand the action near a point in the space of phases to compute the response function at finite frequency. We define the tensor quantity $B_{\alpha\beta}$ (Eq. 2.21) as a first term in the expansion of the response function at small frequency. This quantity would have been Berry curvature if the spectrum were entirely discrete.

We analyze the topological properties of the computed quantity. Like for Berry curvature, the topological charge associated with divergence of $B_{\alpha\beta}$ is concentrated in the singular points of 3d phase space where ABS cross zero energy — Weyl points. Unlike Berry curvature, the quantity $B_{\alpha\beta}$ has a non-topological contribution that is constant over the space of phases (Eq. 2.27). This in general adds a non-quantized part to "Chern" numbers defined as integrals of $B_{\alpha\beta}$ over two superconducting phases, and to the corresponding transconductances. This contribution is determined by the scattering matrix at $\epsilon \to \infty$. It vanishes if the scattering matrix without superconducting phases is time-reversible and if the scattering matrix approaches isolation limit $S_c = 1$ at large energies. For an energy-independent scattering matrix, the non-topological term is associated with the anti-symmetrized part of the conductance matrix of the structure in the normal state.

We consider in detail the case of weak energy dependence of the scattering matrix. We separate the contributions of the discrete and continuous spectrum, find them equally important and derive a compact relation for $B_{\alpha\beta}$ (Eq. 2.29).

We analyze in detail the Berry curvature in the vicinity of Weyl points. We have found a violation of topological protection of "Chern" number in case of weak spin-orbit coupling. This, however, is rather trivially related to the transition between the ground states of different parity near the Weyl point and associated discontinuity of the wave functions. The topological protection is restored if one considers a ground state of a fixed parity.

We also investigate the properties of $B_{\alpha\beta}$ for the scattering matrices that essentially depend on energy at the energy scale $\simeq \Delta$.

2.9. APPENDIX A: DERIVATION OF THE ACTION

In this Appendix, we derive the effective action for a multi-terminal superconducting junction within the scattering approach. We follow the lines of Ref.[48]. In contrast to Ref.[48] we proceed in Matsubara formalism. Let us start with the formulation of a concrete microscopic model. Since the scattering formalism is universal, there is a great degree of arbitrariness in the choice of the model: all models that are characterized by the same scattering matrix will result in the same action. Properties of the scatterer are to be completely described by an S-matrix, the details of the model that describes the system are not important. So we choose the model in a way we find it convenient (see Fig. 2.10). We consider a system of independent 1-dimensional channels with pairwise op-

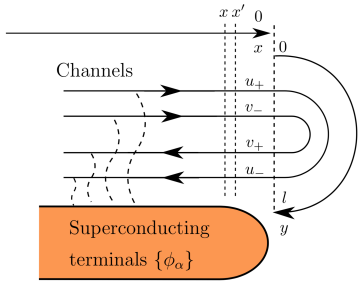

Figure 2.10: The concrete model for the derivation of the action. The electons are moving in $2N$ spin-degenerate channels connected to the corresponding superconducting terminals by tunneling (wavy dashed lines). In the picture, all the terminals in Eq.2.1 are combined into a single superterminal for convenience. Right of the vertical line, the tunnelling between the channels provides the scattering described by $N \times N$ matrix.

posite velocities and a linear spectrum. They are defined in the interval $-\infty < x < 0$. The total number of channels is $2N$, number N includes the spin doubling. Two channels in a pair with opposite velocities are coupled to the same superconducting reservoir: this is required to assure the time-reversibility of the model at this level. The coupling is a tunnel one, and the coupling strength is characterized by the dwell time scale τ: at this time scale, an electron in a channel would tunnel to a reservoir. The tunneling results in an addition of self-energy to Green's functions in the channels, which is proportional to the tunneling rate $1/\tau$ and to a matrix Green's function g characterizing a reservoir (see its concrete definition below). The channels defined in such a way model the electron states coming from and going to the reservoirs that are scattered at the nanoscructure. In the scattering region with a coordinate $y \in [0, l]$, there are N spin-degenerate channels of the same velocity direction. At the boundary $y = 0$ the electron amplitudes in the channels match those in the channels of positive velocity at $x = 0$ (incoming states), while at $y = l$ the amplitudes match those in the channels with the negative velocity(outgoing states). As we will show, the S-matrix relates the amplitudes at $y = l$ and $y = 0$.

To find the action for the nanostructure, we will compute its variation with respect to the variation of g. To this end, we require the values of the Green's functions in the channels $x, x' < 0$ in close points $x \approx x'$. We find the variation in three steps. At the first step, we express the Green's functions at any x in terms of the Green's functions at $x \approx 0$. At the second step, we consider the scattering region that provides a boundary condition. With this, we relate these Green's functions, and solve for them. This permits to find the variation and the action at the third step.

In the channels, we choose the basis in the following form

$$\begin{pmatrix} u_+ \\ v_- \\ u_- \\ v_+ \end{pmatrix} \tag{2.53}$$

where $u_\pm, v_\pm$ are N vectors in the space of the channels associated with the electron and hole amplitudes of the Bogolyubov wave function, and $\pm$ refers to the sign of the velocity

in corresponding channels. In this basis, the equation for Green's function reads

$$\left(i\epsilon\tau_3 + i\upsilon\eta_3\tau_3\partial_x + \frac{i}{2\tau}g\right)G_{\mathrm{Ch}}(x,x') = \delta(x-x') \tag{2.54}$$

where υ is the velocity that we can set the same for all the channels, ϵ is the Matsubara frequency, τ_i are Pauli matrices in Nambu space, and $\eta_3 = \pm$ distinguishes channels with positive and negative velocities. The matrix g is block-diagonal in the channel space. For a given reservoir, it is given by

$$g = \frac{1}{\sqrt{\epsilon^2+|\Delta|^2}}(\epsilon\tau_3 + i\sigma_2[\tau_1(\frac{\Delta-\Delta^*}{2}) + i\tau_2(\frac{\Delta+\Delta^\star}{2})]), \tag{2.55}$$

$g^2 = 1$, Δ being the superconducting order parameter in the corresponding reservoir.

We define a block structure

$$G_{\mathrm{Ch}} = \begin{pmatrix} G_1 & G_3 \\ G_4 & G_2 \end{pmatrix} \tag{2.56}$$

We are only interested in the diagonal blocks $G_{1;2}$ since the off-diagonal blocks will not contribute to the variation of the action. We integrate the equation assuming $\epsilon\tau \ll 1$ for $G(x,x')$ at $x < x'$ we obtain

$$G_1(x,x') = [(\frac{1-g}{2}e^{\frac{(x-x')}{2\upsilon\tau}} + \frac{1+g}{2}e^{-\frac{(x-x')}{2\upsilon\tau}})]G_1^-(x') \tag{2.57}$$

$$G_2(x,x') = [(\frac{1+g}{2}e^{\frac{(x-x')}{2\upsilon\tau}} + \frac{1-g}{2}e^{-\frac{(x-x')}{2\upsilon\tau}})]G_2^-(x') \tag{2.58}$$

where we use special notations for the Green's functions in the close points

$$G_1^-(x') = G_1(x'-0,x'), \quad G_2^-(x') = G_2(x'-0,x') \tag{2.59}$$

Since the solution for the Green's function should not grow $x \to -\infty$, these Green's functions should satisfy the following conditions

$$\Pi_+ G_1^- = 0, \quad \Pi_+ = \frac{1+g}{2}, \quad G_1^- = \lim_{x'\to-0} G_1^-(x') \tag{2.60}$$

$$\Pi_- G_2^- = 0, \quad \Pi_- = \frac{1-g}{2}, \quad G_2^- = \lim_{x'\to-0} G_2^-(x') \tag{2.61}$$

These matrices $G_{1;2}^-$ can be fixed if we consider the boundary conditions, that can be obtained by solving the equations for the Green's functions in the the scattering region $y \in [0;l]$. To derive these condition, let us introduce the amplitude vectors $\Psi(y) = G(y,x)$, $X(y) = G(x,y)$ that have Nambu structure $\begin{pmatrix} u(y) \\ v(y) \end{pmatrix}$ and satisfy the equations

$$\left(i\epsilon\tau_3 + i\upsilon\tau_3\partial_y - \begin{pmatrix} U(y) & 0 \\ 0 & U^T(y) \end{pmatrix}\right)\Psi(y) = 0 \tag{2.62}$$

$$\left(i\epsilon\tau_3 - i\upsilon\tau_3\partial_{y'}\right)X(y') - X(y')\begin{pmatrix} U(y') & 0 \\ 0 & U^T(y') \end{pmatrix} = 0 \tag{2.63}$$

where $U(y,\epsilon)$ is the $N \times N$ matrix potential acting on electrons inside the scattering region and mixing different channels. The solution of the Eq.(2.63) gives a linear relation on the amplitudes

$$X(y=l) = X(y=0)\hat{S}^{\dagger}_{-\epsilon} \tag{2.64}$$

where we define the S-matrix for electrons and holes arranged in Nabmu structure

$$\hat{S}_{\epsilon} = \begin{pmatrix} S_e(\epsilon) & 0 \\ 0 & (S_h(\epsilon))^{-1} \end{pmatrix} \tag{2.65}$$

$$(S_h(\epsilon))^{-1} \equiv S^{T}_{-\epsilon}. \tag{2.66}$$

The electron scattering matrix is given by

$$S_e(\epsilon) = S_{\epsilon} = e^{-\frac{\epsilon l}{v}} \times T_y e^{-\frac{i}{v}\int_0^l dy U(y,\epsilon)} \tag{2.67}$$

where T_y implies the ordering of the $U(y)$ operators in the exponent according to the values of y in the increasing order. We do not need to specify the energy dependence fo the S-matrix except for the general condition $S_{\epsilon}S^{\dagger}_{-\epsilon} = 1$.

The relation on the amplitude (2.64) gives the relation between the diagonal and off-diagonal blocks of the Green's function (2.56) outside the scattering region but close to it $|x\epsilon/v| \ll 1, |x'\epsilon/v| \ll 1$

$$G_3(x,x) = G_1(x,x')\hat{S}^{\dagger}_{-\epsilon} = G^{-}_1\hat{S}^{\dagger}_{-\epsilon}, \quad (x<x') \tag{2.68}$$

The solution of Eq. (2.62)

$$\Psi(y=l) = \hat{S}_{\epsilon}\Psi(y=0) \tag{2.69}$$

yields another relation between the blocks

$$G_2(x',x) = G^{+}_2 = \hat{S}_{\epsilon}G_3(x,x), \quad (x<x') \tag{2.70}$$

Combining Eq. (2.70) and (2.68) we obtain the required boundary condition that relates the diagonal sub-blocks

$$\hat{S}_{\epsilon}G^{-}_1\hat{S}^{\dagger}_{-\epsilon} = G^{+}_2 \tag{2.71}$$

Combining the equations (2.71), (2.60) and (2.61), and the condition

$$G^{+}_{\mathrm{Ch}} - G^{-}_{\mathrm{Ch}} = -\frac{i}{v}\tau_3\eta_3 \tag{2.72}$$

that follows directly from (2.54) we solve the complete linear system of the equations to obtain the follwing for the diagonal blocks of the general Green's function (2.56)

$$G^{-}_1 = \frac{i}{v}\frac{1}{\Pi_+ + \Pi_-\hat{S}_{\epsilon}}\Pi_-\hat{S}_{\epsilon}, \quad G^{+}_1 = \frac{-i}{v}\frac{1}{\Pi_+ + \Pi_-\hat{S}_{\epsilon}}\Pi_+ \tag{2.73}$$

$$G^{-}_2 = \frac{-i}{v}\frac{1}{\Pi_- + \Pi_+\hat{S}^{\dagger}_{-\epsilon}}\Pi_+\hat{S}^{\dagger}_{-\epsilon}, \quad G^{+}_2 = \frac{i}{v}\frac{1}{\Pi_- + \Pi_+\hat{S}^{\dagger}_{-\epsilon}}\Pi_- \tag{2.74}$$

Next, we employ the formula that expresses the action variation in terms of Green's functions. We vary the reservoir Green's function g keeping normalization $g^2 = 1$, so that $\{g, \delta g\} = 0$, then the variation of the action L is

$$\delta L = \int dx \mathrm{Tr}[\delta\Sigma(x) G_{\mathrm{Ch}}(x,x)] \tag{2.75}$$

where $\delta\Sigma = \frac{-i}{2\tau}\delta g$ is the variation of self-energy of electrons in channels and $G_{\mathrm{Ch}}(x,x)$ is their Green's function at coinciding points. We note here that indeed only the diagonal blocks $G_{1;2}$ in Eq.(2.56) contribute since Σ is diagonal in this basis. The contribution from the channels corresponding to G_1 gives

$$2\delta L_{in} = + \int_{-\infty}^{0} dx \mathrm{Tr}[\delta\Sigma G_{\mathrm{Ch}}(x,x)] =$$

$$= \frac{-i}{2\tau}\int_{-\infty}^{0} dx \mathrm{Tr}[\delta g G_{\mathrm{Ch}}(x,x)] = \frac{-1}{2}\mathrm{Tr}[\delta g \frac{1}{\Pi_+ + \Pi_- \hat{S}_\epsilon}\Pi_+] \tag{2.76}$$

The futher calculations is convenient to do in the basis that diagonalizes g. In this basis,

$$\delta g = \begin{pmatrix} 0 & V \\ W & 0 \end{pmatrix}, \quad g = \begin{pmatrix} 1 & 0 \\ 0 & -1 \end{pmatrix}, \quad \hat{S} = \begin{pmatrix} S_1 & S_2 \\ S_3 & S_4 \end{pmatrix}$$

$$Y^{-1}(g + \delta g)Y = g, \quad Y(\hat{S} + \delta\hat{S})Y^{-1} = \hat{S} \tag{2.77}$$

we find

$$Y = \begin{pmatrix} 1 & \frac{-V}{2} \\ \frac{W}{2} & 1 \end{pmatrix}, \quad \delta S_4 = -S_3\frac{V}{2} - \frac{W}{2}S_2$$

$$2\delta L_{in} = \frac{1}{2}\mathrm{Tr} V S_4^{-1} S_3 \tag{2.78}$$

where all the realtions are valid up to the first order in variations. The contribution from the outgoing channels reads

$$2\delta L_{out} = \frac{1}{2}\mathrm{Tr}[\delta g \frac{1}{\Pi_- + \Pi_+ \hat{S}_{-\epsilon}^\dagger}\Pi_-] =$$

$$= \frac{1}{2}\mathrm{Tr}[\delta g S_\epsilon \frac{1}{\Pi_- S_\epsilon + \Pi_+}\Pi_-] = \frac{1}{2}\mathrm{Tr} W S_2 S_4^{-1} \tag{2.79}$$

Summing both contributions, we obtain

$$2\delta L = -\mathrm{Tr}[\delta S_4 S_4^{-1}] \tag{2.80}$$

Hence

$$2L = -\mathrm{Tr}\log S_4 = -\mathrm{Tr}\log[\Pi_+ + \Pi_- \hat{S}_\epsilon] \tag{2.81}$$

This so-called block-determinant result for the action is similar to the one obtained previously [48] within the Keldysh formalism.

2.10. APPENDIX B: DERIVATION OF THE RESPONSE FUNCTION

In this Appendix, we present the details of the derivation of the Eq.(2.18) and Eq.(2.21). We start with the action as given by Eq. (2.6). In order to derive the response function, we assume that the time-dependent deviation ($\delta\phi(\tau)$) from the stationary phase denoted as ϕ is small ($\delta\phi(\tau) \ll 2\pi$) so we can expand the action in Taylor series in $\delta\phi(\tau)$. We also note that in time representation the total phase operator is diagonal ($\phi_{\tau\tau'} = \delta_{\tau\tau'}\phi(\tau)$), which implies that the energy representation of ϕ reads

$$\phi_{nm} = \phi(\omega), \quad \omega = \epsilon_n - \epsilon_m \tag{2.82}$$

We consider here the general case of the energy-dependent scattering matrix. The action from Eq.(2.6) reads

$$-2L = \mathrm{Tr}\log[B + B^T], \quad B = A_\epsilon e^{\frac{-i\phi}{2}} S_\epsilon e^{\frac{i\phi}{2}} A_\epsilon \tag{2.83}$$

T implies the complete operator transposition that includes the reversing of the sign of energy. We remind the definition

$$A_\epsilon = \sqrt{\frac{E+\epsilon}{2E}}, \quad E = \sqrt{\epsilon^2 + |\Delta|^2}, \tag{2.84}$$

We ascribe the stationary part of the phases to an S-matrix $S_\epsilon \to S_\epsilon(\phi)$ and expand in small nonstationary deviation $\delta\phi(\tau)$.

$$B \simeq B_0 + B_1 + B_2 = B_0 + \frac{\partial B}{\partial \phi^\alpha_\omega}\delta\phi^\alpha_\omega + \frac{1}{2}\frac{\partial^2 B}{\partial\phi^\alpha_\omega \partial\phi^\beta_{-\omega}}\delta\phi^\alpha_\omega \delta\phi^\beta_{-\omega} \tag{2.85}$$

We introduce

$$Q_\epsilon = B_0 + B_0^T = A_\epsilon^2 S_\epsilon + A^2_{-\epsilon} S^T_{-\epsilon} \tag{2.86}$$

With this,

$$\delta\mathrm{Tr}\log[B + B^T] \simeq \mathrm{Tr}Q^{-1}(B_1 + B_1^T + B_2 + B_2^T) - \frac{1}{2}\mathrm{Tr}Q^{-1}(B_1 + B_1^T)Q^{-1}(B_1 + B_1^T). \tag{2.87}$$

We remind the definition of the matrix, that projects on the channels connected to a given terminal α:

$$(I^\alpha)^{ab} = \delta^{ab}\begin{cases} 1, & a = \alpha \\ 0, & a \neq \alpha \end{cases} \tag{2.88}$$

where a, b indices are in channels. With the help of this matrix the phase variation can be conveniently expressed as

$$(\delta\phi^\alpha)^{ab} = (I^\alpha)^{ab}\delta\phi^\alpha(\tau) \tag{2.89}$$

For simplicity of the notations, we denote the stationary phase derivatives $\partial_{\phi_\alpha} = \partial_\alpha$. With all this we consider the expansion of the S-matrix

$$e^{\frac{-i\delta\phi(\tau)}{2}} S_\epsilon e^{\frac{i\delta\phi(\tau)}{2}} \simeq S_\epsilon + [S_\epsilon, \frac{i\delta\phi(\tau)}{2}] + \frac{\delta\phi(\tau)}{2} S_\epsilon \frac{\delta\phi(\tau)}{2} - \\ - \frac{1}{2}\{(\frac{\delta\phi(\tau)}{2})^2, S_\epsilon\} \tag{2.90}$$

Let us we also note the identities for the derivatives with respect to the stationary phases:

$$\frac{\partial S}{\partial \alpha} = [S, \frac{iI_\alpha}{2}] \tag{2.91}$$

$$\frac{\partial^2 S}{\partial \alpha \partial \beta} = \frac{I_\alpha}{2} S \frac{I_\beta}{2} + \frac{I_\beta}{2} S \frac{I_\alpha}{2} - \delta_{\alpha\beta}\{\frac{I_\alpha}{4}, S\} \tag{2.92}$$

the first term in the expansion (2.87) vanishes since $\delta\phi_{\omega=0} = 0$. The second term is

$$\begin{aligned}
&\mathrm{Tr}Q^{-1}(B_2 + B_2^T) = 2\mathrm{Tr}Q^{-1}B_2 = \\
&\delta\phi^\alpha_\omega \delta\phi^\beta_{-\omega} \int \frac{d\epsilon}{2\pi} \mathrm{Tr}Q_\epsilon^{-1} A_\epsilon^2 [-\delta_{\alpha\beta}\{\frac{I_\alpha}{4}, S_\epsilon\} + \\
&+ \frac{I_\alpha}{2} S_{\epsilon-\omega} \frac{I_\beta}{2} + \frac{I_\beta}{2} S_{\epsilon+\omega} \frac{I_\alpha}{2}] = \\
&= \frac{\delta\phi^\alpha_\omega \delta\phi^\alpha_{-\omega}}{2} \int \frac{d\epsilon}{2\pi} \mathrm{Tr}Q_\epsilon^{-1} [\frac{\partial^2 Q_\epsilon}{\partial\alpha\partial\beta}] + \\
&\delta\phi^\alpha_\omega \delta\phi^\alpha_{-\omega} \int \frac{d\epsilon}{2\pi} \mathrm{Tr}Q_\epsilon^{-1} A_\epsilon^2 [\frac{I_\alpha}{2}(S_{\epsilon-\omega} - S_\epsilon)\frac{I_\beta}{2} + \\
&\frac{I_\beta}{2}(S_{\epsilon+\omega} - S_\epsilon)\frac{I_\alpha}{2}]
\end{aligned} \tag{2.93}$$

The first term here does not depend on frequency and does not vanish in the limit $\omega \to 0$. The second term up to linear order in ω can be rewritten as

$$\begin{aligned}
&2\omega\delta\phi^\alpha_\omega \delta\phi^\alpha_{-\omega} \int \frac{d\epsilon}{2\pi} \mathrm{Tr}[Q_\epsilon^{-1} A_\epsilon^2 \frac{I_\beta}{2} \frac{\partial S_\epsilon}{\partial \epsilon} \frac{I_\alpha}{2}] = \\
&\omega\delta\phi^\alpha_\omega \delta\phi^\alpha_{-\omega} \int \frac{d\epsilon}{2\pi} \mathrm{Tr}Q_\epsilon^{-1} A_\epsilon^2 \partial_\beta \{\frac{\partial S_\epsilon}{\partial \epsilon}, \frac{iI_\alpha}{2}\}
\end{aligned} \tag{2.94}$$

The second term in the expansion (2.87) reads

$$\begin{aligned}
&-\frac{1}{2}\mathrm{Tr}Q^{-1}(B_1 + B_1^T)Q^{-1}(B_1 + B_1^T) = \\
&\frac{-\delta\phi^\alpha_\omega \delta\phi^\beta_{-\omega}}{2} \int \frac{d\epsilon}{2\pi} \mathrm{Tr}Q_1^{-1}(A_{-1}(\frac{iI_\alpha}{2} S^T_{-2} - S^T_{-1}\frac{iI_\alpha}{2})A_{-2} - \\
&A_1(\frac{iI_\alpha}{2} S_2 - S_1 \frac{iI_\alpha}{2})A_2) Q_2^{-1}(A_{-2}(\frac{iI_\beta}{2} S^T_{-1} - \\
&S^T_{-2}\frac{iI_\beta}{2})A_{-1} - A_2(\frac{iI_\beta}{2} S_1 - S_2 \frac{iI_\beta}{2})A_1)
\end{aligned} \tag{2.95}$$

where subscripts mean taking the function at the frequency $\epsilon_{1,2}$: $\epsilon_1 = \epsilon_2 + \omega$ and we denoted $\epsilon_2 = \epsilon$. Summing it with (2.93) we get the general response function as in Eq. (2.18).

To perform the adiabatic expansion in the small parameter $\omega/|\Delta|$ here we keep ω as an independent parameter. We will use the identities

$$\frac{iI_\alpha}{2} S_2 - S_1 \frac{iI_\alpha}{2} = -\frac{\partial S_{cl}}{\partial \alpha} - \{S_q, \frac{iI_\alpha}{2}\} \tag{2.96}$$

where we introduced "classical" and "quantum" S-matrices as

$$S_{cl} = \frac{S_1 + S_2}{2}, \quad S_q = \frac{S_1 - S_2}{2} \tag{2.97}$$

With this, we rewrite the term

$$\begin{aligned} &\frac{-\delta\phi^{\alpha}_{\omega}\delta\phi^{\beta}_{-\omega}}{2}\int\frac{d\epsilon}{2\pi}\mathrm{Tr}Q_1^{-1}[A_1A_2(\frac{\partial S_{cl}}{\partial\alpha}+\{S_q,\frac{iI_\alpha}{2}\})+\\ &A_{-1}A_{-2}(\frac{\partial S^T_{cl}}{\partial\alpha}-\{S_q,\frac{iI_\alpha}{2}\})]Q_2^{-1}[A_1A_2(\frac{\partial S_{cl}}{\partial\alpha}-\{S_q,\frac{iI_\alpha}{2}\})\\ &+A_{-1}A_{-2}(\frac{\partial S^T_{cl}}{\partial\alpha}+\{S_q,\frac{iI_\alpha}{2}\})] \end{aligned} \tag{2.98}$$

Next, we expand the terms that are taken at $\epsilon_1 = \epsilon_2 + \omega$. Thery come from three factors here. The expansion of the first factor $Q_1^{-1} \simeq Q_2^{-1} + \omega\frac{\partial Q_\epsilon^{-1}}{\partial\epsilon}$ gives rise to

$$\frac{\omega}{2}\delta\phi^{\alpha}_{\omega}\delta\phi^{\beta}_{-\omega}\int\frac{d\epsilon}{2\pi}\mathrm{Tr}Q_\epsilon^{-1}\frac{\partial Q_\epsilon}{\partial\epsilon}Q_\epsilon^{-1}\frac{\partial Q_\epsilon}{\partial\alpha}Q_\epsilon^{-1}\frac{\partial Q_\epsilon}{\partial\beta} \tag{2.99}$$

The expansion of the product of the classical parts is symmetric with respect to α,β, so it vanishes. The product of quantum parts vanishes in linear order in ω. So we only need to consider quantum times classical and expand the quantum one

$$S_q \simeq \frac{\omega}{2}\frac{\partial S_\epsilon}{\partial\epsilon} \tag{2.100}$$

it yields

$$\begin{aligned} &-\frac{2}{2}\delta\phi^{\alpha}_{\omega}\delta\phi^{\beta}_{-\omega}\int\frac{d\epsilon}{2\pi}\mathrm{Tr}Q^{-1}\frac{\omega}{2}(A^2_\epsilon\{\frac{iI_\alpha}{2},\frac{\partial S_\epsilon}{\partial\epsilon}\}-\\ &-A^2_{-\epsilon}\{\frac{iI_\alpha}{2},\frac{\partial S^T_{-\epsilon}}{\partial\epsilon}\})\frac{\partial Q}{\partial\beta}Q^{-1}=\\ &=\omega\delta\phi^{\alpha}_{\omega}\delta\phi^{\beta}_{-\omega}\int\frac{d\epsilon}{2\pi}\mathrm{Tr}\frac{\partial Q^{-1}}{\partial\beta}A^2_\epsilon\{\frac{\partial S_\epsilon}{\partial\epsilon},\frac{iI_\alpha}{2}\} \end{aligned} \tag{2.101}$$

where the first doubling is due to the same contribution with $\alpha \leftrightarrow \beta$. Summing it with (2.94) we obtain the total response function as given by (2.21)

$$\begin{aligned} &-\frac{2_S}{2}\omega\delta\phi^{\alpha}_{\omega}\delta\phi^{\beta}_{-\omega}\int\frac{d\epsilon}{2\pi}(\frac{1}{2}\mathrm{Tr}Q_\epsilon^{-1}\frac{\partial Q_\epsilon}{\partial\epsilon}Q_\epsilon^{-1}\frac{\partial Q_\epsilon}{\partial\alpha}Q_\epsilon^{-1}\frac{\partial Q_\epsilon}{\partial\beta}+\\ &\frac{\partial}{\partial\beta}\mathrm{Tr}[Q_\epsilon^{-1}A^2(\epsilon)\{\frac{\partial S_\epsilon}{\partial\epsilon},\frac{iI_\alpha}{2}\}]) \end{aligned} \tag{2.102}$$

2.11. ACKNOWLEDGEMENTS

This project was supported by the Netherlands Organization for Scientific Research (NWO/OCW), as part of the Frontiers of Nanoscience (NanoFront) program, and has received funding from the European Research Council (ERC) under the European Union's Horizon 2020 research and innovation programme (Grant Agreement No. 694272).

REFERENCES

[1] C. Xu and L. Balents, Phys. Rev. Lett. **121**, 087001 (2018).

[2] S. Yao and Z. Wang, Phys. Rev. Lett. **121**, 086803 (2018).

[3] M. J. Pacholski, C. W. J. Beenakker, and i. d. I. Adagideli, Phys. Rev. Lett. **121**, 037701 (2018).

[4] M. S. Hossain, M. K. Ma, M. A. Mueed, L. N. Pfeiffer, K. W. West, K. W. Baldwin, and M. Shayegan, Phys. Rev. Lett. **120**, 256601 (2018).

[5] X. Tan, D.-W. Zhang, Q. Liu, G. Xue, H.-F. Yu, Y.-Q. Zhu, H. Yan, S.-L. Zhu, and Y. Yu, Phys. Rev. Lett. **120**, 130503 (2018).

[6] M. R. Brems, J. Paaske, A. M. Lunde, and M. Willatzen, Phys. Rev. B **97**, 081402 (2018).

[7] C.-C. Tang, K. Ikushima, D. C. Ling, C. C. Chi, and J.-C. Chen, Phys. Rev. Applied **8**, 064001 (2017).

[8] M. Götte, T. Paananen, G. Reiss, and T. Dahm, Phys. Rev. Applied **2**, 054010 (2014).

[9] J. Maciejko, E.-A. Kim, and X.-L. Qi, Phys. Rev. B **82**, 195409 (2010).

[10] H. Chen, W. Zhu, D. Xiao, and Z. Zhang, Phys. Rev. Lett. **107**, 056804 (2011).

[11] C. Nayak, S. H. Simon, A. Stern, M. Freedman, and S. Das Sarma, Rev. Mod. Phys. **80**, 1083 (2008).

[12] D. Aasen, M. Hell, R. V. Mishmash, A. Higginbotham, J. Danon, M. Leijnse, T. S. Jespersen, J. A. Folk, C. M. Marcus, K. Flensberg, and J. Alicea, Phys. Rev. X **6**, 031016 (2016).

[13] C. L. Kane and E. J. Mele, Phys. Rev. Lett. **95**, 226801 (2005).

[14] C. Wu, B. A. Bernevig, and S.-C. Zhang, Phys. Rev. Lett. **96**, 106401 (2006).

[15] L. Fu, C. L. Kane, and E. J. Mele, Phys. Rev. Lett. **98**, 106803 (2007).

[16] X.-L. Qi, T. L. Hughes, S. Raghu, and S.-C. Zhang, Phys. Rev. Lett. **102**, 187001 (2009).

[17] X.-L. Qi, T. L. Hughes, and S.-C. Zhang, Phys. Rev. B **82**, 184516 (2010).

[18] A. Das, Y. Ronen, Y. Most, Y. Oreg, M. Heiblum, and H. Shtrikman, Nature Physics **8**, 887 EP (2012).

[19] L. Fu and E. Berg, Phys. Rev. Lett. **105**, 097001 (2010).

[20] F. D. M. Haldane, Phys. Rev. Lett. **61**, 2015 (1988).

[21] N. Regnault and B. A. Bernevig, Phys. Rev. X **1**, 021014 (2011).

[22] Y. Zhang and X.-L. Qi, Phys. Rev. B **89**, 195144 (2014).

[23] T. Thonhauser and D. Vanderbilt, Phys. Rev. B **74**, 235111 (2006).

[24] X.-L. Qi and S.-C. Zhang, Rev. Mod. Phys. **83**, 1057 (2011).

[25] J. E. Moore and L. Balents, Phys. Rev. B **75**, 121306 (2007).

[26] E. Witten, Nuclear Physics B **223**, 422 (1983).

[27] Z. Wang, X.-L. Qi, and S.-C. Zhang, Phys. Rev. Lett. **105**, 256803 (2010).

[28] Z. Wang, X.-L. Qi, and S.-C. Zhang, New Journal of Physics **12**, 065007 (2010).

[29] A. M. Essin and V. Gurarie, Phys. Rev. B **84**, 125132 (2011).

[30] Q. Niu, D. J. Thouless, and Y.-S. Wu, Phys. Rev. B **31**, 3372 (1985).

[31] D. J. Thouless, M. Kohmoto, M. P. Nightingale, and M. den Nijs, Phys. Rev. Lett. **49**, 405 (1982).

[32] F. R. S. M. V. Berry, Proceedings of the Royal Society of London A: Mathematical, Physical and Engineering Sciences **392**, 45 (1984).

[33] R.-P. Riwar, M. Houzet, J. S. Meyer, and Y. V. Nazarov, Nature Communications **7**, 11167 EP (2016).

[34] A. Andreev, Sov. Phys. JETP **19**, 1228 (1964).

[35] P. de Gennes and D. Saint-James, Physics Letters **4**, 151 (1963).

[36] C. W. J. Beenakker and H. van Houten, Phys. Rev. Lett. **66**, 3056 (1991).

[37] A. Kitaev, AIP Conference Proceedings **1134**, 22 (2009).

[38] L. Lu, Z. Wang, D. Ye, L. Ran, L. Fu, J. D. Joannopoulos, and M. Soljačić, Science **349**, 622 (2015).

[39] A. A. Soluyanov, D. Gresch, Z. Wang, Q. Wu, M. Troyer, X. Dai, and B. A. Bernevig, Nature **527**, 495 EP (2015).

[40] Y. Nazarov and Y. Blanter, *Quantum Transport* (Cambridge University Press, 2009).

[41] G. Schön and A. Zaikin, Physics Reports **198**, 237 (1990).

[42] C. W. J. Beenakker, Rev. Mod. Phys. **69**, 731 (1997).

[43] G. Eilenberger, Zeitschrift für Physik A Hadrons and nuclei **214**, 195 (1968).

[44] X. Qi, T. Hughes, and S. Zhang, Phys. Rev. B **78** (2008), 10.1103/PhysRevB.78.195424.

[45] R. Landauer, IBM Journal of Research and Development **1**, 223 (1957).

[46] T. Yokoyama and Y. V. Nazarov, Phys. Rev. B **92**, 155437 (2015).

[47] A. A. Golubov, M. Y. Kupriyanov, and E. Il'ichev, Rev. Mod. Phys. **76**, 411 (2004).

[48] Y. V. Nazarov, Physica E: Low-dimensional Systems and Nanostructures **74**, 561 (2015).

3

TOPOLOGICAL NUMBERS OF QUANTUM SUPERPOSITIONS OF TOPOLOGICALLY NON-TRIVIAL BANDS

Topological properties of the wavefunction manifolds - bands are in focus of modern condensed matter research. In this Article, we address the definition and values of topological numbers of quantum superpositions of the topologically distinct bands. The problem, although simple in essence, can be formulated as a paradox: it may seem that quantum superposition implies non-integer topological numbers.

We show that the results are different for superpositions that are created dynamically and for those obtained by stationary mixing of the bands. For dynamical superpositions, we have found that an observable commonly witnessing a topological number is non-integer indeed. For static superpositions, the resulting bands retain integer topological numbers. We illustrate how the quantization of topological number is restored upon avoided crossing of topologically distinct subbands. The band crossings may result in the exchange of topological numbers between the bands upon changing the parameters describing the bandstructure. This is a phase transition between the phases defined as sequences of topological numbers of the bands. We consider complex phase diagrams arising in this context and show the absence of triple critical points and abundance of quadruple critical points that are rare in common phase diagrams. We illustrate these features with a bilayer Haldane model.

arxiv:1905.12376, submitted to PRB; http://doi.org/10.5281/zenodo.4377127

3.1. INTRODUCTION

The notion of the topology of the wavefunction manifolds has been being discussed for many years (see e.g. Refs.[1, 2]). In addition to the topological applications in the fields such as cosmology[3], quantum field theory[4], classical integrable Hamiltonian dynamics[5], etc. it has also been understood that the topology may play an important role in condensed matter[6], in particular in the quantum description of crystal solids[7, 8]. The Chern insulator[9] is an example of such an application. Let us describe the simplest case of a 2-dimensional Chern insulator. The Hamiltonian of this periodic solid is a matrix defined in the compact space of two quasimomenta q_α, $\alpha = 1,2$ and is continuous. The eigenbasis of the Hamiltonian is also parameter-dependent and the resulting manifolds of parameter-dependent wavefunctions that belong to a certain eigenvalue are usually called bands. It is important to note that continuity of the Hamiltonian does not immediately imply the continuity of these wavefunctions. Since the eigenfunctions are defined upon the phase factor $e^{i\chi(\vec{q})}$, they have to be continuous only upon a phase factor. Let us call this property a quasi-continuity.

Mathematically a band can be regarded as a section of a 1-dimensional linear bundle that can be characterized by an integer Chern number in a standard way[2, 10]. It is common to define the Berry curvature of the band k is commonly defined as[2] $B^{(k)}_{\alpha\beta} = -2\mathrm{Im}\langle\partial_{q_\alpha}\psi_k(\vec{q})|\partial_{q_\beta}\psi_k(\vec{q})\rangle$. The first Chern number is an integral of the Berry curvature over the compact space of $\vec{q}$ and has to reduce to an integer times (2π). One can also define the Hamiltonian in the space of $\vec{q}$ with more dimensions. Then the first Chern number is defined as the integral over any 2-dimensional compact subspace of $\vec{q}$.

In physical terms first Chern number can be directly related to the transconductance of the system. To establish this, one may utilize the description in terms of the semi-classical equations of motion. As known[11], a nonzero value of the Berry curvature brings about a nonzero drift velocity transverse to the external force F^β. Average of this drift velocity over the $\vec{q}$-space is expressed in terms of the first Chern number. This explains the transverse conductance quantization in the QHE setups[1, 12]. We note that the above consideration implies that the initial wavefunction is the eigenstate of the Hamiltonian. It is not evident if the conclusion is valid for more complex initial wavefunctions.

The linearity is one of the basic postulates of quantum mechanics: a linear superposition of two wavefunctions is also a valid wavefunction of the system. What are the topological properties of the superposition of topologically distinct bands? To comprehend why the question is not trivial let us consider a short example. Let us take two bands of quasi-continuous wavefunctions $|\psi_0(\vec{q})\rangle$, $|\psi_1(\vec{q})\rangle$ with different first Chern numbers $C_0 = 0$ and $C_1 = 1$. Let us consider a superposition of those bands with parameter-independent coefficients $a, b \neq 0$

$$|\psi(\vec{q})\rangle = a|\psi_0(\vec{q})\rangle + b|\psi_1(\vec{q})\rangle \tag{3.1}$$

What is the Chern number of this superposition? It is a weighted sum of two Chern numbers, $|b|^2$ which is generally not integer. The topology dictates that the Chern number must be integer[10]. So, this presents an apparent paradox.

The solution is simple: the superposition of two quasi-continuous wavefunctions is not quasi-continuous and is not subject to topological classification. The superposition

can be made quasi-continuous by choosing the proper parameter dependence of a and b. This restores the quantization of Chern number.

This sets the goal of this Chapter: to investigate the topological properties of superpositions. We address the superpositions of two kinds. A *dynamic* superposition is created at a given value of $\vec{q}$ and then evolves in accordance with the Hamiltonian dynamics. A *static* superposition is obtained by modification of the stationary Hamiltonian that mixes the bands. Let us shortly describe the results. Firstly, we consider dynamic superpositions. We investigate the time evolution of a particle in the Chern insulator that is prepared initially in a superposition state. In such insulators the transverse current response - the transconductance is supposed to witness the Chern number. The quantization of transconductance is related to the quantization of transmobility that gives a transverse velocity. We find for a superposition that the resulting transmobility is indeed proportional to the weighted sum of Chern numbers, so it is not a subject of topological quantization. This can be deduced that the wavefunction is not periodic in time and its time-dependence is complex. Although dynamics are equivalent to the slow change of parameters $\vec{q}$ in the Hamiltonian the wavefunction does not remain quasi-continuous on a closed trajectory in a parameter space. This is different from the dynamics of the eigenfunctions. Thus the resulting wavefunction is not a subject of topological classification.

Next, we investigate the static superpositions, made by adding the mixing matrix elements between the bands into the Hamiltonian. We investigate the topological properties of the resulting eigen-bands. These eigen-bands are quasi-continuous and we establish the topological restriction on the parametric dependence of the mixing matrix element: it must be zero at least in one point in $\vec{q}$-space. The Chern number of a static superposition is thus integer and may change abruptly upon changing of the parameters of the bandstructure. Such an abrupt change is a topological phase transition, so this naturally brings us to the consideration of possible phase diagrams. The phases we consider are defined by a set of first Chern numbers attributed to each band with Chern numbers being ordered with increasing energy of the bands. We investigate the critical points in these phase diagrams and find no triple points. The critical points are quadruple connecting 4 regions in 2d parameter space. There are two kinds of quadruple points with either 4 or 3 different phases in the adjacent regions. This is different from the case of phase diagrams for usual phase transitions where generically triple points are present[13]. We extensively illustrate these features of phase diagrams with a specific example of a bilayer Haldane model.

The Chapter is organized as follows. In Sec. 3.2 we derive the value of the transconductance of a particle prepared initially in the superposition state. The discussion of the restrictions imposed by general topological considerations on the mixing matrix element between two topological bands is given in Sec. 3.3. In Sec. 3.4 we address the properties of the topological numbers exchange for between two static superpositions. In Sec. 3.5 we investigate the case of multiple bands introducing and discussing the general features of the phase diagrams. In Sec. 3.6 we illustrate these general features inspecting the phase diagrams of the topological phase transitions in the bilayer Haldane model. We conclude in Sec. 3.7. The present a note on a specific degenerate case of the bilayer Haldane model in App.3.8.

3.2. ADIABATIC EVOLUTION OF THE SUPERPOSITION

In this Section we consider the adiabatic evolution of a particle initially prepared in a superposition of two states that belong to different bands. We will compute the transmobility μ of a particle defined as the proportionality coefficient between the drift velocity in the direction perpendicular to the external force and the external force, $v_\alpha = \mu e_{\alpha\beta} F_\beta$. As we will show below, for a particle in a certain band

$$\mu = -\frac{2\pi C}{\hbar \Omega} \tag{3.2}$$

where C is an integer Chern number of the band and is the volume of the Brillouin zone $\Omega = \int dq_1 dq_2$. The transverse current density of a many-body system at zero temperature is a sum over filled bands labeled by j

$$j_\alpha = e \sum_j v_\alpha^j n^j = e^2 \sum_j \mu_j n^j \epsilon_{\alpha\beta} E^\beta \tag{3.3}$$

where μ_j is the transmobility in the band j and the particle density $n_j = \frac{\Omega}{(2\pi)^2}$ in a filled band does not depend on a band . With this, the transconductance[14], the proportionality coefficient between the transverse current and the voltage $I_x = G_{xy} V_y$ is quantized in the units of $e^2/(2\pi\hbar)$,

$$G_{xy} = -\frac{e^2}{2\pi\hbar} \sum_j C_j \tag{3.4}$$

This is a well-established result[1].

Thus, the problem of the computation of the current can be reduced to the problem of the computation of the transmobility. It can be computed by solving the Schrodinger evolution equation for the wavefunction and computing the expectation value of the velocity operator that is defined as

$$\hat{\dot{x}}_\alpha = \frac{1}{\hbar} \frac{\partial \hat{H}}{\partial q_\alpha} \tag{3.5}$$

where q_α is a quasi-momentum parameter of the system. In the case of the milti-terminal superconducting junction it would be the global phase of one of the leads[15].

The computation of transmobility of a particle in a single band is standard. A weak force doesn't cause interband transitions but changes the wavevector in time $\hbar \dot{q}_\alpha = F_\alpha$. For constant F_α

$$\hbar \vec{q}(t) = \vec{F} t + \text{const} \tag{3.6}$$

for a resulting trajectory in $\vec{q}$-space sweeps over the whole Brillouin zone at long time scale $t \sim \hbar\sqrt{\Omega}/|\vec{F}|$ at least for incommensurate direction of force.

In the case when the initial state is the eigenstate of the Hamiltonian, the mean current reduces to the Berry curvature of the initial state. It follows from the semi-classical equations of motion[11] that the Berry curvature brings an addition to the velocity:

$$\vec{\dot{x}} = \frac{1}{\hbar} \frac{\partial E(q,x)}{\partial \vec{q}} - B^{\alpha\beta} \dot{q}_\beta = \frac{1}{\hbar} \frac{\partial E(q,x)}{\partial \vec{q}} - B^{\alpha\beta} \frac{F_\beta}{\hbar} \tag{3.7}$$

We consider this equation at the long time scales such that the whole Brillouin zone is swept over. Upon the sweeping desribed by Eq.(3.6) the first term in (3.7) describes Bloch oscillations and averages to zero since it is a derivative over $\vec{q}$. The second term reduces to the average of the Berry curvature

$$\frac{1}{\Omega}\int d\vec{q}B^{\alpha\beta} = \frac{2\pi C e^{\alpha\beta}}{\Omega} \tag{3.8}$$

which is an integer Chern number C, and gives the drift in the direction perpendicular to the applied force

$$\langle \dot{x}_\alpha \rangle = -\frac{2\pi C}{\hbar\Omega} \times \epsilon_{\alpha\beta}F^\beta, \quad \mu = -\frac{2\pi C}{\hbar\Omega} \tag{3.9}$$

in agreement with Eq.(3.2).

Let us compute the transmobility for a superposition. One can make such a superposition by an oscillating modification[16] of bandstructure parameters. A pulse of these oscillations brings a number of particles to the superposition state in a narrow region in $\vec{q}$-space where the frequency of the oscillations matches the energy difference between the bands $|\psi_{0,1}\rangle$ with different Chern numbers $\hbar\omega = \epsilon_1(\vec{q}_0) - \epsilon_0(\vec{q}_0)$. After the pulse, wavefunction of one particle with the quasi-momentum $\vec{q}_0$ is

$$|\psi(t=0)\rangle = a|\psi_0(\vec{q}_0)\rangle + b|\psi_1(\vec{q}_0)\rangle \tag{3.10}$$

a, b being the superposition coefficients. We need to solve

$$i\hbar\frac{\partial\psi(t)}{\partial t} = H(\vec{q}(t))\psi(t), \quad \vec{q}(t) = \vec{q}_0 + \vec{F}t \tag{3.11}$$

where we treat the quasi-momentum of the particle as an adiabatically changing parameter of the Hamiltonian. We seek for the wavefunction in the instantaneous eigenbasis of $\hat{H}(t)$, $|\psi(t)\rangle = \sum_k c_k(t)|\psi_k(t)\rangle$, k labeling all the bands. The coefficients c_k in the zero order of adiabatic perturbation theory in the parameters $\dot{q}_{\alpha,\beta}$ are

$$c_0^{(0)}(t) = e^{i\theta_0(t)}a, \quad c_1^{(0)}(t) = e^{i\theta_1(t)}b, \quad c_{l>1}^{(0)}(t) = 0 \tag{3.12}$$

where

$$\theta_k(t) = -\int^t d\tau E_k(t) + \int^t \vec{A}^{(k)} \cdot d\vec{q}(t) \tag{3.13}$$

incorporates both the dynamical and geometric phases[2], and $\vec{q}(t)$ being the path in parameter space as in Eq.(3.11). Here $A_\alpha^{(k)}$ is the Berry connection, $A_\alpha^{(k)} = i\langle k|\partial_{q_\alpha}k\rangle$. To compute the expectation value of the drift velocity, $\langle\psi(t)|\hat{\dot{x}}_\alpha|\psi(t)\rangle$, we need to evaluate c_k up to the first order

$$c_0^{(1)}(t) = \frac{ibe^{i\theta_1(t)}\langle\psi_0|\dot{\psi}_1\rangle}{E_0 - E_1}, \quad c_1^{(1)}(t) = \frac{iae^{i\theta_0(t)}\langle\psi_1|\dot{\psi}_0\rangle}{E_1 - E_0} \tag{3.14}$$

$$c_{l>1}^{(1)}(t) = \frac{ibe^{i\theta_1(t)}\langle\psi_l|\dot{\psi}_1\rangle}{E_l - E_1} + \frac{iae^{i\theta_0(t)}\langle\psi_l|\dot{\psi}_0\rangle}{E_l - E_0} \tag{3.15}$$

We average this expectation value over the short time scale $t_s|E_0 - E_1| \gg \hbar$ thereby neglecting the fast oscillating terms $\sim e^{i(\theta_0(t)-\theta_1(t))}$. We obtain

$$\langle \hat{\dot{x}}_\alpha \rangle = \frac{1}{\hbar}(|a|^2 \frac{\partial E_0}{\partial q_\alpha} + |b|^2 \frac{\partial E_1}{\partial q_\alpha} - F^\beta [|a|^2 B^{(0)}_{\alpha\beta} + |b|^2 B^{(1)}_{\alpha\beta}]) \tag{3.16}$$

where the first two terms are of zero order in $\dot{q}_{\alpha,\beta}$ and coming from Eq.(3.12) and the last two are the first order adiabatic correction coming from Eqs.(3.14), (3.15). Thus, Eq.(3.16) generalizes Eq.(3.7) for the case of a superposition. As above, we consider the drift velocity at the long time scale such that the whole Brillouin zone is swept over. Upon the sweeping described by Eq.(3.6) the first two terms in (3.16) average to zero since they are derivatives over $\vec{q}$ with time-independent coefficients. The last two terms reduce to the weighted sum of the averages of two Berry curvatures. Finally, we obtain

$$\langle \dot{x}_\alpha \rangle = -\frac{2\pi C'}{\hbar\Omega} \times \epsilon_{\alpha\beta} F^\beta, \quad C' = |a|^2 C_0 + |b|^2 C_1 \tag{3.17}$$

Thus, the transmobility of a particle in a superposition state is not quantized. The absence of the topological quantization can be explained from the fact that the dynamical superposition is not periodic in $\vec{q}$ even if upon sweeping the wavefunction comes to the same or close point in Brillouin zone. It won't be the same due to the fast oscillating factors $e^{i\theta_{0,1}(t)}$. In other words, the dynamical superpositions do not form a manifold where topological constraints can be imposed.

The experimental observation of this effect is rather straightforward. If we apply sequence of pulses to a sample a number of particles will be brought to a superposition state. This number will be proportional to the intensity of radiation. One would just see deviations from the quantized value of the current proportional to the radiation intensity.

3.3. TOPOLOGICAL CONSTRAINT ON THE MIXING MATRIX ELEMENT

In the previous Section, we have seen that a dynamical superposition shows a non-topological response. Since it is not an eigenfunction of a Hamiltonian. In this Section we consider the static superpositions that are the eigenfunction of a stationary Hamiltonian. We consider a smooth $N \times N$ Hamiltonian $H_0 + H'$ with $N \geq 2$. The Hamiltonian H_0 is assumed to be diagonalized giving rise to a bandstructure that includes topologically non-trivial bands. The addition H' is a perturbation that is generally non-diagonal in this basis. With this, the eigen-bands of the total Hamiltonian will be quantum superpositions of the eigenbands of the unperturbed Hamiltonian with well-defined energies. As above, all the bands and the Hamiltonian are defined on 2-dimensional compact space of parameters $q_{1,2}$. Let us concentrate on two bands $|\psi_{0,1}(\vec{q})\rangle$ with different Chern numbers $C_{0,1} = 0, 1$ introduced above.

We can choose different gauges for wavefunctions in these bands by multiplying it with a phase factor $\chi(\vec{q})$. By a proper choice of the gauge the topologically trivial band $|\psi_0(\vec{q})\rangle$ can be made not only quasi-continuous but truly continuous. In distinction from this the topologically non-trivial band $|\psi_1(\vec{q})\rangle$ cannot be made continuous everywhere.

However, by a proper gauge choice it is possible to make it continuous within the Brillouin zone placing possible discontinuities on its boundary. We will stick to this convenient gauge choice. The effective Hamiltonian in the subspace of those two bands H is obtained by projecting $H_0 + H'$ on that subspace

$$H = \begin{pmatrix} \epsilon_0(\vec{q}) & t(\vec{q}) \\ t^*(\vec{q}) & \epsilon_1(\vec{q}) \end{pmatrix} \tag{3.18}$$

where the mixing matrix element

$$t(\vec{q}) = \langle \psi_0 | H'(\vec{q}) | \psi_1 \rangle \tag{3.19}$$

is a continuous function inside the Brillouin zone by virtue of the gauge choice made.

We will prove now a general and important topological constraint imposed on $t(\vec{q})$: if the Chern numbers of two bands are different, then for any H' there must exist a point in $\vec{q}$-space where the mixing matrix element vanishes

$$\exists (q_1^*, q_2^*) : t(q_1^*, q_2^*) = 0 \tag{3.20}$$

For simplicity, let us consider the case when the parameter space is a torus corresponding to a Brillouin zone of a 2-dimensional crystal, generalization to other types of surfaces is straightforward. According to the general theory of characteristic classes, the wavefunction with a nontrivial Chern number has to have a singularity at some point in parameter space $\vec{q}'$. By choosing the gauge described above we have moved the singularity of $|\psi_1(\vec{q})\rangle$ to the boundary of the 2-disc from which the torus is then obtained by gluing the sides. The wavefunction is continuous inside the Brillouin zone then but not periodic and the boundary conditions are given by

$$\psi(0, q_2) = e^{i\theta(q_2)} \psi(2\pi, q_2), \quad \psi(q_1, 0) = e^{i\theta(q_1)} \psi(q_1, 2\pi) \tag{3.21}$$

the winding of the phase $\theta(q_1, q_2)$ along the boundary yields precisely the first Chern number. Then, according to (3.19) the mixing matrix element $t(q_1, q_2)$ also acquires the same phase winding along the boundary. Due to the discrete nature of this winding it does not change upon smooth variations of the parameters, so one can smoothly deform the contour on which the winding is defined. One will not be able to shrink this contour to a point if $t(q_1, q_2) \neq 0$ everywhere since due to the conservation of the winding. In this case one would obtain a discontinuity of $t(q_1, q_2)$ at some point unless $t(q_1, q_2) = 0$ in this point. So, this proves the topological constraint discussed.

3.4. TOPOLOGICAL TRANSITION AND BERRY CURVATURE DISTRIBUTION

In this Section we consider the avoided crossing of two bands of different topology. We assume that the values of the mixing matrix elements in (3.18) $t(\vec{q})$ are small in comparison with typical width of the bands $\epsilon_{0,1}(\vec{q})$. More precisely,

$$|t(q_1, q_2)| \ll \max_{\vec{q}} \epsilon_{0,1}(\vec{q}) - \min_{\vec{q}} \epsilon_{0,1}(\vec{q}) \tag{3.22}$$

We would like to move the energies of the bands with respect to each other. Let us assume that both energies depend on an additional parameter η

$$\epsilon_{0,1}(\vec{q}) = \epsilon^0_{0,1}(\vec{q}) \pm \eta \tag{3.23}$$

As an example of a concrete physical situation where it can be realized one can consider a bilayer material with weak tunnel coupling between the layers. The bands ϵ_0 and ϵ_1 are situated in different layers, weak tunneling is responsible for matrix mixing elements and to 2η corresponds to the difference of electrostatic potentials between the layers that can be induced by a perpendicular electric field.

We see that at sufficiently large $|\eta|$ the unperturbed band energies never cross: $\eta \to -\infty\ \epsilon_0(q_1,q_2) < \epsilon_1(q_1,q_2)$ for all (q_1,q_2), for $\eta \to +\infty\ \epsilon_0(q_1,q_2) > \epsilon_1(q_1,q_2)$ for all (q_1,q_2). By changing η from large negative to large positive values we move the energies of the bands with respect to each other and make them cross in a certain interval of η.

Let us consider how the Chern numbers of the eigenbands of (3.18) change upon changing η. When the energies of the unperturbed bands do not cross at any point ($|\eta| \to +\infty$) the mixing can be neglected and the Chern numbers of the eigenbands the same as without mixing. However, we see that the topological configurations of the bands are different for $\eta \to \pm\infty$. At $\eta \to -\infty$ the topological charge is concentrated in the lower band while it is transfered to the upper band when $\eta \to +\infty$. We conclude that the topological transition must occur upon the band crossing.

The crossing of the bands is generally avoided at a given value of η. The unperturbed bands cross at the lines where $\epsilon_0(q_1,q_2) = \epsilon_1(q_1,q_2)$, and the area of the space of (q_1,q_2) is separated into parts by these lines. Except for the close vicinity of these lines, the wavefunctions are expected to be close to with the unperturbed ones since the mixing is small. At the lines the crossings are generally avoided and the bands do not actually cross (see Fig.3.1) being separated by an energy difference at least $2|t(\vec{q})|$. The bandmixing is strong in a narrow strip that includes the lines. The typical width of the strip can be estimated as $|\delta\vec{q}_M| \simeq |\frac{t(\vec{q})}{\partial(\epsilon_1(\vec{q})-\epsilon_0(\vec{q}))/\partial q_\alpha}|$. The Chern numbers can be ascribed to the resulting lower and upper energy bands and do not change while the crossing is avoided.

There is however a critical value of $\eta = \eta_c$ at which the crossing lines intersect the special point $\vec{q}^*$ mentioned in the previous Section. At this point $|t(\vec{q}^*)| = 0$ and the crossing is not avoided. Two bands are connected at the point $\vec{q}^*$ and become a single band with the topological charge 1. This is the point of topological phase transition.

In the rest of the Section we consider the distribution of the Berry curvature in the $\vec{q}$-space for the situation of the band crossing. The Chern number is proportional to the integral of the Berry curvature over the space. A naive consideration would neglect the small mixing, so the Chern number of the eigenband reduces to the sum of integrals of Berry curvatures of the unperturbed bands over the corresponding regions. However, this sum is by no means integer.

So motivated, let us consider the situation in detail. Let us assume that the condition for the crossing of the unperturbed levels $\epsilon_0 = \epsilon_1$ is satisfied along a single closed line in the (q_1,q_2) space (see Fig.3.1). Then, under the assumptions described above away from this line the wavefunctions should approach the non-mixed functions up to a phase factor $|\psi_\pm(q_1,q_2)\rangle \to e^{i\chi_{0,1}(q_1,q_2)}|\psi_{0,1}(q_1,q_2)\rangle$. We denote these areas as $D_{1,2}$. We denote the

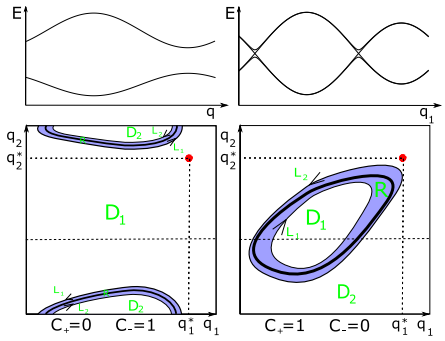

Figure 3.1: Right: separation of the (q_1, q_2) parameter space into 3 regions before the topological transition: D_1 where $\epsilon_1 < \epsilon_0$, D_2 where $\epsilon_1 > \epsilon_0$ and a narrow strip R around the line $\epsilon_1 = \epsilon_0$. The width of the strip is determined by the value of mixing t in (3.18). Oriented boundaries of $D_{1,2}$ are denoted as $L_{1,2}$. Left: after the transition

values of the Berry curvature integrals over these areas as

$$I_i^j = \frac{1}{2\pi}\int_{D_i} B_{12}^{(j)} dq_1 dq_2 \tag{3.24}$$

$j = 0,1$ labeling the unperturbed bands. If we neglect a narrow area that encloses the energy crossing line (denoted as R in Fig.3.1). the "Chern numbers" of the upper ($\tilde{C}_+$) and lower ($\tilde{C}_-$) bands do not reduce to integers

$$\tilde{C}_+ = I_1^{(0)} + I_2^{(1)} \neq C_1 = 1 = I_1^{(1)} + I_2^{(1)} \tag{3.25}$$

$$\tilde{C}_- = I_1^{(1)} + I_2^{(0)} \neq C_0 = 0 = I_1^{(0)} + I_2^{(0)} \tag{3.26}$$

in general, which seems to contradict the general topology statement.

This paradox is resolved by considering the Berry curvature in region R. There, the bands are strongly mixed and thus this narrow region brings a finite contribution to the Chern number so that the typical Berry curvature in this region is $\sim |\delta\vec{q}_M|^{-1}$, that is much bigger that the typical Berry curvature in the regions $D_{1,2}$. We denote the contributions from the region R as

$$I_\pm^R = \frac{1}{2\pi}\int_R B_{12}^{\pm} dq_1 dq_2 \tag{3.27}$$

The true topological charges $C_\pm$ of the eigenbands $|\psi_\pm\rangle$ are

$$C_+ = I_1^{(0)} + I_2^{(1)} + I_+^R \tag{3.28}$$

$$C_- = I_1^{(1)} + I_2^{(0)} + I_-^R \tag{3.29}$$

and must be integer.

To see that we shall evaluate $I_\pm^R$. In order to do this, we consider the Berry connections of the superpositions. It is defined as $A_\alpha^\pm = i\langle\psi_\pm|\partial_{q_\alpha}\psi_\pm\rangle$. For two superpositions under consideration, $|\psi_\pm\rangle = a_\pm|\psi_0\rangle + b_\pm|\psi_1\rangle$ where superposition coefficients $a_\pm, b_\pm$ are

obtained by diagonalizing (3.18). We express the connections in terms of superposition coefficients

$$A_\alpha^\pm = i a_\pm^* \partial_{q_\alpha} a_\pm + i b_\pm^* \partial_{q_\alpha} b_\pm + |a_\pm|^2 A_\alpha^{(0)} + |b_\pm|^2 A_\alpha^{(1)} + \\ + (i a_\pm^* b_\pm \langle \psi_0 | \partial_{q_\alpha} \psi_1 \rangle + c.c) \tag{3.30}$$

We see that in addition to the weighted sum of connections there are extra contributions to $A_\alpha^\pm$. We will see that they are responsible for the resulting Chern numbers being integer. At distances from the crossing line that $\gg |\delta \vec{q}_M|$ but still much smaller than the typical size of the Brillouin zone, the coefficients a_- and b_+ vanish in D_1 and the coefficients a_+ and b_- vanish in D_2 (see Fig.3.1). With this we obtain the following asymptotics for $\vec{q} \in D_1$

$$\begin{cases} A_\alpha^+ = i\partial_{q_\alpha}(\log a_+) + A_\alpha^{(0)} \\ A_\alpha^- = i\partial_{q_\alpha}(\log b_-) + A_\alpha^{(1)} \end{cases} \tag{3.31}$$

and for $\vec{q} \in D_2$

$$\begin{cases} A_\alpha^+ = i\partial_{q_\alpha}(\log b_+) + A_\alpha^{(1)} \\ A_\alpha^- = i\partial_{q_\alpha}(\log a_-) + A_\alpha^{(0)} \end{cases} \tag{3.32}$$

We denote the contour integrals of the Berry connections over two oriented boundaries $L_i = -\partial D_i$ of the regions D_i

$$J_i^j = -\frac{1}{2\pi} \int_{L_i} \vec{A}^j \cdot d\vec{q} \tag{3.33}$$

It is crucial to note that in the absence of singularities of all the functions away from the boundary of the (q_1, q_2)-space one may use the Stokes theorem to reduce the surface integrals of the Berry curvature I_i^j to the contour integrals of the Berry connection. Applying this we express the contributions of D_i in terms of the contour integrals (3.33)

$$\begin{cases} I_1^j = J_1^j \\ I_2^j = J_2^j + C_j \end{cases}$$

As for the contributions from region R, they are expressed in terms of I_i^j and the contour integrals of the gradients of the phases of superposition coefficients (the latter holds since $|a_-|, |b_+| \to 1$ in D_2 and $|a_+|, |b_-| \to 1$ in D_1)

$$I_+^R = \frac{1}{2\pi} \int_{L_1} \vec{A}^+ \cdot d\vec{q} + \frac{1}{2\pi} \int_{L_2} \vec{A}^+ \cdot d\vec{q} = \\ = -I_2^{(1)} + C_1 - I_1^{(0)} + \frac{i}{2\pi} \int_{L_2} d\vec{l} \cdot \vec{\nabla} \log b_+ + \\ + \frac{i}{2\pi} \int_{L_1} d\vec{l} \cdot \vec{\nabla} \log a_+ \tag{3.34}$$

$$I_-^R = \frac{1}{2\pi} \int_{L_1} \vec{A}^- \cdot d\vec{q} + \frac{1}{2\pi} \int_{L_2} \vec{A}^- \cdot d\vec{q} = \\ = -I_2^{(0)} + C_0 - I_1^{(1)} + \frac{i}{2\pi} \int_{L_2} d\vec{l} \cdot \vec{\nabla} \log a_- + \tag{3.35}$$

$$+\frac{i}{2\pi}\int_{L_1} d\vec{l}\cdot\vec{\nabla}\log b_- \tag{3.36}$$

The last two terms in Eqs. (3.36) and (3.34) are integer multiples of 2π since they are equal to the sum of the windings of the phases of superposition coefficients along the closed contours $L_{1,2}$. In order to compute these phases, we diagonalize the effective Hamiltonian in the vicinity of the crossing line

$$H^{(\text{eff})} = \begin{pmatrix} \varepsilon & t \\ t^* & -\varepsilon \end{pmatrix} \tag{3.37}$$

where the small energy difference is $\varepsilon = (\epsilon_0 - \epsilon_1)/2$, the limits $\varepsilon/|t| \to \pm\infty$ bring us to the region D_1, D_2 correspondingly. We approximate the mixing matrix element by its value exactly at line disregarding its dependence on ε. We diagonalize (3.37) to find two eigenfunctions $|\psi_\pm\rangle = a_\pm(\varepsilon)|\psi_0\rangle + b_\pm(\varepsilon)|\psi_1\rangle$. To remove the ambiguity of the phases we will choose the phase of $|\psi_+\rangle$ to coincide with the phase of $|\psi_1\rangle$ and the phase of $|\psi_-\rangle$ to coincide with the phase of $|\psi_0\rangle$ in the region D_2 so that

$$a_-(-\infty) = 1, \quad b_+(-\infty) = 1 \tag{3.38}$$

Diagonalizing (3.37) with the phase fixing conditions (3.38), we obtain the superposition coefficients in the region R

$$\begin{cases} b_-(\varepsilon) = \\ a_-(\varepsilon) = \end{cases} \frac{1}{\sqrt{|t|^2 + (\varepsilon + \sqrt{|t|^2+\varepsilon^2})^2}} \begin{matrix} \frac{-t^*(\varepsilon+\sqrt{\varepsilon^2+|t|^2})}{|t|} \\ |t| \end{matrix}$$

$$\begin{cases} b_+(\varepsilon) = \\ a_+(\varepsilon) = \end{cases} \frac{1}{\sqrt{|t|^2 + (-\varepsilon + \sqrt{|t|^2+\varepsilon^2})^2}} \begin{matrix} \sqrt{|t|^2+\varepsilon^2} - \varepsilon \\ t \end{matrix}$$

With this we can find their asymptotics at $\varepsilon \to +\infty$ that correspond to the values of superposition coefficients on L_1

$$b_- \to -t^*/|t|, \quad a_+ \to t/|t| \tag{3.39}$$

with this one can compute the last contributions in (3.36) and (3.34)

$$\int_{L_2} d\vec{l}\cdot\vec{\nabla}\log a_- = 0 = \int_{L_2} d\vec{l}\cdot\vec{\nabla}\log b_+ \tag{3.40}$$

$$\frac{i}{2\pi}\int_{L_1} d\vec{l}\cdot\vec{\nabla}\log a_+ = -\frac{i}{2\pi}\int_{L_1} d\vec{l}\cdot\vec{\nabla}\log b_- =$$

$$= \int_{L_1} d\vec{l}\cdot\vec{\nabla}\log t = w \tag{3.41}$$

where we denoted the winding of the phase of the mixing matrix element along L_1 as w. Before the transition when the point $\vec{q}^*$ is outside L_1 we have $w = 0$. After the transition

by definition of the mixing matrix element (3.19) the value of w coincides with the value of C_1 with the opposite sign. Then from Eqs. (3.36), (3.34), (3.40), (3.41) we obtain

$$C_+ = 1 + \frac{w}{2\pi}, \quad C_- = -\frac{w}{2\pi} \tag{3.42}$$

So, in the case before the transition we have

$$C_+ = 1, \quad C_- = 0 \tag{3.43}$$

and after the transition

$$C_+ = 0, \quad C_- = 1 \tag{3.44}$$

as shown in Fig.3.1. The above reasonings can be straightforwardly generalized to the crossing of two bands with arbitrary Chern numbers m, n. We note that in this case the mixing matrix element has $|n-m|$ zeroes, so we expect $|n-m|$ phase transitions upon the crossing.

3.5. MANY BANDS: GENERAL PROPERTIES OF THE PHASE DIAGRAMS

In this Section, we consider the topological phases and the transitions between the phases for an arbitrary number of bands N. Let us assume that the bandstructure depends on M additional parameters. At arbitrary point in the space of M parameters the bands do not cross and can be sorted in the order of increasing energy. The first Chern numbers of each band are well-defined. With this, we define a topological phase as an enumeration of the first Chern numbers of the bands in the order of ascending energy. It is convenient to describe it with a Greek letter milti-index that consists of enumeration of the first Chern numbers of the bands in the order of ascending energy (e.g. $\beta \equiv \{n_i\}$, $i = 1, .., N$).

To achieve a 2-band generic crossing one has to tune 3 independent parameters[17], two of them might be quasi-momenta. Therefore, the band crossings occur in a $(M-1)$-subspace of the space of additional parameters and this is a subspace of the topological transition points.

For many bands there can be the singularities of higher order, e.g. 3- and 4-bands crossing. They occur in the subspaces of dimension $M-6$ and $M-13$. We restrict our consideration to smaller dimensions where all transitions correspond to pairwise crossings of the bands.

We start with $M = 1$. Two quasi-momenta and single additional parameter form a 3-dimensional parameter space. The 2-band crossings correspond to isolated Weyl points in this 3-dimensional space. These points are topologically stable bearing a topological charge related to the point-like divergence of the 3-dimensional Berry curvature. Two bands exchange Chern number 1 upon the change of the additional parameter. Let us note that the crossings of different pairs of the bands bear distinct topological charges. We will call them colors: there are $N-1$ distinct colors. Generically the positions of Weyl points do not coincide. The accidental coincidence of the positions of two Weyl points corresponding to two pairs with one mutual band would lead to a 3-band crossing at

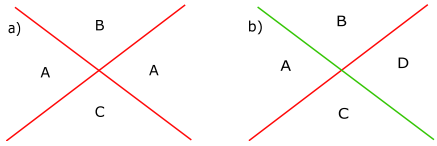

Figure 3.2: Triple points are generically absent in the phase diagrams under consideration. The critical points are quadruple with 4 phases meeting at the point. There are two types of the quadruple points. a) Type-I: crossing of the lines of the same color. always connects three different phases. The crossing point is stable upon small variations of parameters. The exchange of Chern number by 1 guarantees that two of the four phases are the same and the only possibility for phases is: $A = (..., n_i, n_{i+1}, ...)$, $B = (..., n_i \pm 1, n_{n+1} \mp 1, ...)$ and $C = (..., n_i \mp 1, n_{i+1} \pm 1, ...)$. b) Type-II: crossing of the lines of different colors. All 4 phases are different. There may be several options for those phases depending on colors and signs of Weyl points, e.g.: $A = (..., n_i, ..., n_j, ...)$, $B = (..., n_i - 1, n_{i+1} + 1, ..., n_j, ...)$, $C = (..., n_i, ..., n_j - 1, n_{j+1} + 1, ...)$ and $D = (..., n_i - 1, n_{i+1} + 1, ..., n_j - 1, n_{j+1} + 1)$

this mere point. As discussed, that we do not consider. The phase diagram consists of intervals separated by the projections of the Weyl poins onto the axis of additional parameter. This implies the following rule: the phase transition cannot occur between two arbitrary phases, since the transitions involve the Chern number exchange between neighboring bands $(\{..., n_i, n_{i+1}, ...\} \leftrightarrow \{..., n_i + 1, n_{i+1} - 1, ...\})$

Let us consider $M = 2$ and phase diagrams in the space of two additional parameters $s_{1,2}$. Weyl points develop into singularity lines in the resulting 4-dimensional space. These lines come in distinct colors. The phase diagram is obtained by the projection of these lines onto (s_1, s_2) plane. Therefore, the critical points where more than two phases coexist, are quadruple (see Fig.3.2). In such a critical point there are two 2-band crossings in the Brillouin zone. Generically these crossings occur at different $\vec{q}$.

There are two types of critical points. Type-I corresponds to the crossing of two lines with the same color (Fig. 3.2(a)). Since each line corresponds to the exchange of Chern numbers by 1 in the neighbouring bands, 2 of the 4 phases meeting at the point must be the same. For instance, two identical phases $A = (..., n_i, n_{i+1}, ...)$ and two different ones: $B = (..., n_i \pm 1, n_{n+1} \mp 1, ...)$ and $C = (..., n_i \mp 1, n_{i+1} \pm 1, ...)$ (see Fig.3.2). If we consider $M > 2$ and give small variations to extra parameters (s_3, etc), these point will be stable with respect to these small variations of extra parameters. However, upon the larger variation of at least two extra parameters one can annihilate two 2-band crossings and thereby eliminate the critical point. Type-II corresponds to the crossings of the lines of distinct colors. In this case all 4 phases must be distinct. These points are even more stable than Type-I points. The Type-II crossing may change upon changing 4 extra parameters. More are needed to change the crossings of the lines of more distinct colors.

The most common features of the usual phase diagrams (e.g. for not topological phase transitions[13]) are very distinct from the ones under consideration. In that case the critical points in 2-dimensional parametric space are triple.

3.6. EXAMPLE: BILAYER HALDANE MODEL

To illustrate the above general considerations, we investigate the phase diagrams of a bilayer Haldane model. The Haldane model[18] for a single layer describes electrons in a periodic hexagonal lattice with two orbitals per site, $\mathbf{a}_i$ $i = 1, 2, 3$ being the nearest neigh-

bor vector distances and $\mathbf{b}_i$ being the next to nearest neighbor vector distances in the lattice. The Hamiltonian is a $\vec{q}$-dependent 2×2 matrix, the matrix structure describing 2 sublattices in hexagonal lattice, and reads

$$H_H = \left\{ M + 2t_{nnn} \sum_{j=1}^{3} \sin \vec{q}\cdot\vec{b}_j \right\} \tau_z + \\ + t_n \left\{ \sum_{i=1}^{3} \cos \vec{q}\cdot\vec{a}_i \tau_x - \sin \vec{q}\cdot\vec{a}_i \tau_y \right\} \tag{3.45}$$

M being the parameter corresponding to a mass coefficient, $t_n^{(\eta)}$ is the real amplitude of the next-neighbor hopping and a purely imaginary next-nearest neighbors hopping amplitude $t_{nnn}^{(\eta)}$. The Hamiltonian gives rise to two bands that are topologically trivial provided $|t_{nnn}| < |M/(3\sqrt{3})|$ and the lower and upper bands have Chern numbers $-\mathrm{sgn}(t_{nnn})$ and $+\mathrm{sgn}(t_{nnn})$ correspondingly for[18] $|t_{nnn}| > |M/(3\sqrt{3})|$. The band crossings occur at $t_{nnn} = \pm M/(3\sqrt{3})$ occur at high symmetry at the boundary of the Brillouin zone where C_3 rotational symmetry is preserved.

The phase diagram for the single layer model was investigated previously[18]. The phase diagram possessed two critical points of Type-I. According to the general analysis done in Sec3.5 those points are stable upon small variations of parameters of the model.

Stacking two layers together, arranging an energy shift and a tunnel coupling between the two will give rise to (avoided) band crossings and the associated topological transitions that we investigate. We put the layers exactly on the top of each other, exactly matching the site positions in lateral directions. This preserves the original C_3 rotational symmetry. We only take into account the tunneling between layers for the nearest neighbors. The Hamiltonian of the bilayer model in use is thus a 4×4 matrix

$$\hat{H} = \begin{pmatrix} H_H^{(1)} & \mathrm{T} \\ \mathrm{T}^\dagger & H_H^{(2)} \end{pmatrix} \tag{3.46}$$

the block structure is in the space of 2 layers. Each diagonal block is a single layer Haldane Hamiltonian with $M^{(\eta)}, t_n^{(\eta)}, t_{nnn}^{(\eta)}$ $(\eta = 1,2)$ and energy shifts $(\eta - 1)\times s$.

The quasi-momentum-independent tunneling operator is diagonal in the sublattice space

$$\mathrm{T} = \begin{pmatrix} T_a & 0 \\ 0 & T_b \end{pmatrix} \tag{3.47}$$

We concentrate on the case $\arg(T_a) \neq \arg(T_b)$. If the phases of these two tunneling amplitudes are the same, the model possesses an extra degeneracy and does not suit to illustrate the generic situation. The degenerate case is addressed in Sec.3.8.

This Hamiltonian describes $N = 4$ bands. The bandstructure depends on $M = 10$ additional parameters: pairs of parameters describing the layers $t_n^{(\eta)}$, $t_{nnn}^{(\eta)}$ and $M^{(\eta)}$, absolute values of $T_{a,b}$ and their mutual phase difference and the energy shift s. For phase diagrams we need to choose two independent parameters. A natural parameter is the energy shift s and the second natural parameter would be the bandwidth W. With this

$$t_n^{(\eta)}/a^{(\eta)} = t_{nnn}^{(\eta)}/b^{(\eta)} = M^{(\eta)}/c^{(\eta)} = W \tag{3.48}$$

where we fix the coefficients $a^{(\eta)}, b^{(\eta)}, c^{(\eta)}$ to some values ~ 1. For some diagrams we implement an alternative choice where $M^{(\eta)}$ are fixed.

One has to find the phase separation lines. To this end, one has to find the positions of the band crossings in a 4-dimensional parameter space $q_{1,2}$, s and W. For the Hamiltonian (3.46), this looks like a challenging numerical task. In fact, it is not. Owing to C_3 symmetry, a band crossing in an arbitrary point of the Brillouin zone would come in a triple. The associated phase transition would correspond to exchange of Chern numbers of 3 topological charges between the bands. This is an interesting possibility we have searched for yet didn't find it for the model under consideration. A possible reason for that is a general difficulty to achieve high topological numbers. In fact, in our examples we didn't see Chern numbers bigger than 1.

Another possibility is to have the band crossings in the high-symmetry points K or K'. The associated topological transitions correspond to the exchange of unity topological charge, as in generic case. In these points, the eigenenergies can be readily found analytically,

$$\epsilon_{1,2} = \frac{s+S}{2} \pm \sqrt{|T_a|^2 + \left(\frac{s+A}{2}\right)^2}$$

$$\epsilon_{3;4} = \frac{s-S}{2} \pm \sqrt{|T_b|^2 + \left(\frac{s-A}{2}\right)^2} \tag{3.49}$$

where we define

$$S = M^{(1)} + M^{(2)} - 3\sqrt{3}\sigma(t^{(1)}_{nnn} + t^{(2)}_{nnn}) \tag{3.50}$$

$$A = M^{(2)} - M^{(1)} - 3\sqrt{3}\sigma(t^{(2)}_{nnn} - t^{(1)}_{nnn}) \tag{3.51}$$

$\sigma = \pm$ corresponding to K and K', respectively. In this model the transition lines come in three colors. We associate the blue color with the crossing of the two lowest in energy bands, green color with that of the second and third band and the red color with that of the third and forth. The red lines emerge at

$$\epsilon_1 = \epsilon_3 \tag{3.52}$$

for the blue lines emerge at

$$\epsilon_2 = \epsilon_4 \tag{3.53}$$

and the green ones emerge either emerge at $\epsilon_1 = \epsilon_4$ or $\epsilon_2 = \epsilon_3$. At a given W the 4 conditions above can be regarded as equations for s. Only 2 of 4 equations can have roots at either K or K'. This implies that at a given W one finds 0 or 2 or 4 phase transitions at different values of s.

The examples of the phase diagrams are presented in Figs. 3.3, 3.4, 3.5. In all these diagrams we see the features predicted in Sec.3.5. The critical points are all quadruple. There are Type-I critical points where 3 phases coexist and Type-II critical points where all 4 phases are different.

In the upper panel of Fig. 3.3 we see two red transition lines separating single domain of phase α from the phases β and $\overline{\beta}$ correspondingly. Upon tuning a parameter

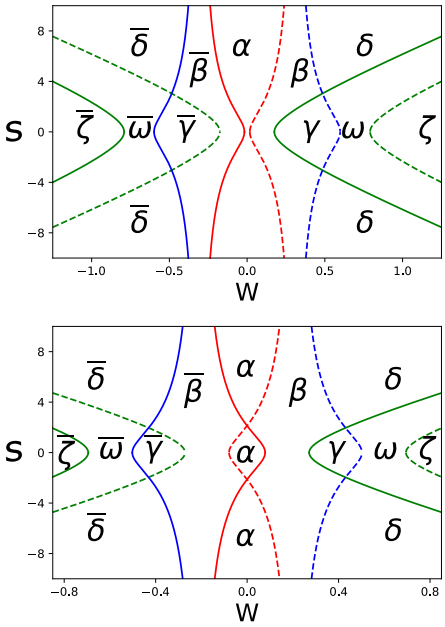

Figure 3.3: Examples of the phase diagrams for the bilayer Haldane model. The phase transition lines of three colors (see the text) correspond to the crossings at K point (dashed) or K' (solid). The parameters are: $b^{(1)} = b^{(2)} = 0.5$, $T_a = 0.5$, $T_b = 2 + 0.2i$. Different choices of masses are made for the upper and lower panel, upper: $M^{(1)} = M^{(2)} = 0.8$ and lower: $M^{(1)} = M^{(2)} = 0.55$. The phases are given by enumeration of Chern numbers: $\alpha = (0,0,0,0)$, $\beta = (0,0,-1,1)$, $\gamma = (0,-1,0,1)$, $\delta = (-1,1,-1,1)$, $\zeta = (-1,-1,1,1)$, $\omega = (-1,0,0,1)$. Overline indicates the change of sign of all Chern numbers, e.g $\overline{\delta} = (1,-1,1,-1)$. The extra region of the phase α between two critical points seen in the lower panel disappears upon variation of the masses.

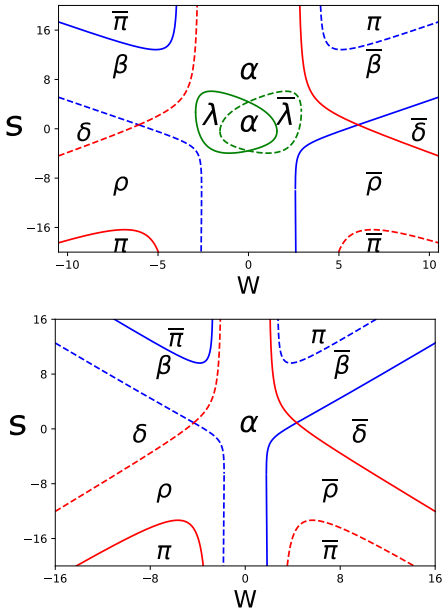

Figure 3.4: Examples of the phase diagrams for the bilayer Haldane model. Choice of parameters $-3b^{(1)} = b^{(2)} = -0.3$, $T_a = 3$, $T_b = 1.5 + 0.2i$ and in the upper panel: $2M^{(1)} = M^{(2)} = 4.2$ and in the lower panel: $2M^{(1)} = M^{(2)} = 3$. In addition to the phases in Fig.3.3 we also have: $\rho = (-1,1,0,0)$, $\pi = (-1,1,1,-1)$, $\lambda = (0,-1,1,0)$. The regions of the phases $\lambda, \overline{\lambda}, \alpha$ in the center of the Figure disappears upon the variation of the masses.

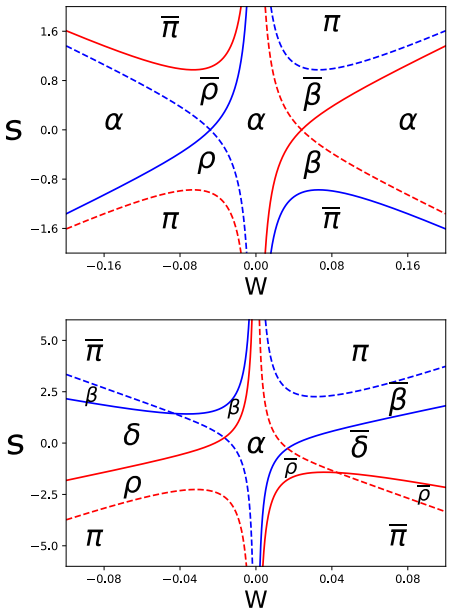

Figure 3.5: Examples of the phase diagrams for the bilayer Haldane model. Choice of the parameters: $M^{(\eta)} = c^{(\eta)} * W$, $c^{(1)} = c^{(2)} = 3.6$, $T_a = 1 + 0.3i$, $T_b = 0.3 + 1.5i$ and for upper panel $b^{(1)} = -b^{(2)} = 5$, for lower panel $b^{(2)} = -10$. In the upper panel only the Type-I critical points are seen at $s = 0$ and $W \approx \pm 0.05$. Upon variation of $b^{(2)}$ the blue and red solid lines interchange at positive as well as at negative W. This leads to the emergence of the Type-II critical points where the lines of different color cross and the non-compact regions of the phases δ and $\bar{\delta}$.

continuously, we can make these 2 lines intersect. Two Type-I critical points are formed at $s = \approx \pm 2$ and $W = 0$ in the lower panel of Fig.3.3. We also see three domains of phase α instead of one as in the upper panel.

With 3.4 we illustrate more complex scenarios of this kind. In the center of the top panel we see isolated compact domains of the phases $\lambda, \overline{\lambda}$ coexisting with the phase α. Upon tuning a parameter continuously, we can make these domains disappear. In the lower panel these domains are absent. We stress that in this case two compact transition lines disappear together with a pair of Type-I critical points.

We illustrate another scenario with Fig. 3.5. There are two main distinctions between upper and lower panel. The first one is the presence of non-compact domains of phases $\delta, \overline{\delta}$ in the lower panel contrary to the case of upper panel. This is in contrast to the case of the Fig.3.4 where the disappearing domains were compact. The second distinction between panels is the presence of the Type-II critical points in the lower one in addition to the Type-I critical points in the upper one. Both changes are produced upon continuous variation of the parameter of the model. We stress that in this case the Type-II crossings are not produced at finite values of parameters but come from infinitely large positive and negative W. This is in contrast to the case of Fig.3.3 where the critical points were produced pairwise at a given point on the phase diagram.

3.7. SUMMARY AND CONCLUSIONS

In this Chapter, we address the topological properties of superpositions of the quantum bands. This involves definition and values of the topological numbers of the superposition of bands.

The naive expectation for the Chern number of the superpositions of the states to also be a weighted sum of Chern numbers should fail due to the general theory of characteristic classes. Therefore, this is a problem of general interest and we investigate the topological properties of the superpositions created in different ways.

The first way is to create the dynamic superposition by resonant quantum manipulation[16] and investigate its time evolution. Thus we can compute the transmobility of the particle initially prepared in the superposition state. In this case we find that the transmobility reduces to the weighted sum and is non-topological therefore. This can be traced to the fact that the dynamic evolution of the state is generally not periodic. The second way to create a superposition is to add a nonzero mixing matrix elements mixing the bands. We have considered the topological properties of so created static superposition of two states. In this case we investigate in detail how the integer values of the Chern numbers of the superposition states are restored in accordance with the general theory of characteristic classes. We show a general and important property of the matrix element between two topologically distinct phases that it must vanish at some point in parameter space. This allows the topological transitions to happen.

Within the approach of investigation of static superpositions we also analyze the properties of many-band Hamiltonians. If the number of parameters is not large then it is not possible generically to tune the system to the more than two bands crossing point in parameter space. Therefore we conclude that in this case the topological properties of separate bands in terms of the first Chern numbers are sufficient to describe the system completely. More precisely, all the relevant information about the topological properties

can be presented in the phase diagram. Those show the quadruple points which is in contrast to usual phase transitions where triple points are common[13]. These quadruple points come in two types: the ones that connect 3 or 4 different phases. The Type-II points can be continuously annihilated pairwise or sent to infinity by tuning an additional parameter. The points of the Type-I can in addition to those mechanisms be annihilated by tuning two opposite topological charges in 3-dimensional parameter subspace to the same point. This requires one additional parameter to tune. Therefore, all the crossings are stable with respect to small deviations of the parameters.

Finally, we investigate in detail the phase diagrams for the bilayer Haldane model at some specific choices of parameters. We see the realization of the general features discussed above. In addition, the disappearance of the whole compact region of the topological phase can be achieved by tuning the parameters.

3.8. APPENDIX A: EXTENDED SINGULARITIES IN THE BILAYER HALDANE MODEL

In this Appendix we investigate a particular choice of the parameters in Eq.(3.46) when $\arg(T_a) = \arg(T_b)$. This case is somewhat degenerate. In the generic case described in the main text one only has Weyl point singularities in the 3-dimensional space of $q_{1,2}$ and one additional parameter. Those are situated in the corners of the Brillouin zone K, K'. Contrary to this, in the degenerate case we find that there is a possibility to have extended 1-dimensional singularities in the 3-dimensional parameter space. Moreover, these can be situated away from the points K, K'. We note that the case $|T_a| = |T_b|$ is even more degenerate and opens a possibility to have 2-dimensional singularities in the 3-dimensional parameter space. We do not consider this case here. We also note that the extended singularities are present in the non-generic case, so they can be removed by complicating the model. We report this cone-formation mechanism in this Appendix anyway.

In order to investigate the possibility of the extended singularities away from high-symmetry points K, K' in $\vec{q}$-space for a Hamiltonian (3.46) it is convenient to rewrite the diagonal blocks (3.45) as spin Hamiltonians which is always possible for a 2×2 matrix, so

$$H_H^{(\eta)} = \vec{B}^{(\eta)}\vec{\sigma} \tag{3.54}$$

where the "magnetic fields" have components $\vec{B}^{(1)} = |B^{(1)}|(\sin\theta\cos\phi, \sin\theta\sin\phi, \cos\theta)$ and $\vec{B}^{(2)} = |B^{(2)}|(\sin\theta'\cos\phi', \sin\theta'\sin\phi', \cos\theta')$. The lengths of $B^{(1,2)}$ and the angles are the functions of initial parameters in (3.45). The peculiarity of our model is that $\phi = \phi'$ always, which directly follows from (3.45). One can diagonalize these diagonal blocks in (3.46) applying a block-diagonal unitary transformation to (3.46). Upon doing that the upper off-diagonal block is transformed

$$\tilde{T} = \begin{pmatrix} \cos\frac{\theta}{2}\cos\frac{\theta'}{2}T_a + \sin\frac{\theta}{2}\sin\frac{\theta'}{2}T_b & \cos\frac{\theta}{2}\sin\frac{\theta'}{2}T_a - \sin\frac{\theta}{2}\cos\frac{\theta'}{2}T_b \\ \sin\frac{\theta}{2}\cos\frac{\theta'}{2}T_a - \cos\frac{\theta}{2}\sin\frac{\theta'}{2}T_b & \sin\frac{\theta}{2}\sin\frac{\theta'}{2}T_a + \cos\frac{\theta}{2}\cos\frac{\theta'}{2}T_b \end{pmatrix} \tag{3.55}$$

where we have used that $\phi = \phi'$. We see from (3.55) that if the phases of $T_{a,b}$ are different, the matrix elements never vanish, so we always expect avoided crossing away from K, K'.

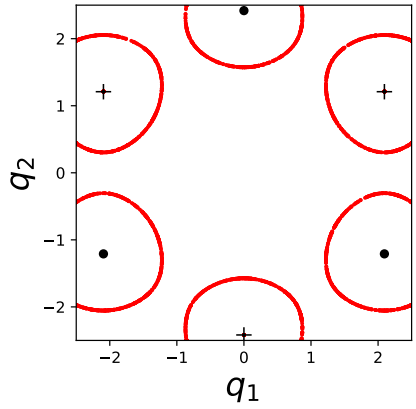

Figure 3.6: Singular manifolds in the $\vec{q}$-space of the model Eq.(3.46) in the degenerate case. These are obtained by projection of the Weyl points and extended line singularities from the 3-dimensional space of parameters $q_{1,2}, W$ (see main text) onto the $((q_1, q_2))$-plane. The extended singularities can be present in the case when $T_{a,b} \in \Re$. Choice of parameters $-3b^{(1)} = b^{(2)} = -0.3$, $T_a = 1$, $T_b = 0.5$, $2M^{(1)} = M^{(2)} = 2.2$, $\mu = -2$, $W \in [-4;4]$. The projections of the Weyl points are situated in the corners of the Brillouin zone and shown as black dots (point K) and black crosses (point K'). Extended singularities are shown in red.

If the phases are the same it opens a possibility to set some matrix elements to zero, so the singularities away from high-symmetry points become possible. In fact, if the phases coincide one can gauge them out by another unitary transformation of (3.46) and bring it to a symmetric form. Due to this additional symmetry there is a possibility to have extended singularities in 3-dimensional parameter space. We indeed see this cone-generation (see Fig.3.6).

3.9. ACKNOWLEDGEMENTS

This work was supported by the Netherlands Organisation for Scientific Research (NWO/OCW), as part of the Frontiers of Nanoscience (NanoFront) program.

REFERENCES

[1] Q. Niu, D. J. Thouless, and Y.-S. Wu, Phys. Rev. B **31**, 3372 (1985).

[2] F. R. S. M. V. Berry, Proceedings of the Royal Society of London A: Mathematical, Physical and Engineering Sciences **392**, 45 (1984).

[3] A. Vilenkin and E. Shellard, *Cosmic Strings and Other Topological Defects* (Cambridge University Press, 2000).

[4] E. Witten, Nuclear Physics B **223**, 422 (1983).

[5] A. Fomenko and D. Fuchs, *Homotopical Topology* (Springer International Publishing, 2016).

[6] S. Ryu, A. P. Schnyder, A. Furusaki, and A. W. W. Ludwig, New Journal of Physics **12** (2010).

[7] X. Qi and S. Zhang, Rev. Mod. Phys. **83** (2011), 10.1103/RevModPhys.83.1057.

[8] M. Z. Hasan and C. L. Kane, Rev. Mod. Phys. **82**, 3045 (2010).

[9] T. Thonhauser and D. Vanderbilt, Phys. Rev. B **74**, 235111 (2006).

[10] M. Nakahara, *Geometry, topology and physics* (INSTITUTE OF PHYSICS PUBLISHING, Bristol and Philadelphia, 2003).

[11] G. Sundaram and Q. Niu, Phys. Rev. B **59**, 14915 (1999).

[12] K. v. Klitzing, G. Dorda, and M. Pepper, Phys. Rev. Lett. **45**, 494 (1980).

[13] L. Landau and E. Lifshitz, *Statistical Physics* (ELSEVIER, 1980).

[14] Y. Nazarov and Y. Blanter, *Quantum Transport* (Cambridge University Press, 2009).

[15] R.-P. Riwar, M. Houzet, J. S. Meyer, and Y. V. Nazarov, Nature Communications **7**, 11167 EP (2016).

[16] J. M. Nichol, L. A. Orona, S. P. Harvey, S. Fallahi, G. C. Gardner, M. J. Manfra, and A. Yacoby, npj Quantum Information **3** (2017), 10.1038/s41534-016-0003-1.

[17] H. B. Nielsen and M. Ninomiya, Nuclear Physics B **185**, 20 (1981).

[18] F. D. M. Haldane, Phys. Rev. Lett. **61**, 2015 (1988).

4

BRAIDING AND ALL QUANTUM OPERATIONS WITH MAJORANA MODES IN 1D

We propose a scheme to perform braiding and all other unitary operations with Majorana modes in 1D. The scheme is based on resonant manipulation involving the first excited state extended over the modes. The detection of the population of the excited state also enables initialization and read-out. We provide an elaborated illustration of the scheme with a concrete device.

arxiv:2009.06578, accepted to PRL; http://doi.org/10.5281/zenodo.4377165

4.1. BRAIDING AND ALL QUANTUM OPERATIONS WITH MAJORANA MODES IN 1D

The paradigm of topological quantum computation [1, 2] provides an elegant solution to the most important problem in quantum manipulations: decoherence problem. It implements a topologically protected degenerate ground state as a computational basis. The degenerate state can be visualized as a set of localized anyons while unitary operations are performed by adiabatic exchange of the anyons, that is, braiding of their world lines [2]. The braiding is feasible in 2D and impossible in 1D since anyons should not collide in the course of operation. The intrinsically slow speed of adiabatic manipulation, as well as the difficulties of read-out and initialization of the protected states, should be compensated by the intrinsic fault-tolerance of the operations.

Of all numerous physical realizations of topologically protected degenerate ground state proposed, the Majorana zero-energy states in hybrid semiconductor-superconductor devices[3, 4] seems to be the most technologically advanced and elaborated. After pioneering experiments [5], an enormous outgoing research effort [6–8] resulted in considerable improvement of the technology and new observations, yet the quantum coherence in degenerate subspace still awaits experimental demonstration [9]. An obvious difficulty is that Majorana modes are realized in 1D nanowires, making direct braiding impossible. In principle, the 1D wires can be combined into a 2D network. There are elaborated schemes to realize braiding in various nanowire networks, for instance, in T- or Y-junctions [10–12]. A enormous technological challenge to make such networks with necessary controls is being addressed [13], but the progress is slow so far.

In this Chapter, we propose a scheme to realize Majorana braiding in a single 1D nanowire. Eventually, with this scheme one can realize any unitary transformation in the degenerate subspace, as well as initialization and read-out in this subspace. The scheme uses resonant manipulation technique, the resonance being between the degenerate subspace and the lowest excited state that extends over all Majorana modes. The initialization and read-out is possible if the population of the excited state is detected.

Strictly speaking, the scheme compromises the quantum computation paradigm since the topological protection fails during the operation. The system is subject to relaxation while being in the excited state. There are standard means to reduce this only source of decoherence, and make the operation time shorter than the corresponding relaxation time. It is important that the protection is preserved between the operations. This makes the scheme an ideal tool to demonstrate persistence of quantum superpositions in the degenerate subspace, and quantify the macroscopically long decoherence time expected. In the final part of the Chapter, we discuss the use of the scheme in wider context. We illustrate the scheme on the example of a minimum concrete setup, at general level as well as with a concrete microscopic model and numbers.

The setup under consideration (Fig. 4.1) encompasses a finite 1D wire brought in proximity with a superconductor. It hosts 4 localized Majorana modes, two at the ends and two in the middle. This is achieved by a gap inversion in the middle section of the wire by a nearby gate. The wire sections at the sides are thus in topological regime of parameters while the middle section is topologically trivial. It is important for us that the first excited state right above the gap extends over the whole wire. This is achieved

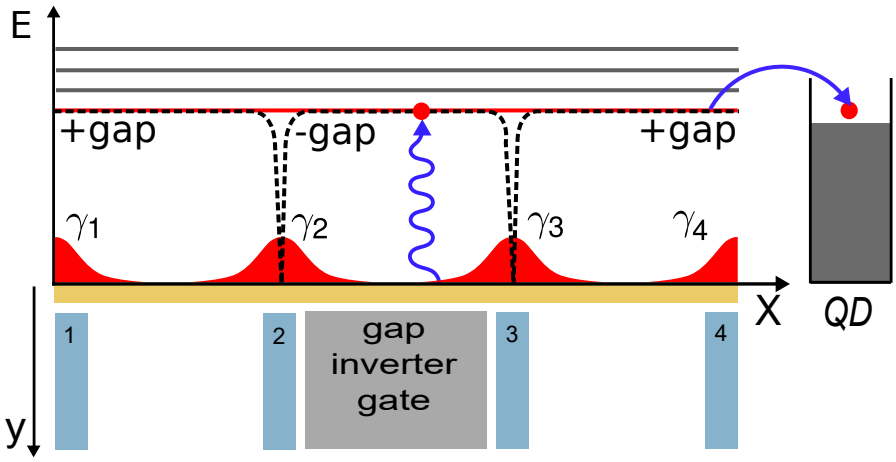

Figure 4.1: The setup for the resonant manipulation of Majorana modes. The proximitized nanowire (orange rectangle) with the inverted gap in the middle section hosts four Majorana modes (γ_{1-4}) formed on the edges of the sections of different topology. The four gates in the vicinity of the modes are used to apply a pulse sequence for the resonant manipulation, the resonance being with the lowest excited state (red line) extented over the modes. A quantum dot on the left can be used to detect the population of the excited state.

by matching the absolute values of the gap in the middle and side sections by the gap inverter gate. To achieve efficient resonant manipulation, we require four more gates near the positions of Majorana modes. This is all we need for resonant manipulation. To detect a possible quasiparticle in the excited state, we put a quantum dot nearby (it can be in the same nanowire). The addition energy of the dot is tuned such that a quasiparticle in the excited state tunnels to the dot changing its charge, which is measured. For effective detection, the tunnel rate should exceed the relaxation rate. The tunnel coupling can be switched on only for duration of measurement.

To start with, let us understand the basis involving the Majorana modes and the first excited state. Let $c_L = (\gamma_1 + i\gamma_2)/2$, $c_R = (\gamma_3 + i\gamma_4)/2$ be the quasiparticle annihilation operators in Majorana subspace, and c_{ex} to be that in the excited state. A basis state is defined as $|n_L, n_R\rangle|n_{ex}\rangle$, where $n_L, n_R, n_{ex} = 0, 1$ are the respective occupation numbers. We thus have 8 states. They separate into two groups of four corresponding to two possible total parities. There can be no coherence between the states of different parities. We define the bases as follows:

$$\Phi_e = \{|00\rangle|0\rangle,\ |11\rangle|0\rangle,\ |01\rangle|1\rangle,\ |10\rangle|1\rangle\}, \tag{4.1}$$

for the even parity, and

$$\Phi_o = \{|01\rangle|0\rangle,\ |10\rangle|0\rangle,\ |00\rangle|1\rangle,\ |11\rangle|1\rangle\}, \tag{4.2}$$

for the odd parity. The first two states for each parity form Majorana subspace. We can thus realize a Majorana qubit for each parity. We would like to perform unitary operations in Majorana subspace. A particular unitary operation is a braiding of two Majorana

modes defined as $U_{ij} = \frac{1}{\sqrt{2}}(1+\gamma_i\gamma_j)$. For instance, the braiding of the second and the third mode in the odd basis Φ_e is given by

$$U^o_{23} = \frac{1}{\sqrt{2}}(1+\gamma_2\gamma_3) = \frac{1}{\sqrt{2}}\begin{pmatrix} 1 & i & 0 & 0 \\ i & 1 & 0 & 0 \\ 0 & 0 & 1 & i \\ 0 & 0 & i & 1 \end{pmatrix}. \tag{4.3}$$

As we see, it is separated into blocks of Majorana and excited subspace, as these operations are independent. Since we wish to operate in Majorana subspace, the excited block is irrelevant. The corresponding matrix in the even subspace is obtained from (4.3) by the following transformation

$$U^e = \Sigma_y\sigma_y U^{o*}\sigma_y\Sigma_y. \tag{4.4}$$

σ_y, Σ_y being Pauli matricies acting within and over the blocks, respectively. Eventually, this relation holds for all braidings as well as for any 4×4 matrix we consider here. So we wish to perform braidings, as well as any unitary operations in Majorana subspace. This task by its own is senseless unless we have means to initialize to a state in this subspace and measure the result. Let us see how we can realize this by resonant manipulation.

A resonant manipulation is performed by applying the oscillating voltages to the gates $1-4$ with the frequency matching the energy spacing. At constant amplitudes, the general Hamiltonian in rotating wave approximation reads:

$$H_{\rm rm} = \left(\alpha_1 c_L + \alpha_2 c_R + \alpha_3 c_L^\dagger + \alpha_4 c_R^\dagger\right) c_{\rm ex} + h.c. \tag{4.5}$$

The four complex coefficients α_{1-4}, are in linear relation with the four complex voltage amplitudes at the gates, so 4 gates suffice to control all coefficients. Applying a pulse of duration t makes a unitary operation $U = e^{-iH_{\rm rm}t}$ in 8-dimensional basis. The manipulation conserves parity, so the matrix separates in two 4×4 blocks U_e, U_o in the bases Φ_e, Φ_o. It is simple and important to show that these matrices satisfy the same relation (4.4) as the braiding matrices.

Let us stress that our aim is to find a unitary transformation that works in Majorana subspace only. To this end, we require a special form of the resulting U: that separated in two 2×2 blocks, like in Eq. 4.3. In other words, the excited state should not be populated at the end of the resonant manipulation if we start in Majorana subspace. This is impossible to achieve with a single pulse. A key observation is that this can be achieved combining *several* pulses. Two pulses with 8 complex parameters in total in principle suffice to realize our aim: an arbitrary 2×2 unitary transformation in Majorana basis. We describe the concrete methods of the pulse design and give examples further in the text.

Let us describe the protocol for initialization and read out starting from an unknown state of unknown parity in Majorana subspace. We will show that this requires two resonant pulse sequences, that is, unitary transformations, and a measurement after each sequence. We dub these sequences a developer and a fixer. To start with, let us assume

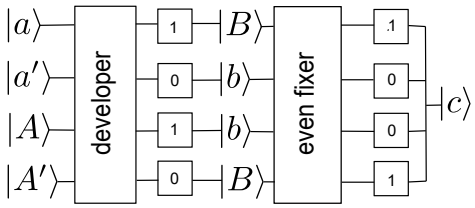

Figure 4.2: Initialization and read-out in Majorana subspace is achieved by two resonant pulse sequences: developer and fixer, and subsequent measurements of the excited quasiparticle. Upper(lower)case letters refer to Majorana superpositions of odd(even)parity, prime indicates orthogonality, $\langle a'|a\rangle = 0$. The measurement outcomes are in square boxes. The protocol brings the system to the state $|c\rangle$ from an unknown state. The probabilities of the measurement outcomes give the probabilities of the states $|a\rangle, |a'\rangle, |A\rangle, |A'\rangle$. See the text for details.

that we start in a Majorana state of even parity. Let us understand the effect of the following 4×4 unitary transformation:

$$D^e = |B\rangle|1\rangle\langle a|\langle 0| + |b\rangle|0\rangle\langle a'|\langle 0| \\ +|B'\rangle|1\rangle\langle A|\langle 1| - |b'\rangle|0\rangle\langle A'|\langle 1|. \tag{4.6}$$

Here, lowercase letters denote the Majorana states in the even subspace ($|00\rangle$, $|11\rangle$ or their linear combination) while capital ones denote those in the odd subspace ($|01\rangle$, $|10\rangle$ or their linear combination). The prime denotes a corresponding orthogonal state, $|a'\rangle \equiv (i\sigma_y|a\rangle)^*$, $\langle a|a'\rangle = 0$ (note that $i\sigma_y i\sigma_y|a\rangle = -|a\rangle$). If the initial state is $|a\rangle$, this developer brings the system to the excited subspace. The quasiparticle tunnels to the dot, we measure outcome "1" and the system is in the state of the opposite parity, $|B\rangle|0\rangle$. (Fig. 4.2). If the initial state is orthogonal, no excitation occurs, we measure output "0" and get to the state $|b\rangle|0\rangle$. We see that the developer can be used to measure the probability of $|a\rangle$ if the initial parity is known to be even, and the final state is known from the measurement result. However, the parity is generally unknown.

Let us see how the same developer works in the odd subspace. We apply Eq. (4.4) to obtain:

$$\begin{aligned} D^o &= -|B'\rangle|0\rangle\langle a'|\langle 1| - |b'\rangle|1\rangle\langle a|\langle 1| - \\ &- |B\rangle|0\rangle\langle A'|\langle 0| + |b\rangle|1\rangle\langle A|\langle 0|. \end{aligned} \tag{4.7}$$

We see that now the developer tries to distinguish between $|A\rangle$ and $|A'\rangle$, while the final states for the same output are opposite: $|b\rangle|0\rangle$ for "1" and $|B\rangle|0\rangle$ for "0". Thus, we do not know the final state if the parity is unknown, neither we know which state has been measured.

However, the situation can be fixed if we apply another unitary transformation. While this transformation does *not* depend on the result of the first measurement, it depends on the desired parity of the final state. In any case, the incoming states of a fixer are the same as the output states of the developer in the Majorana subspace. Let us consider the

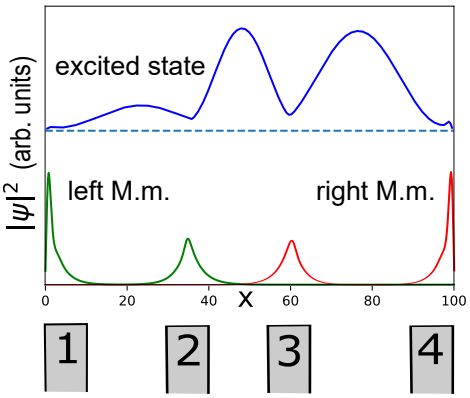

Figure 4.3: The concrete illustrative setup. The probability densities of eigenfunctions and the positions of modulation gates $1-4$ chosen at $[0;10]$, $[30;40]$, $[55;65]$ and $[90;100]$.

even fixer F_e first. Its representation for two parities reads:

$$\begin{aligned} F_e^e &= |c\rangle|0\rangle\langle b|\langle 0| + |C\rangle|1\rangle\langle b'|\langle 0| + \\ &+ |C'\rangle|1\rangle\langle B|\langle 1| + |c'\rangle|0\rangle\langle B'|\langle 1|, \end{aligned} \tag{4.8}$$

$$\begin{aligned} F_e^o &= |c'\rangle|1\rangle\langle b'|\langle 1| + |C'\rangle|0\rangle\langle b|\langle 1| - \\ &- |C\rangle|0\rangle\langle B'|\langle 0| - |c\rangle|1\rangle\langle B|\langle 0|. \end{aligned} \tag{4.9}$$

After the fixer, and the second measurement, the final state is always $|c\rangle|0\rangle$, this solves the initialization task. If the outcomes of the first and second measurements are "11" or "00", the initial parity was even. Otherwise, it was odd.

The odd fixer F_o has a similar structure,

$$\begin{aligned} F_o^e &= |C\rangle|1\rangle\langle b|\langle 0| + |c\rangle|0\rangle\langle b'|\langle 0| + \\ &+ |c'\rangle|0\rangle\langle B|\langle 1| + |C'\rangle|1\rangle\langle B'|\langle 1|, \end{aligned} \tag{4.10}$$

$$\begin{aligned} F_o^o &= -|C'\rangle|0\rangle\langle b'|\langle 1| - |c'\rangle|1\rangle\langle b|\langle 1| + \\ &+ |c\rangle|1\rangle\langle B'|\langle 0| + |C\rangle|0\rangle\langle B|\langle 0|. \end{aligned} \tag{4.11}$$

In any case, the final state is $|C\rangle|0\rangle$. The measurement outcomes "11" and "00" manifest even initial parity, "01" and "10" manifest odd initial parity. So both fixers not only solve the initialization task: they determine the initial parity.

We see that the protocol described at the same time provides a measurement tool. Suppose we are able to arrange an unknown state of unknown parity, and reproduce it on demand. To characterize the state, one just repeats the protocol collecting the statistics of outcomes. The probabilities of outcomes "11","00","10","01" give the probabilities of the basis states $|a\rangle, |a'\rangle, |A\rangle, |A'\rangle$, respectively. The developer and fixer pulse sequences can be designed and realized for any choice of the superpositions $|a\rangle, |b\rangle, |c\rangle, |A\rangle, |B\rangle, |C\rangle$. In Supplemental Material 4.2, we provide the concrete choice example.

To show the feasibility of the setup and the suggested pulse sequence design, we now specify a microscopic model and provide extensive numerical study for a concrete

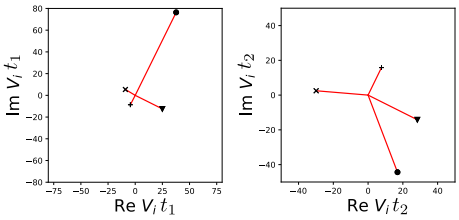

Figure 4.4: Designed two-pulse sequence for the braiding U_{23}. The gate voltage amplitudes V_{1-4} times pulse durations $t_{1,2}$ are given by circle, plus sign, triangle and x-mark, respectively.

set of parameters. We make use of the Hamiltonian [3, 4] to model a semiconducting nanowire with spin-orbit spectrum splitting, in the presence of applied uniform magnetic field B, and proximity-induced superconducting gap Δ. The gap inverter gate is described by a coordinate-dependent potential $\mu(x)$ such that its values in the middle and outer sections, μ_m, μ_o satisfy the conditions of trivial $B < \sqrt{\Delta^2 + \mu_m^2}$ and non-trivial $B > \sqrt{\Delta^2 + \mu_o^2}$ topology. The modulation gates are described by a time-dependent addition $\mu(x,t) = \sum_i V_i(t)\Theta(x-x_i)\Theta(y_i-x)$, x_i, y_i giving the start and end position of the gate i (see Fig. 4.3). The Hamiltonian in use reads

$$
\begin{aligned}
H_0 = \int dx \Psi^\dagger(x) \Big[\Big(-\frac{1}{2m}\frac{\partial^2}{\partial x^2} - i\alpha_{SOI}\sigma_z \frac{\partial}{\partial x} - \mu(x) \Big) \tau_z \\
+ B\sigma_x + \Delta\tau_x \Big] \Psi(x), \\
\Psi(x) = \{\psi_\uparrow(x), \psi_\downarrow(x), \psi_\downarrow^\dagger(x), -\psi_\uparrow^\dagger(x)\},.
\end{aligned}
\tag{4.12}
$$

$\psi_\sigma(x)$ being the electron field operators.

We measure length and energy in units of $(m\alpha_{SOI})^{-1}$ and $m\alpha_{SOI}^2$, respectively. We compute the spectrum and wavefunctions diagonalizing the discrete-in-space appoximation of the Hamiltonian (4.12), with the discretization step 0.2. We choose a relatively long wire with length $L = 100$ and the material parameters are of the order of 1: $B = 3$, $|\Delta| = 2.5$, $\mu_m = -1.91, \mu_o = -1.34$, see 4.2 for details. The transition between these two values are smoothed at the lenght scale of 3, and the setup has been made slightly asymmetric. The bulk energy gaps correspondig to these parameters are $G_e = 0.146$ and $G_m = 0.164$, they are not precisely equal because of the finite size of the middle section. With this, the lowest excited state at $E_1 = 0.175$ is extended over the wire(see Fig. 4.3). Higher excited states are situated at $E_2 = 0.180$ and $E_3 = 0.187$. For the resonant signal to address the lowest excited state only, the inverse pulse duration should not exceed the level spacing $E_2 - E_1$, this gives $t > 10^3$.

The wave functions are presented in Fig. 4.3. There are 4 Majorana localized modes with the width ≈ 5. We neglect a marginal overlap between the states setting them at zero energy. The wave function of the first excited state reminds the first particle-in-the box state with noticeable dips owing to orthogonality with Majorana peaks, and is extended over the whole length of the wire. With these wave functions, we compute the matrix elements of voltages applied to 4 gates whose positions are given in Fig. 4.3. This gives as a 4×4 matrix $\hat{M}$ that relates the voltage amplitudes and the resonant manipu-

lation coefficients α_i (Eq. (4.5)). To design a pulse sequence corresponding to a unitary operation, we compute the resulting matrix depending on the parameters α_i and time duration of each pulse, and iteratively minimize in α_i the distance between the resulting and target matrix. Using the matrix $\hat{M}$, we convert to the gate voltage amplitudes. The design for the braiding of the second and the third Majorana mode is presented in Fig. 4.4, extensive examples are to be found in 4.2.

To conclude, we propose a scheme that allows to realize braiding and all other unitary operations, as well as the measurement and initialization, for a Majorana qubit in a single 1D wire. It suits ideally to demonstrate macroscopically long coherence in Majorana space. The topological protection fails only during the operation. We illustrate the scheme with a concrete elaborated example.

Let us shortly present necessary discussions in a wider context. No experimental system can be modelled with the accuracy we did. However, to design the pulse sequencies, one only needs E_1 and the matrix M: the latter can be determined from the analysis of the spectra of the dressed resonant state at varying V_i. The resonance with the lowest state only is essential since it minimizes dissipation. Moreover, the excitation to many excited states is exponentially suppressed owing to destructive interference. The scheme can be readily extended to *more* Majorana modes within the single wire. While this can be done with a single state extended over the wire, but a simpler design would involve separate excited states, each extended over a group of Majorana modes. This can be achieved by proper profile of $\mu(x)$. At the moment, the technological efforts are aimed to increase transparency of the barrier between the wire and the superconductor. As it is shown, for instance, in [14] at sufficiently high transparency the wire is not described by the Hamiltonian [3, 4] and eventually looses the localized excited states. So the moderate transparency is required for experimental realization of our idea. The idea presented may be also useful in the context of more traditional 2D Majorana braiding: one can set a localized excited state, switch on a resonant field, and move the modes passing the state to achieve the resonant manipulation and read out.

4.2. SUPPLEMENTAL MATERIALS

In this Supplemental Material, we present additional details and calculations regarding the example setup under consideration, as well as concrete designs of unitary transformations for quantum manipulation, initialization, and measurement.

4.2.1. WAVE FUNCTIONS AND MATRIX ELEMENTS OF GATE VOLTAGES

To find the wave functions, we diagonalize numerically the Hamiltonian (4.12). Owing to BdG symmetry, they come in pairs with positive and negative energies. We fix the phases of these wavefunctions in such a way that $|\psi^*(E)\rangle = \sigma_x|\psi(E)\rangle$ and $|\psi(-E)\rangle = -i\tau_y\sigma_z|\psi(E)\rangle$.

This suffices for the wave functions of the excited state, $|\mathrm{ex}_\pm\rangle$, $\pm$ corresponding to positive/negative energy. More work is required for wave functions in Majorana subspace. Owing to a residual overlap of Majorana modes (see Section S5), the eigenfunctions of the Hamiltonian are rather arbitrary linear combinations of the wave functions corresponding to the modes. To establish a proper basis in the Majorana subspace, we

proceed as follows. We take 4 Hamiltonian eigenfunctions with lowest (residual) energies, form a matrix of elements of the operator x in this 4-dimensional basis, and diagonalize it. The 4 eigenvalues correspond to 4 positions of the localized modes, and the corresponding eigenvectors are those of the modes. Next, we pick up two modes (1 and 2) on the left, and diagonalize 2×2 matrix of the elements of an operator τ_z (any operator with BdG symmetry would suffice). As the result, we obtain two eigenfunctions $|L_\pm\rangle$ of the Majorana quasiparticle on the left. Picking up two modes on the right (3 and 4), we construct $|R_\pm\rangle$.

Next, we compute the matrix elements of the perturbation $H_{\rm rm}$ brought by the gate voltage modulations,

$$H_{\rm rm} = -\tau_z \sum_i V_i(t)\Theta(x-x_i)\Theta(y-y_i), \tag{4.13}$$

x_i, y_i being start and end positions of the gate i. We rewrite $H_{\rm rm}$ in the second-quantization form (Eq. 4.5) to the BdG form which allows us to express the coefficients α_i in terms of eigenstates of the BdG Hamiltonian with positive (+) and negative (−) energy eigenvalue, and find the following relations for the matrix elements,

$$\alpha_1 = \langle L_-|H_{\rm rm}|{\rm ex}_+\rangle;\ \alpha_2 = \langle R_-|H_{\rm rm}|{\rm ex}_+\rangle;\ \alpha_3 = \langle L_+|H_{\rm rm}|{\rm ex}_+\rangle;\ \alpha_4 = \langle R_+|H_{\rm rm}|{\rm ex}_+\rangle. \tag{4.14}$$

4.2.2. RELATION BETWEEN PULSE PARAMETERS AND GATE VOLTAGE AMPLITUDES

The Hamiltonian for each resonant pulse is written in terms of resonant parameters α_{1-4}. In odd subspace, it reads:

$$H = \begin{pmatrix} 0 & 0 & \alpha_4 & \alpha_1 \\ 0 & 0 & \alpha_3 & -\alpha_2 \\ \alpha_4^* & \alpha_3^* & 0 & 0 \\ \alpha_1^* & -\alpha_2^* & 0 & 0 \end{pmatrix} \tag{4.15}$$

Its form in even subspace is obtained from the relation $H_e = -\Sigma_y\sigma_y H_o^*\sigma_y\Sigma_y$.

To find the relation between the resonant parameters and the gate voltage amplitudes, we evaluate Eqs. (4.14) for each V_i independently, and invert the corresponding matrix. We obtain the linear relation $V_i = M_{ij}\alpha_j$ where the 4×4 real matrix M is given by

$$M = \begin{pmatrix} 27.9300 & -0.0009 & -27.8803 & 0.0009 \\ -5.8723 & -0.0219 & -5.8375 & 0.0219 \\ 0.0083 & 4.6067 & 0.0082 & -4.5970 \\ 0.0002 & -13.8756 & 0.0002 & -13.8682 \end{pmatrix} \tag{4.16}$$

4.2.3. PULSE SEQUENCES REQUIRED FOR BRAIDING

For 4 Majorana modes, there are six possible braiding matrices U_{ij}. We list here the explicit form of these matrices in the odd subspace:

$$U_{13}^o = \frac{1}{\sqrt{2}}\begin{pmatrix} 1 & -1 & 0 & 0 \\ 1 & 1 & 0 & 0 \\ 0 & 0 & 1 & -1 \\ 0 & 0 & 1 & 1 \end{pmatrix} \tag{4.17}$$

$$U_{12}^{o}=\frac{1}{\sqrt{2}}\begin{pmatrix}1+i & 0 & 0 & 0\\ 0 & 1-i & 0 & 0\\ 0 & 0 & 1+i & 0\\ 0 & 0 & 0 & 1-i\end{pmatrix} \tag{4.18}$$

$$U_{23}^{o}=\frac{1}{\sqrt{2}}\begin{pmatrix}1 & i & 0 & 0\\ i & 1 & 0 & 0\\ 0 & 0 & 1 & i\\ 0 & 0 & i & 1\end{pmatrix} \tag{4.19}$$

$$U_{14}^{o}=\frac{1}{\sqrt{2}}\begin{pmatrix}1 & -i & 0 & 0\\ -i & 1 & 0 & 0\\ 0 & 0 & 1 & i\\ 0 & 0 & i & 1\end{pmatrix} \tag{4.20}$$

$$U_{24}^{o}=\frac{1}{\sqrt{2}}\begin{pmatrix}1 & -1 & 0 & 0\\ 1 & 1 & 0 & 0\\ 0 & 0 & 1 & 1\\ 0 & 0 & -1 & 1\end{pmatrix} \tag{4.21}$$

$$U_{34}^{o}=\frac{1}{\sqrt{2}}\begin{pmatrix}1-i & 0 & 0 & 0\\ 0 & 1+i & 0 & 0\\ 0 & 0 & 1+i & 0\\ 0 & 0 & 0 & 1-i\end{pmatrix} \tag{4.22}$$

As mentioned, their form in the even subspace is obtained by transformation (4.4) given in the main text.

To design the corresponding pulse sequence for a given target matrix U, we consider 2 pulses of resonant field with the Hamiltonians given by (4.15),

$$\Pi_2 = e^{-iH_2t_2}e^{-iH_1t_2} \tag{4.23}$$

Π_2 being the resulting matrix. We concentrate on the odd subspace. The resulting matrix depends on 8 complex parameters $\alpha_i^{(j)}t_j$, $j=1,2$, t_j being the pulse durations. We define a distance in the space of unitary matrices,

$$D=\mathrm{Tr}\left((U-\Pi_2)(U-\Pi_2)^{\dagger}\right). \tag{4.24}$$

We mininize D iteratively in the space of $\alpha_i^{(j)}t_j$ starting a random initial point. If the minimum is achieved at $D=0$, we have the solution. If $D\neq 0$ at the minimum, we repeat the procedure.

For all braiding matrices (4.17), (4.18), (4.19), (4.20), (4.21), (4.22) we obtain the required parameters $\alpha_i^{(j)}t_j$ with the relative accuracy $\sim 10^{-3}$. Using the matrix M given by Eq. (4.16) we obtain the corresponding voltage amplitudes for each pulse. The results for all braiding matrices are collected in the Table 4.1.

U^o_{13}		
first pulse	3.5626+1.4379i	104.8326 -3.3360i
	6.2875-0.7429i	-51.6591 +8.0068i
	2.5388-0.6246i	-17.5693 +0.4805i
	-0.2746+1.5416i	-45.5943-41.3344i
second pulse	-0.2407+1.3738i	-79.6332 +2.4531i
	-2.0651+1.3088i	7.5805-14.8275i
	0.7874+1.2231i	-10.5582 +0.3552i
	-2.5298+1.4434i	38.4411-39.0808i
U^o_{12}		
first pulse	-1.8112+0.9887i	-38.0629-103.3642i
	3.1254-3.2631i	-44.6421 +16.6691i
	4.4961+0.4385i	8.8887 -14.0691i
	0.1083-2.0622i	23.6168 +14.9035i
second pulse	1.2309-3.2858i	72.2241+133.8673i
	0.4281+1.5560i	10.0026 +9.7060i
	-2.1617-3.2428i	21.4980 +18.1660i
	3.4413+0.6674i	-30.6798i +36.3059i
U^o_{23}		
first pulse	-2.3878+1.1627i	37.7004+76.3880i
	1.0442+2.1060i	-4.4629 -8.6305i
	-0.3063-0.6299i	24.9729-12.4763i
	3.0368-1.5506i	-9.0232 +5.3913i
second pulse	-2.0021+1.4490i	16.9146-44.3686i
	-0.3673-2.1380i	7.7136+15.8356i
	-0.9749-0.5503i	28.3286-14.1843i
	4.1538-1.6281i	-29.8720 +2.4944i
U^o_{14}		
first pulse	0.6530+2.2008i	-127.1431-100.2741i
	-2.3252-3.1458i	0.7380 +15.8719i
	2.2310+0.4450i	-22.5744 +0.7148i
	-4.2483+2.3562i	49.8913 -63.2159i
second pulse	-3.5774-2.0921i	102.6599-51.9062i
	0.6735-0.5148i	13.4862 -4.8453i
	-3.0076+1.3460i	24.2822 +2.3053i
	1.7053+1.5887i	25.9498+51.0587i
U^o_{24}		
first pulse	-2.3317+0.5118i	-69.7238-53.0538i
	0.6100+0.1589i	-21.7916-12.9138i
	3.1119+2.0622i	9.0500-12.1150i
	-0.3689-2.1230i	37.4569+22.3599i
second pulse	4.4745+2.1958i	144.9705+13.2449i
	2.2551+0.0303i	3.9829 +2.4324i
	-2.9404-0.4445i	-12.7219 -3.2558i
	1.7047+1.4852i	-85.7087-51.0616i
U^o_{34}		
first pulse	-0.5448-1.7311i	-138.1478-32.2069i
	-1.6033-4.3352i	-10.1538+43.9911i
	3.3487-3.1879i	4.3630+16.0604i
	0.4002+1.7723i	2.0034 -0.5854i
second pulse	-0.4689-0.3569j	-41.7639+44.2386i
	-1.9545-0.3445j	14.1960+13.3048i
	-0.4600-1.9318i	-6.8107 -0.8697i
	-1.9420-0.5408i	33.4493+12.4548i

Table 4.1: Matrix elements of resonant perturbation for all braiding transformations. Left: from top to bottom $\alpha_4, \alpha_1, \alpha_3, \alpha_2$. Right: from top to bottom V_1, V_2, V_3, V_4

4.2.4. DEVELOPER AND FIXER FOR INITIALIZATION AND MEASUREMENT

As discussed in the main text, we need two pulse sequences for measurement and initialization: a developer D and a fixer F. For this illustration, we choose an even fixer F_e. In odd subspace, the corresponding unitary matrices are given by (4.7) and (4.10). Applying two pulses brings the Majorana subsystem to $|c\rangle$. As mentioned, the eigenstates involved can be chosen in arbitrary way. The concrete choice we made for this example is as follows:

$$|a\rangle = \begin{pmatrix}1\\0\end{pmatrix}, \quad |a'\rangle = \begin{pmatrix}0\\-1\end{pmatrix}, \quad |b\rangle = \frac{1}{\sqrt{2}}\begin{pmatrix}1\\-i\end{pmatrix}, \quad |\beta'\rangle = \frac{1}{\sqrt{2}}\begin{pmatrix}i\\-1\end{pmatrix}, \quad |c\rangle = \frac{1}{2}\begin{pmatrix}\sqrt{3}\\1\end{pmatrix}, \quad |c'\rangle = \frac{1}{2}\begin{pmatrix}1\\-\sqrt{3}\end{pmatrix} \tag{4.25}$$

$$|B\rangle = \frac{1}{\sqrt{2}}\begin{pmatrix}1\\1\end{pmatrix}, \quad |B'\rangle = \frac{1}{\sqrt{2}}\begin{pmatrix}1\\-1\end{pmatrix}, \quad |A\rangle = \begin{pmatrix}i\\0\end{pmatrix}, \quad |A'\rangle = \begin{pmatrix}0\\i\end{pmatrix}, \quad |C\rangle = \frac{1}{3}\begin{pmatrix}1\\2\sqrt{2}i\end{pmatrix}, \quad |C'\rangle = \frac{1}{3}\begin{pmatrix}-2\sqrt{2}i\\-1\end{pmatrix} \tag{4.26}$$

To design the corresponding pulse sequence, we apply the same numerical method as above. A peculiarity that the convergence for two pulses is rather poor. So for these transformations we implement three-pulse design:

$$\Pi_3 = e^{-iH_3t_3}e^{-iH_2t_2}e^{-iH_1t_3}. \tag{4.27}$$

to achieve the relative accuracy $\sim 10^{-3}$. The resulting matrix elements $\alpha_i^{(j)}t_j$ and corresponding voltage amplitudes for these three pulses are presented in Table 4.2.

4.2.5. RESIDULAL OVERLAP OF MAJORANA MODES

For the example setup under consideration, we still have a remaining overlap between the separated Majorana modes, since their width $\simeq 5$ is only a factor of 5 smaller than the minimal distance. Owing to the overlap, the two lowest eigenergies are finite, $4.14e-03$, and $2.33402015e-05$. If we express this as a Hamiltonian in the left-right basis in use, it reads

$$\begin{pmatrix} 0.00049355 & 0.00205414 & -0.00205413 & 0 \\ 0.00205414 & 0.00019598 & 0 & 0.002054132 \\ -0.00205413 & 0 & -0.00019598 & -0.002054143 \\ 0 & 0.002054132 & -0.002054143 & -0.00049355 \end{pmatrix} \begin{pmatrix} L_- \\ R_- \\ L_+ \\ R_+ \end{pmatrix} \tag{4.28}$$

This Hamiltonian, in principle, results in unitary evolution at time scale $\simeq 1000$. We did not take this evolution into account neglecting the corresponding Hamiltonian. The overlap can be easily made exponentially smaller for longer setups.

4.3. ACKNOWLEDGEMENTS

We acknowledge useful discussions with Anton Akhmerov, Kim Pöyhänen and Felix von Oppen. This project has received funding from the European Research Council (ERC) under the European Union's Horizon 2020 research and innovation programme (grant agreement No. 694272). This project was supported by the Netherlands Organisation for Scientific Research (NWO/OCW), as part of the Frontiers of Nanoscience (NanoFront) program.

D_o		
first pulse	-2.0495+2.0042i -4.0966+4.5633i -1.9107+2.7887i 1.4154+0.6030i	-61.1507+49.7052i 35.1354-43.0467i 15.8924 -6.3745i 8.7827-36.1612i
second pulse	6.5586-1.2382i -1.3629-5.4106i -3.1199-2.9906i 2.7259-1.5108i	48.9201i-67.7397i 26.3007+49.2372i -17.6294 -1.3374i -128.7829+38.1339i
third pulse	-1.4867-0.6612i 0.5468i-0.1334i 1.1283+0.6907i -2.5564+1.8971i	-16.1835-22.9873i -9.7742 -3.3047i -4.9286+11.7841i 56.0909-17.1536i
F_e^o		
first pulse	0.6126-0.8434i -1.8684 +0.2338i -0.5092-2.3555i -1.0239-1.3748i	-37.9861+72.2040i 13.9809+12.3891i -7.5534 -2.4738i 5.7111+30.7735i
second pulse	-0.3808+2.1101i 0.0977 -0.4129i -1.3286+2.1820i 1.3150+1.1225i	39.7697-72.3703i 7.1449-10.2913i 7.7986 -4.5144i -12.9653-44.8405i
third pulse	0.3121-1.2087i -0.9123+0.4286i -1.4933-0.0448i 1.7204+0.4916i	16.1518+13.2206i 14.0443 -2.2930i 6.4710 +7.8246i -28.2014 +9.9404i

Table 4.2: Matrix elements of resonant perturbation for 2 necessary unitary transformations in parity measurement scheme. Left: from top to bottom $\alpha_4, \alpha_1, \alpha_3, \alpha_2$. Right: from top to bottom V_1, V_2, V_3, V_4

REFERENCES

[1] A. Kitaev, Annals of Physics **303**, 2 (2003).

[2] C. Nayak, S. H. Simon, A. Stern, M. Freedman, and S. Das Sarma, Rev. Mod. Phys. **80**, 1083 (2008).

[3] R. M. Lutchyn, J. D. Sau, and S. Das Sarma, Phys. Rev. Lett. **105**, 077001 (2010).

[4] Y. Oreg, G. Refael, and F. von Oppen, Phys. Rev. Lett. **105**, 177002 (2010).

[5] V. Mourik, K. Zuo, S. M. Frolov, S. R. Plissard, E. P. A. M. Bakkers, and L. P. Kouwenhoven, Science **336**, 1003 (2012), https://science.sciencemag.org/content/336/6084/1003.full.pdf .

[6] M. T. Deng, C. L. Yu, G. Y. Huang, M. Larsson, P. Caroff, and H. Q. Xu, *Nano Letters*, Nano Letters **12**, 6414 (2012).

[7] A. Das, Y. Ronen, Y. Most, Y. Oreg, M. Heiblum, and H. Shtrikman, Nature Physics **8**, 887 (2012).

[8] A. D. K. Finck, D. J. Van Harlingen, P. K. Mohseni, K. Jung, and X. Li, Phys. Rev. Lett. **110**, 126406 (2013).

[9] H. Zhang, D. E. Liu, M. Wimmer, and L. P. Kouwenhoven, NATURE COMMUNICATIONS **10** (2019), 10.1038/s41467-019-13133-1.

[10] J. Alicea, Y. Oreg, G. Refael, F. von Oppen, and M. P. A. Fisher, Nature Physics **7**, 412 (2011).

[11] F. Harper, A. Pushp, and R. Roy, Phys. Rev. Research **1**, 033207 (2019).

[12] Z.-C. Yang, T. Iadecola, C. Chamon, and C. Mudry, Phys. Rev. B **99**, 155138 (2019).

[13] S. Gazibegovic, D. Car, H. Zhang, S. C. Balk, J. A. Logan, M. W. A. de Moor, M. C. Cassidy, R. Schmits, D. Xu, G. Wang, P. Krogstrup, R. L. M. Op het Veld, K. Zuo, Y. Vos, J. Shen, D. Bouman, B. Shojaei, D. Pennachio, J. S. Lee, P. J. van Veldhoven, S. Koelling, M. A. Verheijen, L. P. Kouwenhoven, C. J. Palmstrøm, and E. P. A. M. Bakkers, Nature **548**, 434 (2017).

[14] T. D. Stanescu, R. M. Lutchyn, and S. Das Sarma, Phys. Rev. B **84**, 144522 (2011).

5

WEYL POINTS IN THE MULTI-TERMINAL HYBRID SUPERCONDUCTOR-SEMICONDUCTOR NANOWIRE DEVICES

The technology of superconductor-semiconductor nanowire devices has matured in the last years in the quest for topological quantum computing. This makes it feasible to make more complex and sophisticated devices. We investigate multi-terminal superconductor-semiconductor wires to access feasibility of another topological phenomenon: Weyl singularities in their spectrum. We have found an abundance of Weyl singularities for devices with intermediate size of the electrodes. We describe their properties and the ways the singularities emerge and disappear upon variation of the setup parameters.

arxiv:2010.11494, submitted to PRB Rapid Communications; http://doi.org/10.5281/zenodo.4377239

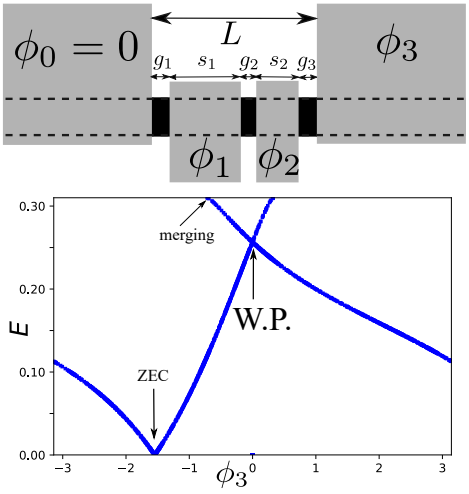

Figure 5.1: Top: The family of the hybrid superconductor-semiconductor setups under consideration. A long semiconducting nanowire is covered by 4 superconducting leads kept at three independent superconducting phases $\phi_{1,2,3}$. A setup is characterized by overall length L and the lengths of electrodes and gaps, $s_{1,2}, g_{1,2,3}$. Bottom: A typical spectrum of Andreev bound states along the line passing a Weyl point where the bands cross. Other features worth attention are zero-energy crossing that occur at a 2D surface in 3D space of the phases, and merging of the second energy band with the gap edge (top egde of the plot).

5.1. MULTI-TERMINAL HYBRID SUPERCONDUCTOR- SEMICONDUCTOR NANOWIRE DEVICES

Topological properties of solids have been a subject of intense research for last years[1, 2]. The prominent examples of topological materials include topological superconductors[3] that may host Majorana modes[4], and Weyl semimetals[5] with Weyl points[6] in the electron spectrum. Despite a big interest, the fabrication, purification and experimental analysis of topological materials is difficult and challenging[7]. This motivates a large effort to realize topologically non-trivial quantum states with topologically trivial materials.[4, 7]

The most known and successful effort of this kind is the realization of zero-energy Majorana states, that can be useful in topological quantum computing [8], in semiconductor nanowires covered by superconducting electrodes, so-called hybrid superconductor-semiconductor nanowire devices. The first experimental observation [9] came only in two years after the first theoretical proposal [10], yet a considerable enhancement of technology was needed for further progress. With the achievement of ballistic superconductivity [11] and experimental verification of topological signatures in Josephson effect [12], the very active sub-field and the technologies in use are mature for next level of experimental sophistication [13, 14]. One of the interesting directions is the fabrication of the multi-terminal nanowire-based devices.[13] Recently proposed Andreev molecules [15] that exhibit non-trivial features in the spectrum of the Andreev states [16, 17] require three superconducting terminals, and the fabrication efforts are underway. In the same manner, one can realize the devices with more terminals.

It has been suggested that the topologically protected spectral singularities - Weyl points - may be realized in multi-terminal superconducting nanostructures[18], potentially, in any nanostructures. The tuning of 3 parameters is required to achieve the singularity, so the minimum number of terminals is four corresponding to three independent superconducting phases. The singularity is pinned to zero energy (counted from Fermi level) in the absence of spin-orbit interaction, and is at finite energy distance if spin-orbit interaction is significant [19]. The topological charge is manifested by transconductance quantization [18, 20] and can be detected by a spectroscopic measurement [21], with some complications brought by the continuous spectrum above the superconducting gap [22]. Four-terminal devices have been fabricated in graphene [23] and 2D semiconducting structures [24]. However, the experimental confirmation of Weyl points is not yet available. The presence or absence of Weyl points in any concrete nanostructure depends on the details of scattering that may be difficult to identify and control, and only 6 % of random scattering matrices provide those. To facilitate the experimental observation and possible applications, it would be good to propose a system where the Weyl points are relatively abundant.

In this Chapter, we investigate the presence of Weyl points in a spectrum of a single-nanowire four-terminal hybrid semiconducting device of a straightforward design and indeed find many of those. This setup is distinct from that of several nanowires with coupled zero-energy Majorana modes [25–27]. In fact, we look for Weyl points at finite energy, where they are present irrespective of the Majorana modes, and find them both in topologically trivial and non-trivial wires.

A typical spectrum with a Weyl point is presented in Fig. 5.1. We set $\phi_{1,2}$ in such a way that the line passes the Weyl point. Other feature of the spectrum is zero-energy crossing (ZEC) [19, 28] that occurs at a 2D surface in the 3D space of phases. If the wire is in non-topological regime, there is an even number of ZEC separating the regions with different parity of the ground state. If, as in Fig. 5.1, the wire is in topological regime, the number of crossings may be odd [10] manifesting so-called 4π periodicity. The parity determination requires consideration of the zero-energy state at far ends of the wire [29].

We concentrate on a family of setups where a (formally infinite)semiconducting nanowire is covered by 4 separate superconducting films (see Fig.5.1). The flims are the superconducting leads kept at the corresponding superconducting phases $\phi_0 = 0, \phi_{1,2,3}$. The widths of 2 intermediate leads $s_{1,2}$ and the gaps between the leads $g_{1,2,3}$ sum up to L. A setup of the family is thus characterized by L and five numbers $\boldsymbol{s} \equiv [g_1/L, s_1/L, g_2/L, s_2/L, g_3/L]$ summing to 1. We investigate the possibility to realize Weyl points in the 3-dimensional phase space of 3 superconducting phases varying L.

The wave function of a Andreev bound state is localized at a typical scale ξ. At $L \ll \xi$ we expect no Weyl points since in this case the localized state hardly feels the middle leads and its energy depends on a single parameter only, $E(\phi_3)$. Neither we expect the Weyl points in the opposite limit $L \gg \xi$: in this case, the states are localized in the corresponding gaps g_i with the energies depending on the local phase differences $\phi_i - \phi_{i-1}$, again depending on a single parameter each. Therefore, we expect Weyl points to appear for each setup at $L \sim \xi$. Indeed, for most choices of $\boldsymbol{s}$ we find one or more intervals of L where the Weyl points are present, both in topological and non-topological regime.

We employ the Lutchin-Sau-Das-Sarma Hamiltonian[10];

$$H = \left(\frac{p^2}{2} - p\sigma_z - \mu\right)\tau_z + \mathrm{Re}\Delta(x)\tau_x + \mathrm{Im}\Delta(x)\tau_y + B\sigma_x \tag{5.1}$$

that we made dimensionless measuring lengths and energies in units of spin-orbit length and spin-orbit energy, τ_i, σ_i being Pauli matrices in Nambu and spin space, respectively. Here, $\Delta(x)$ is the superconducting order parameter induced in the wire. We assume a piecewise-constant spacial dependence where $\Delta(x) = |\Delta|e^{i\phi_i}$ under the leads, ϕ_i being the phase of the corresponding lead and $\Delta(x) = 0$ within the gaps(see Fig.5.1). The wire is in the topological regime[10] provided $|B| > \sqrt{|\Delta|^2 + \mu^2}$, otherwise it is in non-topological one.

The Hamiltonian (5.1) possesses the usual BdG symmetry $H^* = -\sigma_y\tau_y H\tau_y\sigma_y$ that guaranties the symmetry of the spectrum and Weyl points with respect to $E \to -E$. We concentrate at positive energies. Although the Hamiltonian 5.1 is not invariant with respect to time reversal, there is a look-alike extra symmetry

$$H^*(\boldsymbol{\phi}) = \sigma_x H(-\boldsymbol{\phi})\sigma_x \tag{5.2}$$

relating the Hamiltonians at opposite points $\boldsymbol{\phi}$ and $-\boldsymbol{\phi}$ in phase space. Therefore, the Weyl points come in pairs of the same charge at opposite points, as for a time-reversible scattering matrix [18]. It has been suggested in [18] that Weyl points emerge in groups of four conform to conservation topological charge. Here we find notable exceptions from this rule: the Weyl points emerging from the continuous spectrum at the gap edge.

The relevant examples of our numerical results are presented in Figs.5.2,5.3,5.4. In Fig.5.2 we plot the number and the energies of the Weyl points versus the overall setup length L. For each parameter set $\mu, |\Delta|, B$ we normalize L on the localization length ξ that is defined as the slowest decaying exponent under the leads 0,3. For all parameters and setups investigated, we find Weyl points in one or several intervals around $L \simeq \xi$. We observe strong dependence of number and energy dependences on the setup details. This is explained by the fact that the Weyl points emerge from complex interference in the setup, the interference pattern being affected by all details.

In non-topological regime (Figs. 5.2a, 5.2c) the points come in groups of four. Their energy dependence is seen as a closed curve, a trajectory in $L - E$ space, that does not touch the gap edge. The curves may intersect or self-intersect, the intersection corresponding to the points at the same energy but separated in phase space. The number of Weyl points at given L is 2 times number of intersections of the line $L = const$ with all the curves, as we see in the plots. Let us discuss the emergence of Weyl points upon changing L taking Fig. 5.2a as example. There are no points at $L < 0.71$. At $L = 0.71$, a pair of close points of opposite topological charges emerges at some phase settings $\boldsymbol{\phi}$, with close energies. At the same L, another pair emerges near $-\boldsymbol{\phi}$, so 4 points appear in total. Upon changing L up to 0.9, the points got separated in phase settings and energy. As explained in [18, 19], any 2D plane that separates the points in the phase space, acquires a non-trivial Chern number that is manifested as a quantized transconductance at even parity of the setup. Upon further change of L, the points of opposite charges get close together and eventually annihilate at $L = 1.04$. All this is seen as a closed trajectory in

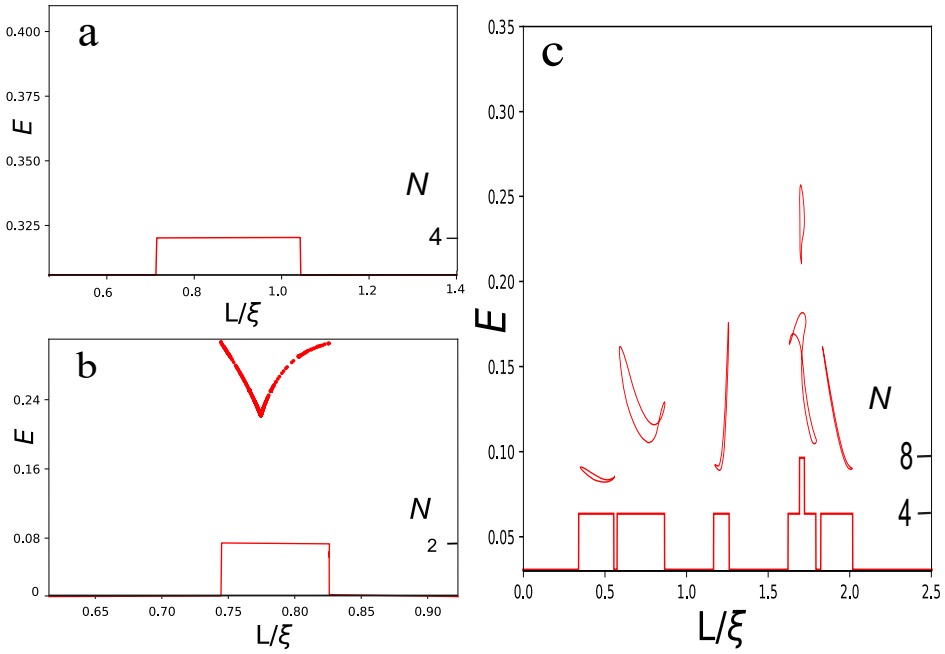

Figure 5.2: Number and energy dependence of Weyl points for several setups. Non-topological regime: a) $\mu, B, |\Delta| = (1,1,2)$, $\xi \approx 1.07$, $\boldsymbol{s} = (0,0.7,0,0.3,0.0)$; c) $\mu, B, |\Delta| = (1,1,0.9)$, $\xi \approx 2.30$, $\boldsymbol{s} = (0.04,0.61,0.09,0.26,0)$ Topological regime: c) $\mu, B, |\Delta| = (0.464,1.144,0.693)$, $\xi \approx 3.26$, $\boldsymbol{s} = (0,0.7,0,0.3,0.0)$; d) $\mu, B, |\Delta| = (0.951,2.407,1.665)$, $\xi \approx 2.1$, $\boldsymbol{s} = (0.05,0.66,0.01,0.28,0.0)$. For b) and c), the gap edge is at the top edge of a plot. For a), the gap edge is at 1.24.

$L-E$ space. More complex picture involving multiple trajectories of the same kind (let us call those type A trajectories) is seen in Fig. 5.2b.

In topological regime, zero-energy states are formed at the far ends of the wire (this is not detected in our approach that concentrates at the states localized at all electrodes). An example is provided in Fig. 5.2b. There are no points for $L < 0.745$. At $L = 0.745$, a Weyl point emerges from the continuous spectrum at some phase setting ϕ. The symmetry implies that another point of the same topological charge emerges at $-\phi$, so two points appear in total. Upon changing L the point changes its phase coordinate. It gets lower in energy first, but eventually returns back to the gap edge and disappears at $L = 0.781$. Such trajectories begin and end at the gap edge: let us call those type B trajectories.

We stress that such merging is not compatible with the presence of a continuous band of localized states throughout the Brillouin zone. This is seen from the following topological argument. Let us consider a 2D plane far from the point where the merging occurs. If there is a continuous band throughout the plane, the Chern number is well-defined. However, it must change upon merging. Since the plane is far from the merging point, this is impossible and proves the absence of such band, which also implies the absence of quantized transconductance. Indeed, a detailed view of the spectrum near the Weyl point merging (Fig. 5.3) shows that the localized states merge with continuous spectrum, and there are regions in the Brillouin zone where no localized state is present.

In total, we have investigated 12 setups, equal number in topological and non-topological regime. Ten of them have Weyl points in the intervals of $L \simeq \xi$. In several cases, we were not able to trace the whole curve and identify its type. The observation is that the type B trajectory we have seen in the topological regime only. However, no fundamental topological restriction can forbid the type B trajectories in non-topological regime or the type A trajectories in topological regime. One can see that if one considers a long but finite wire where the overall spectrum is discrete. Such regularization only affects the states at very small energies. For discrete spectrum, all trajectories are of type A. Presently, we assume that the observation is valid for the specific family of setups under consideration and is explained by the fact that the boundary conditions near the gap edge in the topological regime are more favourable for merging the localized states with continuum. More detailed research is underway.

We illustrate the wave functions of the localized states at a Weyl point in Fig. 5.4. The specifics of the situation is that there are two degenerate wave functions at the point, so eventually one could plot any linear combination of the two. The choice made is as follows: we consider matrix elements of the coordinate operator x in 2-dimensional degenerate subspace, determine and plot the corresponding eigenfunctions. The resulting eigenfunctions are therefore maximally separated in coordinate. We observe the localization of the wave functions at several ξ at the setup, and complex multiple-peak structure that witnesses complex wave interference required for Weyl points. The setup chosen has a mirror symmetry that is however violated by non-symmetric phase settings. Still, the wavefunctions look approximately mirror-symmetric.

To conclude, we have investigated the occurence of Weyl points in the spectrum of Andreev bound states in a family of realistic device setups where a semiconducting nanowire is covered by four superconducting electrodes. It is feasible to realize such setups experimentally and observe the corresponding topological singularities. For most

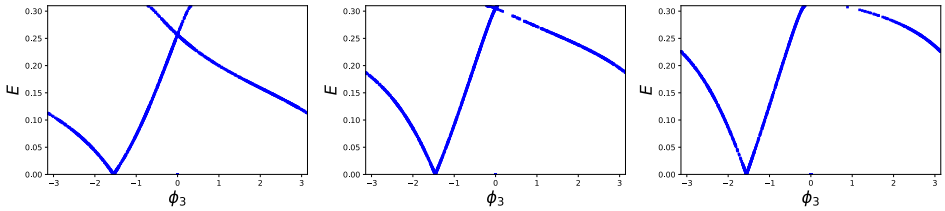

Figure 5.3: Merging of a Weyl point with the gap edge. Choice of the parameters and setup is the same as in Fig. 2c. We plot the spectrum versus ϕ_3 at a line hitting the Weyl point for three values of L. Left: $L/\xi = 0.781$, $\phi_1 = 2.639$, $\phi_2 = 2.629$ and , the Weyl point is $E = 0.256$ and $\phi_3 = 0.002$. Middle: $L/\xi = 0.824$, $\phi_1 = 2.260$, $\phi_2 = 2.256$, the Weyl point is precisely at the gap edge $E_g = 0.31$. Right: $L/\xi = 0.829$, there is no Weyl point, no bound state is found in an interval of ϕ_3.

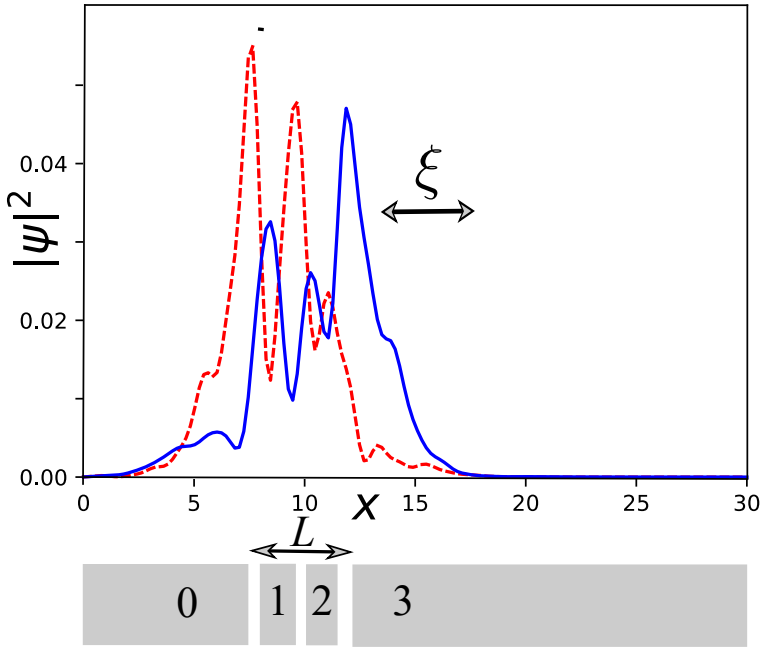

Figure 5.4: The densities $\sum_i |\psi(x)|_i^2$ of two degenerate wave functions (solid and dashed curves) at a Weyl point. The wave functions in the degenerate subspace are chosen to be eigenvectors of the coordinate operator x. The calculations are made for a finite wire of total length $l = 30$, the overlaps with the leads 0−3 are shown below the plot. The parameters are $B, \mu, |\Delta| = (1, 1, 0.9)$, corresponding to $\xi = 4.0$, $\boldsymbol{s} = (1/9, 1/3, 1/9, 1/3, 1/9)$. For $L = 4.5$, the point is found at $\phi_1, \phi_2, \phi_3 = (3.059, -0.448, 1.631)$.

setups, we find Weyl points for $L \simeq \xi$, that is for setup length of the order of the localization length of the bound states. In experiment, an in situ control of the device length is not feasible. However, it is custom for such devices to utilize a set of gate electrodes to control $\mu(x)$. We believe that this permits tuning of the device to the region where Weyl points are present.

We observe two types of the Weyl point trajectories. The type A trajectories do not touch the gap edge, and the Weyl points appear in the groups of 4. For type B trajectories, the Weyl points emerge from the gap edge in pairs. We have found the type B trajectory in topological regime only, this should be specific for the family of setups under consideration.

5.2. SUPPLEMENTARY MATERIAL

5.2.1. FINDING THE SPECTRUM

Here, we outline the method we use to find the spectrum of Andreev bound states in the setup. To start with, we write the Schrodinger equation for the 4-component eigenfunctions $\psi(x)$ of the Hamiltonian (Eq. (5.1)). This equation is of second-order in x-derivative

$$E\psi(x) = [-\frac{\tau_z}{2}\frac{\partial^2}{\partial x^2} + i\sigma_z\tau_z\frac{\partial}{\partial x} + C(x)]\psi(x). \tag{5.3}$$

Here, we define a 4×4 matrix $C(x) = B\sigma_x - \mu\tau_z + \mathrm{Re}\Delta(x)\tau_x + \mathrm{Im}\Delta(x)$. We rewrite it in a form of a first-order differential equation for a new 8-component vector $\Psi(x)$,

$$\frac{\partial\Psi}{\partial x} = \Lambda(x)\Psi, \quad \Psi = \begin{pmatrix}\psi\\ \partial\psi/\partial x\end{pmatrix} \tag{5.4}$$

The matrix $\Lambda(x)$ is defined as

$$\Lambda(x) = \begin{pmatrix}0 & 1\\ 2\tau_z(C(x)-E) & 2i\sigma_z\end{pmatrix} \tag{5.5}$$

The matrix Λ satisfies two symmetries:

$$\Lambda^*(x) = e^{i\frac{\phi(x)\tau_z}{2}}\sigma_x\Lambda(x)\sigma_x e^{-i\frac{\phi(x)}{2}\tau_z} \tag{5.6}$$

and

$$\Lambda\eta_z\sigma_x + \eta_z\sigma_x\Lambda = 0 \tag{5.7}$$

where η_z is a Pauli matrix in the space $\begin{pmatrix}\psi\\ \partial\psi/\partial x\end{pmatrix}$. Owing to these symmetries, the eigenvalues of Λ come in both complex-conjugated and opposite sign pairs: if λ is an eigenvalue, $-\lambda, \lambda^*, -\lambda^*$ are eigenvalues as well. There is also an extra symmetry $\Lambda^*(-E) = \eta_z\tau_y\sigma_y\Lambda(E)\sigma_y\tau_y\eta_z$ that guarantees $\lambda(E) = \lambda(-E)$. For an infinite lead with a constant $C(x)$, a pair of purely imaginary eigenvalues at a given energy E indicates a delocalized state at this energy. Since we are interested in the bound states, we restrict our consideration to the energy interval $0 < E < E_g$, where the spectral gap E_g is the minimum value of E at which the purely imaginary eigenvalue of Λ appears for infinite leads 0, 3.

In an interval where Λ is constant, the solution of Eq.(5.4) reads

$$\Psi(x) = e^{(x-x')\Lambda}\Psi(x') \tag{5.8}$$

For the part of the wire covered by the lead 0, where $\Lambda \equiv \Lambda_0$, we need to require the absence of divergent exponents at $x \to -\infty$. For this, let as introduce a projector on the 4-dimensional subspace spanned by the eigenvectors of Λ. One can compute this projector with using the eigen decomposition of Λ_0,

$$\Lambda_0 = v_0 \lambda_d v_0^{-1}; \tag{5.9}$$

where the diagonal λ_d is sorted in order of increasing Reλ. With this,

$$P_0^- = v_0 P_d^- v_0^{-1}, \tag{5.10}$$

where $P_d^- = \text{diag}\{1,1,1,1,0,0,0,0\}$.

This provides a condition for the wave function Ψ_0 at the right end of the interval covered by the lead 0,

$$P_0^- \Psi_0 = 0 \tag{5.11}$$

Similarly, with the projector P_3^+ that projects on positive eigenvalues of Λ_3, we determine the condition on the wave function Ψ_3 at the left end of the interval covered by the lead 3,

$$P_3^+ \Psi_3 = 0 \tag{5.12}$$

From the other hand, we can implement the relation (5.8) throughout the setup to obtain that $\Psi_3 = U\Psi_0$,

$$U = \exp(g_3\bar{\Lambda}_3)\exp(s_2\Lambda_2)\exp(g_2\bar{\Lambda}_2)\exp(s_1\Lambda_1)\exp(g_1\bar{\Lambda}_1); \tag{5.13}$$

$\bar{\Lambda}$ being the Λ matrices in the corresponding gaps. This gives the second condition on the same vector Ψ_0:

$$P_3^+ U \Psi_0 = 0 \tag{5.14}$$

Next step is to find a proper matrix for which Ψ_0 is an eigenvector with zero eigenvalue, $M\Psi_0 = 0$. It may seem that any linear combination of Eq. 5.11 and Eq. 5.14 with non-degenerate matrix coefficients would provide such a matrix. However, these linear combinations would also have additional zero eigenvalue eigenvectors that are distinct from Ψ_0. To make sure that these additional eigenvectors do not appear, the matrix coefficients in the linear superposition of two conditions should be chosen such that two terms project onto mutually orthogonal subspaces.

The simplest way to achieve this is to multiply Eq. 5.11 with v_0^{-1}, Eq. 5.14 with v_3^{-1}, and add them up. With this,

$$M = P_d^- v_0^{-1} + P_d^+ v_3^{-1} U \tag{5.15}$$

and the energy of the bound state is determined from the condition of zero determinant of this matrix. For technical reasons, we prefer to work with an equvalent matrix, $\bar{M} \equiv M v_0$, and solve for

$$\det(\bar{M}) = 0 \tag{5.16}$$

to find the energies of the bound states. The root finding was implemented as a minimization of the function $F \equiv |\det(\bar{M})|^2$ over the interval of energies $(0, E_g)$, with subsequent check if zero minimum is achieved. The special properties of the matrix Λ guarantees that the zeroes of this complex determinant are achieved at real E.

5.2.2. SEARCH FOR WEYL POINTS

In principle, the presence of a Weyl point can be detected by a thorough scanning of the obtained eigenvalues throughout the whole Brillouin zone of (ϕ_1, ϕ_2, ϕ_3). This, however, is a very time-consuming procedure.

We automate the search for the Weyl points as follows. It is crucial to note that at a Weyl point the determinat has a double zero, that is, in addition to $\det(\bar{M}) = 0$ the condition $\partial_E \det(\bar{M}) = 0$ is also satisfied. So for the search of Weyl points, we fix the setup $\boldsymbol{s}$, the parameters $\mu, B, |\Delta|$ and minimize the function

$$F = |\det(\bar{M})|^2 + |\partial_E \det(\bar{M})|^2 \tag{5.17}$$

in the 5-dimensional parameter space $(E, L, \phi_1, \phi_2, \phi_3)$ starting from a random point and checking if zero minimum is achieved. The output is a set of points in this space that lie at a 1-dimensional manifold. This is how the data plotted in Fig. 2 have been obtained. Once the coordinates of a Weyl point are found, one can compute the spectrum along a line in phase space that passes the point: this is how the plot in Fig. 1 has been obtained. The procedure described also permits finding the wave functions of the localized states. However, for the plots in Fig. 4 we made use of direct diagonalization of a discrete version of the Hamiltonian 5.1.

5

5.3. ACKNOWLEDGEMENTS

We acknowledge useful discussions with Manuel Houzet and Julia Meyer. This project was supported by the Netherlands Organisation for Scientific Research (NWO/OCW), as part of the Frontiers of Nanoscience (NanoFront) program, and has received funding from the European Research Council (ERC) under the European Union's Horizon 2020 research and innovation programme (Grant Agreement No. 694272).

REFERENCES

[1] X. Qi and S. Zhang, Rev. Mod. Phys. **83**, 10.1103/RevModPhys.83.1057 (2011).

[2] B. Bernevig, T. Hughes, and S. Zhang, Science **314**, 10.1126/science.1133734 (2006).

[3] M. Sato and Y. Ando, Reports on Progress in Physics **80**, 076501 (2017).

[4] J. Alicea, Reports on Progress in Physics **75**, 076501 (2012).

[5] N. P. Armitage, E. J. Mele, and A. Vishwanath, Rev. Mod. Phys. **90**, 015001 (2018).

[6] H. Weyl, Zeitschrift für Physik **56**, 330 (1929).

[7] P. Liu, J. R. Williams, and J. J. Cha, Nature Reviews Materials **4**, 479 (2019).

[8] C. Nayak, S. H. Simon, A. Stern, M. Freedman, and S. Das Sarma, REVIEWS OF MODERN PHYSICS **80**, 1083 (2008).

[9] V. Mourik, K. Zuo, S. M. Frolov, S. R. Plissard, E. P. A. M. Bakkers, and L. P. Kouwenhoven, SCIENCE **336**, 1003 (2012).

[10] R. M. Lutchyn, J. D. Sau, and S. Das Sarma, Phys. Rev. Lett. **105**, 077001 (2010).

[11] H. Zhang, O. Gul, S. Conesa-Boj, M. P. Nowak, M. Wimmer, K. Zuo, V. Mourik, F. K. de Vries, J. van Veen, M. W. A. de Moor, J. D. S. Bommer, D. J. van Woerkom, D. Car, S. R. Plissard, E. P. A. M. Bakkers, M. Quintero-Perez, M. C. Cassidy, S. Koelling, S. Goswami, K. Watanabe, T. Taniguchi, and L. P. Kouwenhoven, NATURE COMMUNICATIONS **8**, 10.1038/ncomms16025 (2017).

[12] D. Laroche, D. Bouman, D. J. van Woerkom, A. Proutski, C. Murthy, D. I. Pikulin, C. Nayak, R. J. J. van Gulik, J. Nygard, P. Krogstrup, L. P. Kouwenhoven, and A. Geresdi, NATURE COMMUNICATIONS **10**, 10.1038/s41467-018-08161-2 (2019).

[13] H. Zhang, D. E. Liu, M. Wimmer, and L. P. Kouwenhoven, NATURE COMMUNICATIONS **10**, 10.1038/s41467-019-13133-1 (2019).

[14] S. M. Frolov, M. J. Manfra, and J. D. Sau, NATURE PHYSICS **16**, 718 (2020).

[15] J. D. Pillet, V. Benzoni, J. Griesmar, J. L. Smirr, and C. O. Girit, NANO LETTERS **19**, 7138 (2019).

[16] V. Kornich, H. S. Barakov, and Y. V. Nazarov, Phys. Rev. Research **1**, 033004 (2019).

[17] V. Kornich, H. S. Barakov, and Y. V. Nazarov, PHYSICAL REVIEW B **101**, 10.1103/PhysRevB.101.195430 (2020).

[18] R.-P. Riwar, M. Houzet, J. S. Meyer, and Y. V. Nazarov, Nature Communications **7**, 11167 EP (2016).

[19] T. Yokoyama and Y. V. Nazarov, Phys. Rev. B **92**, 155437 (2015).

[20] E. Eriksson, R.-P. Riwar, M. Houzet, J. S. Meyer, and Y. V. Nazarov, PHYSICAL REVIEW B **95**, 10.1103/PhysRevB.95.075417 (2017).

[21] R. L. Klees, G. Rastelli, J. C. Cuevas, and W. Belzig, PHYSICAL REVIEW LETTERS **124**, 10.1103/PhysRevLett.124.197002 (2020).

[22] E. V. Repin, Y. Chen, and Y. V. Nazarov, Phys. Rev. B **99**, 165414 (2019).

[23] A. W. Draelos, M.-T. Wei, A. Seredinski, H. Li, Y. Mehta, K. Watanabe, T. Taniguchi, I. V. Borzenets, F. Amet, and G. Finkelstein, Nano Letters **19**, 1039 (2019).

[24] N. Pankratova, H. Lee, R. Kuzmin, M. Vavilov, K. Wickramasinghe, W. Mayer, J. Yuan, J. Shabani, and V. E. Manucharyan, The multi-terminal josephson effect (2018), arXiv:1812.06017 [cond-mat.supr-con] .

[25] K. Sakurai, M. T. Mercaldo, S. Kobayashi, A. Yamakage, S. Ikegaya, T. Habe, P. Kotetes, M. Cuoco, and Y. Asano, Phys. Rev. B **101**, 174506 (2020).

[26] J. P. T. Stenger and D. Pekker, Phys. Rev. B **100**, 035420 (2019).

[27] M. Houzet and J. S. Meyer, Phys. Rev. B **100**, 014521 (2019).

[28] B. van Heck, S. Mi, and A. R. Akhmerov, Phys. Rev. B **90**, 155450 (2014).

[29] D. I. Pikulin and Y. V. Nazarov, Phys. Rev. B **86**, 140504 (2012).

ACKNOWLEDGEMENTS

I would like to sincerely thank anyone who had made a positive contribution to this thesis, especially Trần Ngọc Bích for invaluable help with Inkscape, Jupyter notebook and transferable skills. I would also like to appreciate the efforts of the Graduate School (I believe my transferable skills are godlike now).

CURRICULUM VITÆ

Evgeny REPIN

16-07-1993 Born in Tambov, Russia.

EDUCATION

2003–2010 Physical-mathematical Lyceum № 14
Tambov, Russia

2010–2014 BSc. in Physics
Moscow Institute of Phisics and Technology
Landau Institute for Theoretical Physics
Thesis: Landau levels at the surface of 3D topological insulator: The role of hexagonal warping and finite mass
Promotor: Dr. I.S. Burmistrov

2014–2016 MSc. in Physics
Moscow Institute of Phisics and Technology
Landau Institute for Theoretical Physics
Thesis: Mesoscopic fluctuations of single-particle Green's function at Anderson transitions with interactions
Promotor: Dr. I.S. Burmistrov

2016–2020 PhD. in Physics
Kavli Institute of Nanoscience, TU Delft
Thesis: Topological properties of superconducting nanostructures
Promotor: Prof. Dr. Y.V. Nazarov

2021– unemployed

List of Publications

8. **E. V. Repin, Y. V. Nazarov**, *Weyl points in the multi-terminal Hybrid Superconductor-Semiconductor Nanowire devices*, https://arxiv.org/abs/2010.11494, submitted to PRB Rapid Communications.

7. **Viktoriia Kornich, Xiaoli Huang, Evgeny Repin, Yuli V. Nazarov**, *Braiding and all quantum operations with Majorana modes in 1D* , https://arxiv.org/abs/2009.06578, accepted to PRL.

6. **E. V. Repin, Y. V. Nazarov**, *Topological numbers of quantum superpositions of topologically non-trivial bands*, https://arxiv.org/abs/1905.12376, submitted to PRB.

5. **E. V. Repin, Y. Chen, and Y. V. Nazarov**, *Topological properties of multiterminal superconducting nanostructures: Effect of a continuous spectrum*, Phys. Rev. B **99**, 165414 (2019).

4. **I.S. Burmistrov, E.V. Repin**, *Quantum corrections to conductivity of disordered electrons due to inelastic scattering off magnetic impurities*, Phys. Rev. B **98**, 045414 (2018).

3. **E.V. Repin, I.S. Burmistrov**, *Mesoscopic fluctuations of the single-particle Green's function at Anderson transitions with Coulomb interaction*, Phys. Rev. B **94**, 245442 (2016).

2. **E.V. Repin, I.S. Burmistrov**, *Inelastic electron scattering off a quantum dot in the cotunneling regime: The signature of mesoscopic Stoner instability*, Phys. Rev. B **93**, 165425 (2016).

1. **E.V. Repin, I.S. Burmistrov**, *Surface states in a 3D topological insulator: The role of hexagonal warping and curvature*, JETP **148**, 584 (2015).